Graduate School ETD Form 9
(Revised 12/07)

PURDUE UNIVERSITY
GRADUATE SCHOOL
Thesis/Dissertation Acceptance

This is to certify that the thesis/dissertation prepared

By _Cynthia D. Wassall_

Entitled
REACTIVE OXYGEN SPECIES' ROLE IN ENDOTHELIAL DYSFUNCTION
BY ELECTRON PARAMAGNETIC RESONANCE.

For the degree of _Doctor of Philosophy_

Is approved by the final examining committee:

Marvin D. Kemple
_____
Chair

Yogesh Joglekar

Horia I. Petrache

B. D. Nageswara Rao

Stephen M. Durbin

To the best of my knowledge and as understood by the student in the *Research Integrity and Copyright Disclaimer (Graduate School Form 20)*, this thesis/dissertation adheres to the provisions of Purdue University's "Policy on Integrity in Research" and the use of copyrighted material.

Approved by Major Professor(s): _Marvin D. Kemple_

Approved by: _Ricardo S. Decca_   _11/05/2012_
                Head of the Graduate Program   Date

PURDUE UNIVERSITY
GRADUATE SCHOOL

Research Integrity and Copyright Disclaimer

Title of Thesis/Dissertation:

REACTIVE OXYGEN SPECIES' ROLE IN ENDOTHELIAL DYSFUNCTION
BY ELECTRON PARAMAGNETIC RESONANCE.

For the degree of ___Doctor of Philosophy_____

I certify that in the preparation of this thesis, I have observed the provisions of *Purdue University Executive Memorandum No. C-22,* September 6, 1991, *Policy on Integrity in Research.**

Further, I certify that this work is free of plagiarism and all materials appearing in this thesis/dissertation have been properly quoted and attributed.

I certify that all copyrighted material incorporated into this thesis/dissertation is in compliance with the United States' copyright law and that I have received written permission from the copyright owners for my use of their work, which is beyond the scope of the law. I agree to indemnify and save harmless Purdue University from any and all claims that may be asserted or that may arise from any copyright violation.

Cynthia D. Wassall
_____
Printed Name and Signature of Candidate

11/05/2012
_____
Date (month/day/year)

*Located at http://www.purdue.edu/policies/pages/teach_res_outreach/c_22.html

REACTIVE OXYGEN SPECIES' ROLE IN ENDOTHELIAL DYSFUNCTION

BY ELECTRON PARAMAGNETIC RESONANCE

A Dissertation

Submitted to the Faculty

of

Purdue University

by

Cynthia D. Wassall

In Partial Fulfillment of the

Requirements for the Degree

of

Doctor of Philosophy

December 2012

Purdue University

Indianapolis, Indiana

To my children: Thomas, Robert, Marie, Juliet and Rosalind.

TABLE OF CONTENTS

LIST OF TABLES

LIST OF FIGURES

Figure   Page

LIST OF ABBREVIATIONS

PA	pulmonary artery
RCA	right coronary artery
AT1	angiotensin II type 1 receptor
ROS	reactive oxygen species
CFO	chronic flow overload
EPR	electron paramagnetic resonance
DMSO	dimethyl sulfoxide
ST	sliced tissue
WT	whole tissue
NO	nitric oxide
CVD	cardiovascular disease
PBN	N-*tert*-butyl-α-phenylnitrone
RV	right ventricle
WSS	wall shear stress
Q	blood flow rate
D	inner diameter of blood vessel
FO	flow overload
ANOVA	analysis of variation

Ang II	angiotensin II
LAD	left anterior descending
BH_4	tetrahydrobiopterin
eNOS	endothelial nitric oxide synthase
PGI_2	prostacyclin
EDHF	endothelium-derived hyperpolarizing factor
MMPs	matrix metalloproteinases
VSMC	vascular smooth muscle cell
ACh	acetylcholine
PO_2	partial pressure of oxygen
PCO_2	partial pressure of carbon dioxide
PE	phenylephrine
im	intramuscular
PKC	protein kinase C

ABSTRACT

Wassall, Cynthia D. Ph.D., Purdue University, December 2012.   Reactive Oxygen Species' Role in Endothelial Dysfunction by Electron Paramagnetic Resonance. Major Professor: Marvin D. Kemple.

The endothelium is a single layer of cells lining the arteries and is involved in many physiological reactions which are responsible for vascular tone. Free radicals are important participants in these chemical reactions in the endothelium. Here we quantify free radicals, *ex vivo,* in biological tissue with continuous wave electron paramagnetic resonance (EPR). In all of the experiments in this thesis, we use a novel EPR spin trapping technique that has been developed for tissue segments. EPR spin trapping is often considered the 'gold standard' in reactive oxygen species (ROS) detection because of its sensitivity and non-invasive nature. In all experiments, tissue was placed in physiological saline solution with 190-mM PBN (N-*tert*-butyl-α-phenylnitrone), 10% by volume dimethyl-sulphoxide (DMSO) for cryopreservation, and incubated in the dark for between 30 minutes up to 2 hours at 37°C while gently being stirred. Tissue and supernatant were then loaded into a syringe and frozen at -80°C until EPR analysis. In our experiments, the EPR spectra were normalized with respect to tissue volume.

Conducting experiments at liquid nitrogen temperature leads to some experimental advantages. The freezing of the spin adducts renders them stable over a longer period, which allows ample time to analyze tissue samples for ROS. The

dielectric constant of ice is greatly reduced over its liquid counterpart; this property of water enables larger sample volumes to be inserted into the EPR cavity without overloading it and leads to enhanced signal detection. Due to Maxwell-Boltzmann statistics, the population difference goes up as the temperature goes down, so this phenomenon enhances the signal intensity as well.

With the 'gold standard' assertion in mind, we investigated whether slicing tissue to assay ROS that is commonly used in fluorescence experiments will show more free radical generation than tissue of a similar volume that remains unsliced. Sliced tissue exhibited a 76% increase in ROS generation; this implies that higher ROS concentrations in sliced tissue indicate extraneous ROS generation not associated with the ROS stimulus of interest.

We also investigated the role of ROS in chronic flow overload (CFO). Elevation of shear stress that increases production of vascular ROS has not been well investigated. We hypothesize that CFO increases ROS production mediated in part by NADPH oxidase, which leads to endothelial dysfunction. ROS production increased threefold in response to CFO. The endothelium dependent vasorelaxation was compromised in the CFO group. Treatment with apocynin significantly reduced ROS production in the vessel wall, preserved endothelial function, and inhibited expressions of p22/p47phox and NOX2/NOX4. The present data implicate NADPH oxidase produced ROS and eNOS uncoupling in endothelial dysfunction at 1 wk of CFO.

In further work, a swine right ventricular hypertrophy (RVH) model induced by pulmonary artery (PA) banding was used to study right coronary artery (RCA) endothelial function and ROS level. Endothelial function was compromised in RCA of

RVH as attributed to insufficient endothelial nitric oxide synthase cofactor tetrahydrobiopterin. In conclusion, stretch due to outward remodeling of RCA during RVH (at constant wall shear stress), similar to vessel stretch in hypertension, appears to induce ROS elevation, endothelial dysfunction, and an increase in basal tone.

Finally, although hypertension-induced vascular stiffness and dysfunction are well established in patients and animal models, we hypothesize that stretch or distension due to hypertension and outward expansion is the cause of endothelial dysfunction mediated by angiotensin II type 1 (AT1) receptor in coronary arteries. The expression and activation of AT1 receptor and the production of ROS were up regulated and endothelial function deteriorated in the RCA. The acute inhibition of AT1 receptor and NADPH oxidase partially restored the endothelial function. Stretch or distension activates the AT1 receptor which mediates ROS production; this collectively leads to endothelial dysfunction in coronary arteries.

CHAPTER 1: REACTIVE OXYGEN SPECIES IN THE ENDOTHELIUM

Reactive oxygen species (ROS) play important roles in biological systems. Many ROS possess an unpaired electron which causes them to be highly reactive in collisions or interactions with other molecules. Such species are referred to as free radicals. Superoxide anion, hydroxyl radical, nitric oxide (NO) and lipid radicals such as peroxyl and methyl radicals, are some examples of these molecules (Figure 1.1). Some ROS do not possess unpaired electrons but are oxidizing agents nonetheless; two important examples of these types of molecules are peroxynitrite (NOO^-) and hydrogen peroxide (H_2O_2). In general ROS are highly reactive and are essential elements in many physiological processes.

Oxygen free radicals as well as other reactive species are continually generated *in vivo* as a consequence of energy metabolism [1]. Although these free radicals have extremely short lifetimes, they are capable of extensive cellular damage. In particular, ROS cause a variety of harmful effects such as lipid peroxidation, DNA modification, protein oxidation, and cell proliferation (cancer) [2, 3]. The endothelium, a thin layer of cells lining blood and lymphatic vessels, is particularly susceptible to free radical damage.

In contrast, another reactive species, NO, has an ameliorative effect on endothelial function in biological systems and was identified as the endothelium-derived, vascular relaxing factor [4]. NO is the primary determining factor both in blood vessel tone and in

the ability for blood to form clots when it comes into contact with materials (thromogenicity). NO also plays a role in the regulation of many physiological functions such as immune response and neurotransmission [5, 6]. Although there are three nitric oxidase synthases that produce NO from L-arginine in physiological, catalytic reactions, NO is produced in the endothelium by the enzyme, endothelial nitric oxide synthase (eNOS); eNOS takes an electron from the electron donor NADPH oxidase (nicotinamide adenine dinucleotide phosphate-oxidase), and $NADP^+$ is a coenzyme in this reaction (Figure 1.3). Since NADPH oxidase also produces ROS, it is believed to be a major cause for development of atherosclerosis in arteries. In order for the enzyme to transfer an electron to L-arginine to produce NO, eNOS requires the presence of tetrahydrobiopterin (BH_4) [7].

Loss of NO bioactivity in the vessel wall alters anticoagulant and anti-inflammatory properties of the endothelium, impairing modulation of vascular growth and remodeling, a dynamic process of structural alteration that involves changes in cellular processes inside the vascular matrix [8]. Excessive production of ROS leads to oxidative stress, which can attenuate endothelium-dependent vasodilation by inactivating NO [9]. These types of biological dysfunction are intimately associated with disease and aging.

Structure of the Endothelium in Arteries

The arterial vessel wall is composed of three layers: the intima, the media and the adventitia (Figure 1.2). The innermost and thinnest layer, the intima, contains a single-

celled thickness of endothelial cells. These cells are surrounded, moving outward toward the vessel's outer wall, by connective tissue. The second layer, the media, contains connective tissue and vascular smooth muscle, which controls the vessel diameter and vascular tone. The outermost layer, the adventitia, entirely consists of connective tissue, nerves and capillaries. In general, the vascular endothelium is composed of a layer of flat cells that line closed internal spaces such as the inside of blood vessels and internal organs. A section of an artery wall shows the endothelial cells align longitudinally. Vascular smooth muscle cells align circumferentially and form the outer layers. When circumferential stretching of the vessel wall occurs, the underlying pressure acts normal to the vessel wall. Shear stress aligns parallel to the vessel wall and acts longitudinally with respect to blood flow direction.

In this thesis, all experiments employ a pig model because of its similar physiology to humans in size and function. Pigs are omnivorous; they have a cardiovascular system similar to humans and are prone to develop the same cardiovascular diseases as humans.

The Relationship Between ROS and Endothelial Dysfunction

Superoxides are formed through diverse enzymatic pathways involving such molecules as NADPH oxidases, mitochondrial oxidases, cytochrome P-450 enzymes, uncoupled NO synthases and lipoxygenases. When generation of ROS overwhelms antioxidant defenses in the endothelium, a physiological situation is commonly described

as oxidative stress arises. Oxidative stress is believed to be a key contributor to a variety of pathophysiological conditions such as atherosclerosis, hypertension and diabetes.

The renin-angiotensin system regulates pressure and fluid balance in blood vessels. In response to low blood volume, the kidneys release renin into the circulatory system. Renin converts angiotensinogen that is released from the liver to angiotensin I. In turn, angiotensin I is converted to angiotensin II through a reaction with an enzyme found in the lungs. Angiotensin II is a powerful vasoconstrictor that causes blood pressure to increase.

In cardiovascular diseases (CVD) such as hypertension, the balance between NO, an important free radical because of its vasodilation properties, and ROS is disturbed. An increase in superoxide causes an increase in production of peroxynitrite via a reaction with NO, leading to less bioavailability of NO. Inactivation of NO by superoxide increases endothelial dysfunction in patients with CVD [10]. Several animal studies of vascular disease have gleaned evidence that indicates increased superoxide production is responsible for a major proportion of an NO deficit. Oxidative metabolism is central to the biological function and health, so biological situations of high oxygen stress are of critical interest to cardiovascular medicine. Generation of free radicals by inflammatory cells acts as a significant microbiocidal agent and also behaves as a messenger in several mechanisms involved in the inflammatory response.

ROS signaling mechanisms allow cells to survive exposure to increased levels of oxidative stress; however, when damage to cell structure becomes severe, apoptosis occurs. Intracellular oscillation of oxidant levels, redox signaling [11, 12], is associated with preservation of the rate of cell proliferation [13]. NO also plays a pivotal role in the

regulation of many physiological functions such as immune response and neurotransmission [5, 6]. Loss of NO bioactivity in the vessel wall alters anticoagulant and anti-inflammatory properties of the endothelium, impairing modulation of vascular growth and remodeling, a dynamic process of structural alteration that involves changes in cellular processes inside the vascular matrix [8]. Excessive production of ROS leads to oxidative stress, which can attenuate endothelium-dependent vasodilation by inactivating NO [9] (Figure 1.4). These types of biological dysfunction are intimately associated with CVD and other diseases.

Superoxides are generated through several pathways involving mitochondrial oxidases, xanthine oxidases, uncoupled NO synthases, cytochrome P-450 enzymes, NADPH oxidases, and lipoxygenases. In particular, NADPH oxidases are produced in response to mechanical stress, hormones and cytokines. NADPH oxidases are a family of complex enzymes identified as the major ROS source in a number of recent animal studies of CVD [14-18]. Shear stress activates the renin-angiotensin system, which enhances vascular production of ROS [19]. There exists an enlarging body of evidence that suggests oxidative stress plays a crucial role in the development and maintenance of various forms of genetic and acquired hypertension. So developing and exploiting methods for detecting ROS is extremely important in order to follow and to identify the roles of ROS in physiological processes.

Both ROS and NO are compounds which contain an unpaired electron. These free radicals are highly reactive when they come in contact with other molecules as noted above. EPR (electron paramagnetic resonance) spectroscopy is considered the most reliable method of observing free radical species by employing spin traps that stabilize

the radicals, thus allowing *ex vivo* identification of the radicals and measurement of their concentrations. The EPR method provides precise measurement of ROS and NO concentrations, even at levels as low as micromolar at room temperature and one order of magnitude smaller at liquid nitrogen temperature, through chemical reactions with spin traps that render free radicals stable long enough for quantification [20]. The primary subject of this thesis is the application of EPR spin trapping methodology to the detection of ROS of biological importance.

References

[1]   Ashton, T.; Rowlands, C. C.; Jones, E.; Young, I. S.; Jackson, S. K.; Davies, B.; Peters, J. R. Electron spin resonance spectroscopic detection of oxygen-centred radicals in human serum following exhaustive exercise. *Eur J Appl Physiol Occup Physiol* **77:**498-502; 1998.

[2]   Anderson, R. A.; Evans, M. L.; Ellis, G. R.; Graham, J.; Morris, K.; Jackson, S. K.; Lewis, M. K.; Rees, A.; Frenneaux, M. P. The relationships between post-prandial lipaemia, endothelial function and oxidative stress in healthy individuals and patients with type 2 diabetes. *Atherosclerosis* **154:**475-484; 2001.

[3]   Davison, G. W.; George, L.; Jackson, S. K.; Young, I. S.; Davies, B.; Bailey, D. M.; Peters, J. R.; Ashton, T. Exercise, free radicals, and lipid peroxidation in type 1 diabetes mellitus. *Free Radic Biol Med* **33:**1543-1551; 2002.

[4]   Moncada, S.; Palmer, R. M. J.; Higgs, E. A. Nitric oxide: physiology, pathophysiology, and pharmacology. *Pharmacological Reviews* **43:**109-142; 1991.

[5]   Weaver, J.; Porasuphatana, S.; Tsai, P.; Budzichowski, T.; Rosen, G. M. Spin trapping nitric oxide from neuronal nitric oxide synthase: A look at several iron-dithiocrbamate complexes. *Free Radical Research* **39:**1027-1033; 2005.

[6]   Peyrot, F.; Grillon, C.; Vergely, C.; Rochette, L.; Ducrocq, C. Pharmacokinetics of 1-nitrosomelatonin and detection by EPR using iron dithiocarbamate complex in mice. *Biochem J* **387:**473-478; 2005.

[7]   Cai, H.; Harrison, D. G. Endothelial dysfunction in cardiovascular diseases: the role of oxidant stress. *Circ Res* **87:**840-844; 2000.

[8]   Gibbons, G. H.; Dzau, V. J. The emerging concept of vascular remodeling. *N Engl J Med* **330:**1431-1438; 1994.

[9]   Lu, X.; Guo, X.; Wassall, C. D.; Kemple, M. D.; Unthank, J. L.; Kassab, G. S. Vascular function is compromised by reactive oxygen species mediated by NADPH oxidase in flow-overload. 2007.

[10]   Spiekermann, S.; Landmesser, U.; Dikalov, S.; Bredt, M.; Gamez, G.; Tatge, H.; Reepschlager, N.; Hornig, B.; Drexler, H.; Harrison, D. G. Electron spin resonance characterization of vascular xanthine and NAD(P)H oxidase activity in patients with coronary artery disease: relation to endothelium-dependent vasodilation. *Circulation* **107:**1383-1389; 2003.

[11]   Soberman, R. J. The expanding network of redox signaling: new observations, complexities, and perspectives. *J Clin Invest* **111:**571-574; 2003.

[12]   Guzik, T. J.; Mussa, S.; Gastaldi, D.; Sadowski, J.; Ratnatunga, C.; Pillai, R.; Channon, K. M. Mechanisms of increased vascular superoxide production in human diabetes mellitus: role of NAD(P)H oxidase and endothelial nitric oxide synthase. *Circulation* **105:**1656-1662; 2002.

[13]   Irani, K.; Xia, Y.; Zweier, J. L.; Sollott, S. J.; Der, C. J.; Fearon, E. R.; Sundaresan, M.; Finkel, T.; Goldschmidt-Clermont, P. J. Mitogenic signaling mediated by oxidants in Ras-transformed fibroblasts. *Science* **275:**1649-1652; 1997.

[14]   Beswick, R. A.; Dorrance, A. M.; Leite, R.; Webb, R. C. NADH/NADPH Oxidase and Enhanced Superoxide Production in the Mineralocorticoid Hypertensive Rat. *Hypertension* **38:**1107-1111; 2001.

[15]   Zalba, G.; Beaumont, F. J.; Jose, G. S.; Fortuno, A.; Fortuno, M. A.; Etayo, J. C.; Diez, J. Vascular NADH/NADPH Oxidase Is Involved in Enhanced Superoxide Production in Spontaneously Hypertensive Rats. *Hypertension* **35:**1055-1061; 2000.

[16]   Pettit, A. I.; Wong, R. K.; Lee, V.; Jennings, S.; Quinn, P. A.; Ng, L. L. Increased free radical production in hypertension due to increased expression of the NADPH oxidase subunit p22(phox) in lymphoblast cell lines. *J Hypertens* **20:**677-683; 2002.

[17]   Fukui*, T.; Ishizaka*, N.; Rajagopalan, S.; Laursen, J. B.; Capers, Q.; Taylor, W. R.; Harrison, D. G.; de Leon, H.; Wilcox, J. N.; Griendling, K. K. p22phox mRNA Expression and NADPH Oxidase Activity Are Increased in Aortas From Hypertensive Rats. *Circ Res* **80:**45-51; 1997.

[18]   Heymes, C.; Bendall, J. K.; Ratajczak, P.; Cave, A. C.; Samuel, J. L.; Hasenfuss, G.; Shah, A. M. Increased myocardial NADPH oxidase activity in human heart failure. *J Am Coll Cardiol* **41:**2164-2171; 2003.

[19]   Dzau, V. J. Theodore Cooper Lecture: Tissue angiotensin and pathobiology of vascular disease: a unifying hypothesis. *Hypertension* **37:**1047-1052; 2001.

[20]   Janzen, E. D. Formation and removal of oxygen radicals: spin trapping. *Methods in Enzymology* **105:**188-198; 1984.

Figures

(A)

(B)
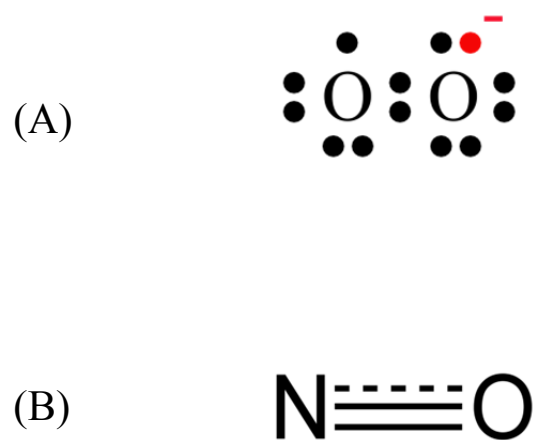
Figure 1.1: (A) superoxide and (B) nitric oxide are two important free radicals in the endothelium.
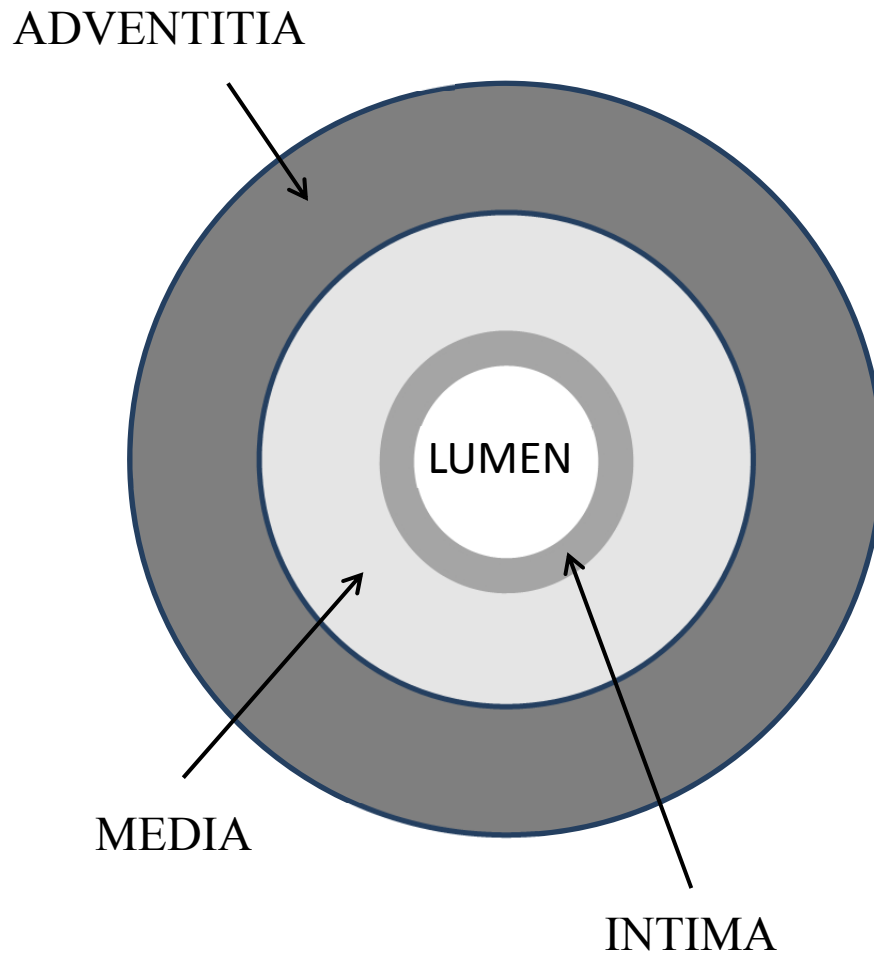
Figure 1.2: An artery cross section with the intima as the innermost layer, which contains the endothelium, as the innermost layer of cells, the media as the next layer out, and the adventitia as the outmost layer. Blood travels through the luman in the central portion of the artery.

$$\text{L-arginine} + 3/2 \text{ NADPH} + \text{H}^+ + 2\text{O}_2 \rightarrow$$

$$\text{citrulline} + \text{nitric oxide} + 3/2 \text{ NADP}^+$$
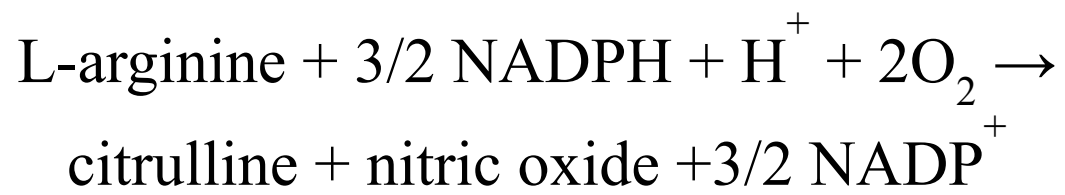
Figure 1.3: The chemical reaction that produces nitric oxide in the endothelium catalyzed by eNOS.
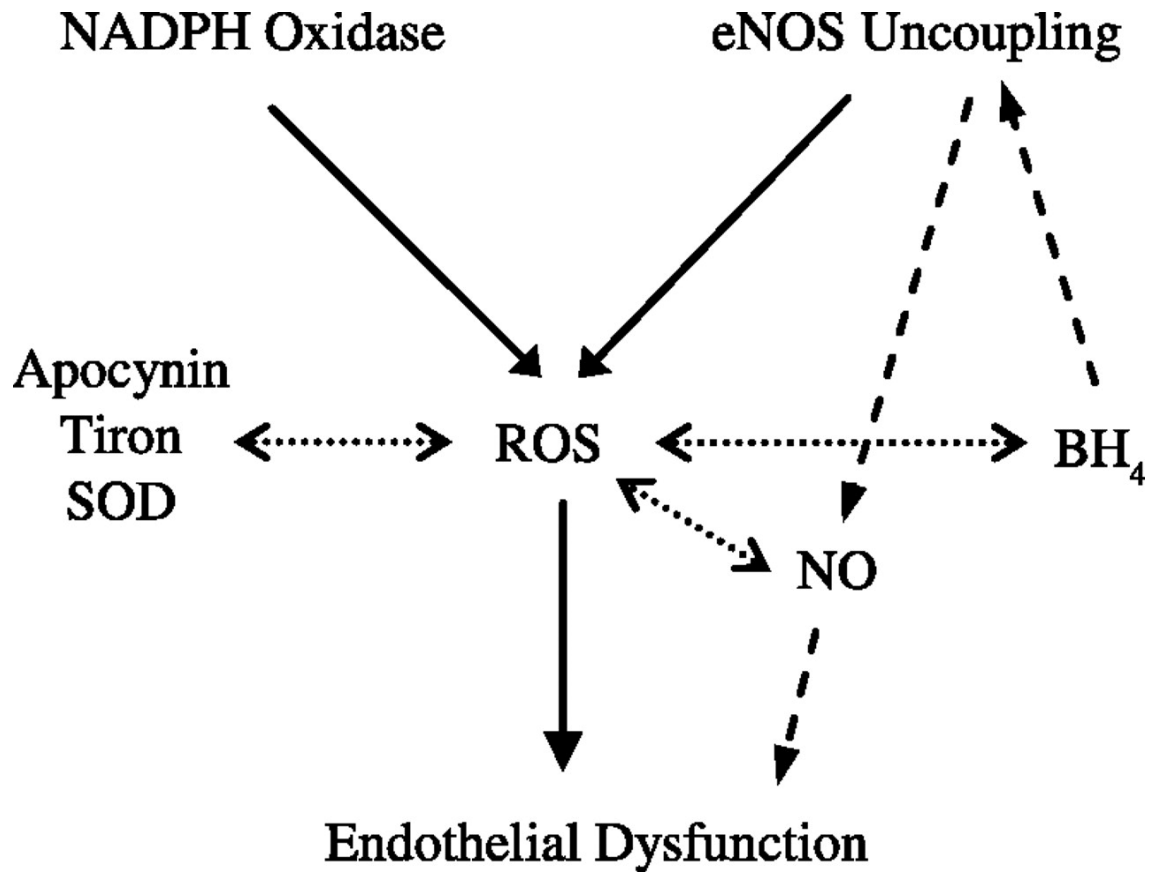
Figure 1.4: Schematic (X. Lu and G. Kassab) of the relation between ROS sources and endothelial dysfunction. Solid line, generation; dashed line, restoration; dotted line, scavenger. eNOS, endothelial nitric oxide synthase; BH_4, tetrahydrobiopterin.

CHAPTER 2: SPIN TRAPPING WITH CONTINUOUS WAVE EPR

Spin Trapping

Many molecules have been developed over the years to react with free radicals to "trap" their magnetic moments (spin); i.e. to lengthen the lifetime of the radicals to allow their detection. With most of the compounds, known as spin traps, experimental pitfalls exist inherent in their application such as a lack of solubility in aqueous solutions, a tendency for the trap to oxidize, and rapid decay of the spin adduct into a EPR silent species. A spin adduct is the compound that results after a spin trapping agent chemically reacts with a free radical, and it is comprised of the spin trap with the incorporated free radical. Although spin traps are more stable than the radical that they capture, the traps are still somewhat reactive since they possess unpaired electrons. Biologically relevant free radicals have short half-lives as noted, which makes accurate measurement of concentrations challenging. N-*tert*-butyl-α-phenylnitrone (PBN) and N-methyl-D-glucamine dithiocarbamate (MGD) form relatively stable spin adducts after trapping ROS and NO respectively; these two spins traps are employed in this study. NO is typically quantified by employing the Griess reaction which is sensitive to only some of the breakdown products of NO. Directly capturing NO through a spin trapping technique is, in general, a more desirable method because EPR can detect NO directly in the extra- and

intra-cellular environment. NO in tissues and cells as well as in physiological fluids (e. g., blood) can be trapped and therefore assayed.

PBN has a very stable spin adduct with a lifetime at room temperature of approximately 24 hours (Figure 2.3) and much longer at liquid nitrogen temperature. PBN traps superoxide and other lipid-derived radicals in whole blood and tissue (Fig. 2.2). PBN is lipid soluble, readily penetrating cell membranes, and can also cross the blood-brain barrier. PBN is utilized to measure oxidative stress directly. PBN spin adducts detected by EPR, gleaned from whole blood and tissue, are typically a secondary species resulting from free radical attack on cell membranes and, therefore, reflective of overall ROS levels [1-4].

MGD forms a stable spin adduct after capturing NO (Figure 2.5). Two MGD molecules combine with Fe^{2+} to form a spin trap with a high affinity for trapping NO. The molecule, MGD, readily traps NO and is soluble in aqueous solutions. However MGD is unable to cross the cell membrane [5-7], and must be shielded from oxygen prior to trapping to avoid oxidation to an EPR silent form.

In Figures 2.3 and 2.6, room temperature spectra show sharply defined peaks because the anisotropic parts of the Zeeman and Hyperfine tensors average to zero. The tensors behave as second order spherical harmonics. This phenomenon occurs because the sample is in solution and there is free tumbling of molecules in this solution. All experiments in this thesis are conducted at liquid nitrogen temperature where the anisotropic parts of the above mentioned tensions do not average to zero. A powder pattern occurs with inhomogeneous broadening of the EPR spectrum.

Basic EPR Theory

The spectroscopic technique of continuous wave EPR is defined as the absorption of microwave radiation by molecules or ions that possess unpaired electrons and are therefore paramagnetic. In the presence of an applied magnetic field, the electron spin states become nondegenerate, as a result of the Zeeman interaction (Figure 2.1). In addition, there often is an interaction present between the spin magnetic moment of the unpaired electron and the magnetic moment of a neighboring nucleus, which is called the hyperfine interaction leading to a further splitting of the energy levels. In our experiments, there is a hyperfine interaction between the unpaired electron and a nitrogen nucleus that possesses a magnetic moment. Since the nuclear spin of ^{14}N, the dominate isotope of nitrogen, is 1, a three-line EPR spectrum is produced characteristic of the multiplicity relation

$$2I + 1 = 3. \qquad\qquad [1]$$

In some traps there also may be nearby hydrogen nuclei influencing the spectrum. In particular, the dominant hydrogen nucleus, a proton, has a spin of ½. In PBN there is one H-nucleus with a substantial hyperfine interaction which splits each of the three energy levels into two and results in a triplet of doublets in the EPR spectrum (Figure 2.3). The selection rules for this system are $\Delta S_z = \pm 1$ and $\Delta I_z = 0$, where z specifies the direction of the applied magnetic field, B [8, 9].

The energy difference between the two spin states is defined as

$$\Delta E = h\nu = g\beta B,$$ [2]

where g is the spectroscopic splitting factor, β is the Bohr magneton, $\dfrac{|e|\hbar}{2m}$, m is the mass

of an electron, and ν is the resonant frequency. In the steady state approximation, the

population difference of the occupied states is

$$n = N_1 - N_2,$$ [3]

where N_1 state with electron is the number of molecules in the spin down, and N_2 is the

number of molecules with electron spin up. This system can be described by Maxwell-

Boltzmann statistics, since it is in thermodynamic equilibrium and the total number of

spins,

$$N = N_1 + N_2$$ [4]

in the sample is constant. Therefore an expression can be written in this form,

$$\frac{N_2}{N_1} = e^{\frac{-\Delta E}{kT}}$$ [5]

Eliminating N_1 and N_2 from equations 3, 4, and 5 results in the expression,

$$n = N \tanh\left[\frac{h\nu}{2kT}\right],$$ [6]

where h is Plank's constant and k is Boltzmann's constant.

The net magnetization in the direction of the magnetic field is defined as,

$$M_\circ = n\vec{m},$$ [7]

where the magnetic moment of one electronic spin is $\vec{m}$. Since $M_\circ$ is proportional to n,

the signal intensity is proportional to the total number of spins in the system, N.

In continuous wave EPR, the microwave frequency is held constant while the magnetic field is swept through a range of approximately 100 Gauss; the signal recorded is displayed as the 1st derivative of the absorption of microwave energy by the sample as depicted in Figure 2.1. To determine the absolute concentration of a sample, a double integration is performed, and the resulting value is compared to the double integration of a precisely known standard. Alternatively, the concentration is calculated from the spectral line width and intensity, and then compared with the spectral line width and intensity of a standard.

References

[1]   Ashton, T.; Rowlands, C. C.; Jones, E.; Young, I. S.; Jackson, S. K.; Davies, B.; Peters, J. R. Electron spin resonance spectroscopic detection of oxygen-centred radicals in human serum following exhaustive exercise. *Eur J Appl Physiol Occup Physiol* **77:**498-502; 1998.

[2]   Anderson, R. A.; Evans, M. L.; Ellis, G. R.; Graham, J.; Morris, K.; Jackson, S. K.; Lewis, M. K.; Rees, A.; Frenneaux, M. P. The relationships between post-prandial lipaemia, endothelial function and oxidative stress in healthy individuals and patients with type 2 diabetes. *Atherosclerosis* **154:**475-484; 2001.

[3]   Bailey, D. M.; Davies, B.; Young, I. S.; Jackson, M. J.; Davison, G. W.; Isaacson, R.; Richardson, R. S. EPR spectroscopic detection of free radical outflow from an isolated muscle bed in exercising humans. *J Appl Physiol* **94:**1714-1718; 2003.

[4]   Davison, G. W.; George, L.; Jackson, S. K.; Young, I. S.; Davies, B.; Bailey, D. M.; Peters, J. R.; Ashton, T. Exercise, free radicals, and lipid peroxidation in type 1 diabetes mellitus. *Free Radic Biol Med* **33:**1543-1551; 2002.

[5]   Vanin, A. F.; Huisman, A.; vanFaassen, E. E. Detection of Nitric Oxide: Iron Dithiocarbamate as Spin Trap for Nitric Oxide. *Methods in Enzymology* **359:**27-42; 2002.

[6]   Fujii, H.; Berliner, L. J. *Ex vivo* EPR detection of nitric oxide in brain tissue. *Magn Reson Med* **42:**599-602; 1999.

[7]   Kleschyov, A. L.; Strand, S.; Schmitt, S.; Gottfried, D.; Skatchkov, M.; Sjakste, N.; Daiber, A.; Umansky, V.; Munzel, T. Dinitrosyl-iron triggers apoptosis in Jurkat cells despite overexpression of Bcl-2. *Free Radic Biol Med* **40:**1340-1348; 2006.

[8]   Pake, G. E. *Paramagnetic Resonance.* New York: W. A. Benjamin, INC.; 1962.

[9]   Nordio, P. L. General Magnetic Resonance Theory. In: Berliner, L. J., ed. *Spin Labeling: theory and applications*. New York: Academic Press, Inc.; 1976: 5-52.

Figures
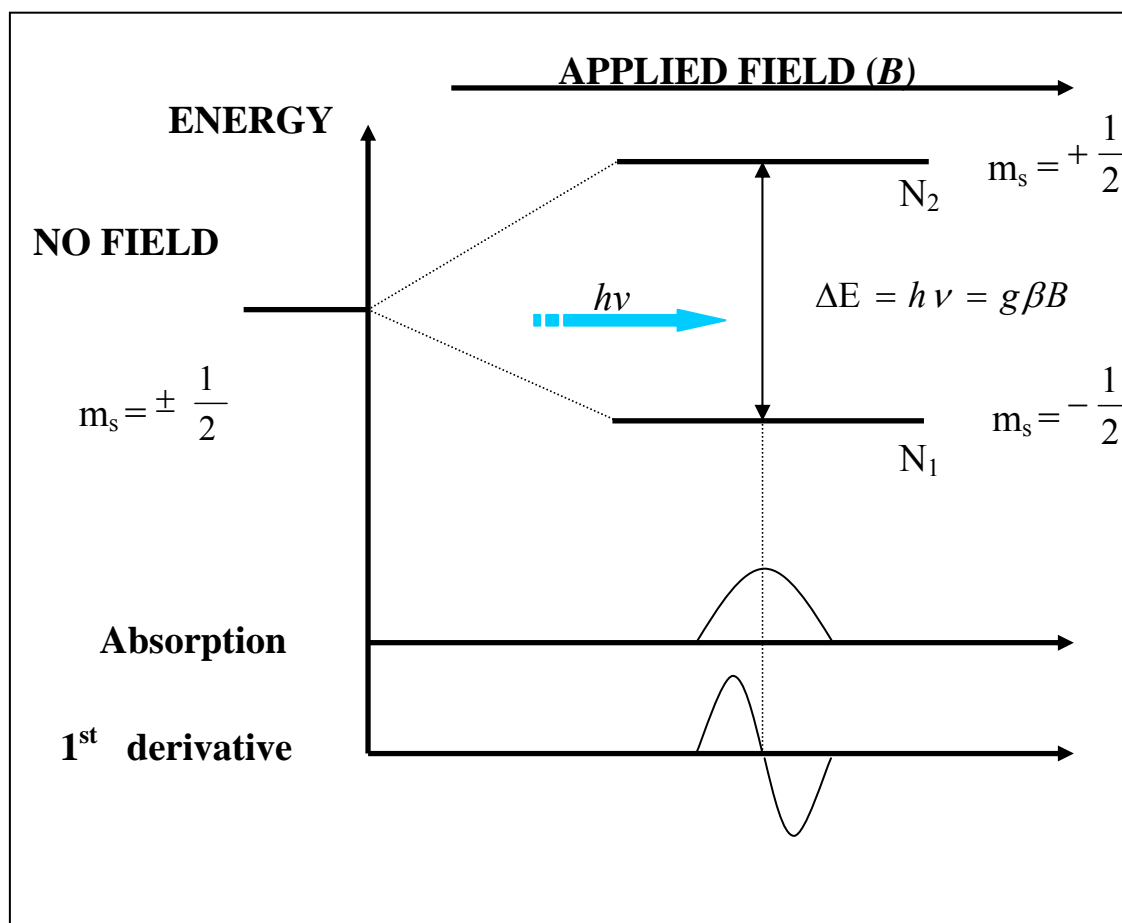
Figure 2.1:   Schematic of electron paramagnetic resonance that occurs when a paramagnetic sample is in the presence of an external magnetic field.   The magnetic field splits its electronic spin states. Microwave irradiation causes energy absorption by the sample which results in a transition to a higher energy state.   The EPR spectrometer shows the 1st derivative of the absorption spectrum.
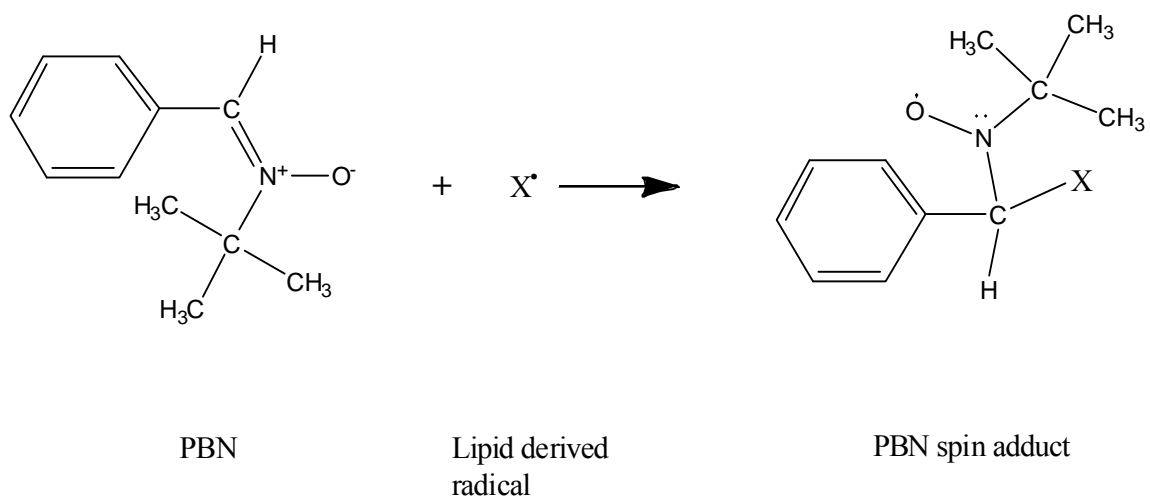
Figure 2.2: The chemical reaction of PBN and lipid-derived radical results in capture of the radical by PBN. This product of the reaction is called the PBN spin adduct.
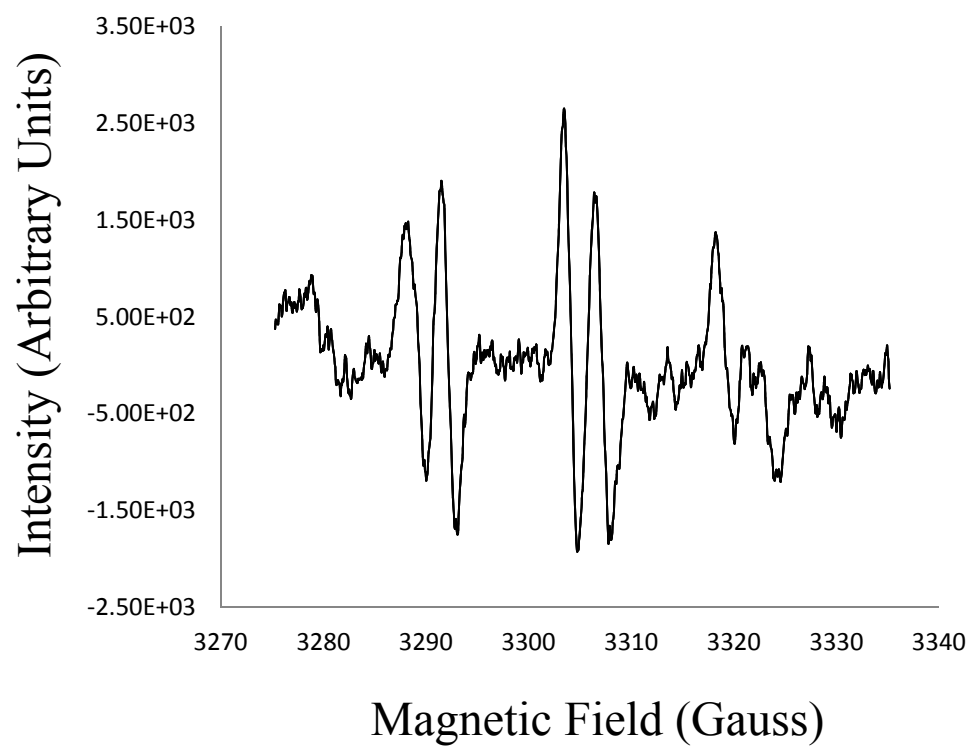
Figure 2.3: A first derivative representative spectrum of superoxide that is trapped by PBN at room temperature. Superoxide was produced in the hypoxanthine/xanthine model system.
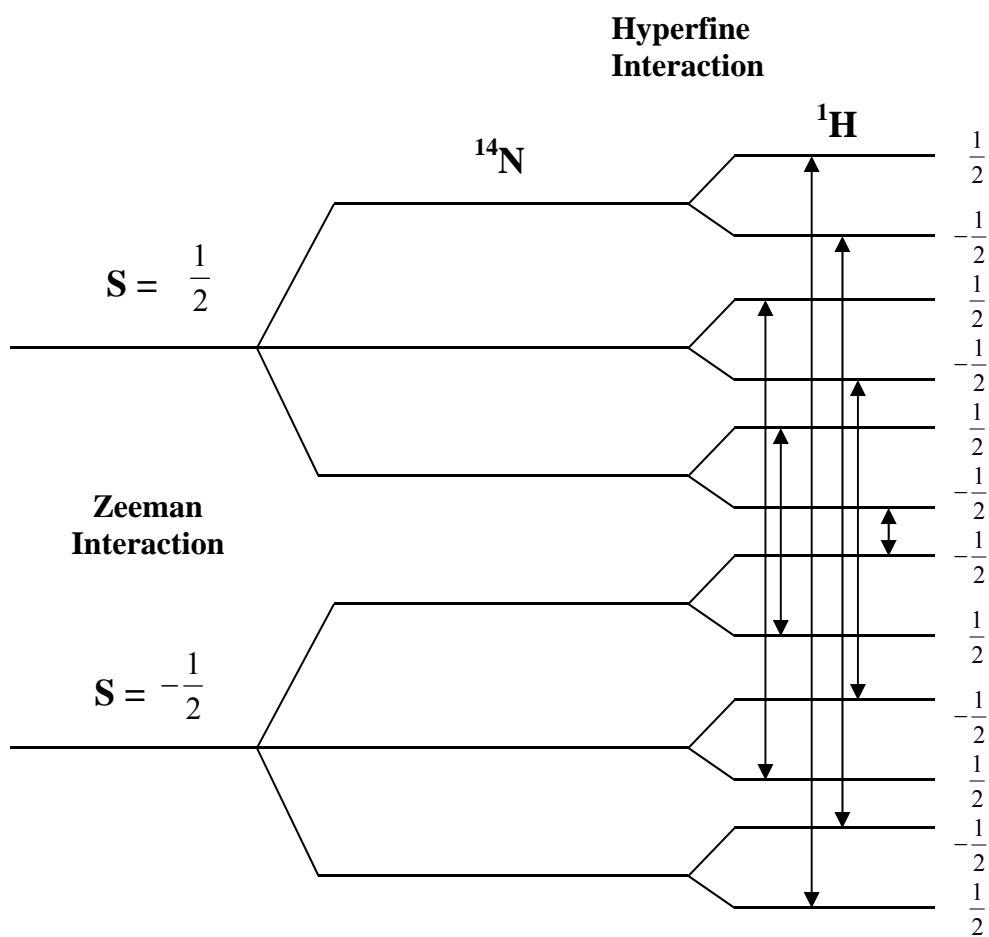
Figure 2.4: Diagram depicting the transitions of the PBN spin adduct.
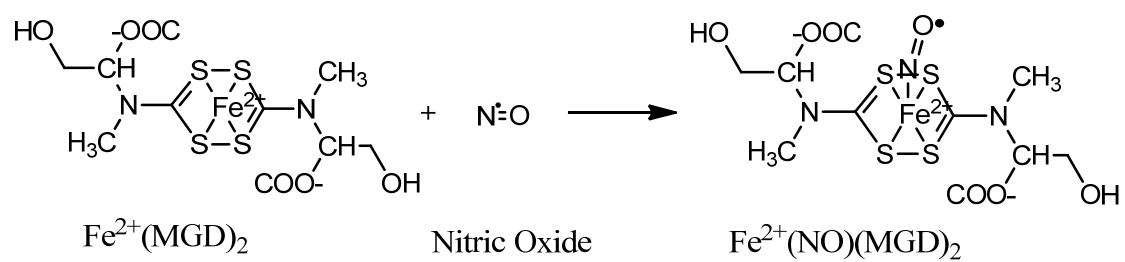
Figure 2.5: The chemical reaction of the MGD spin trap and nitric oxide. The MGD spin adduct is the product of the reaction.
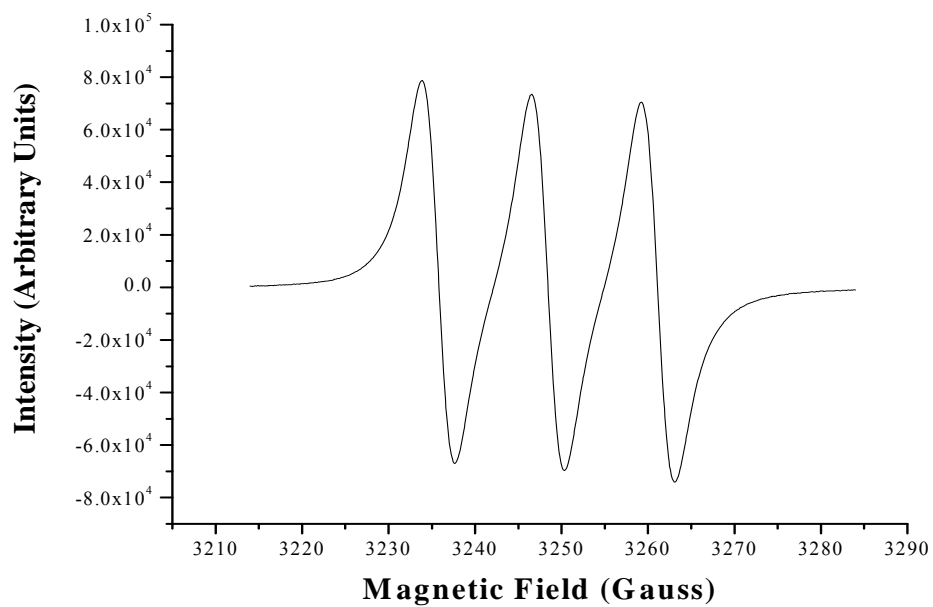
Figure 2.6: The first derivative spectrum of the MGD spin adduct of nitric oxide produced by a slow release NO source (PAPA-NONOate) in aqueous solution, $A_N = 12.6$ and line width = 3.7 G.

CHAPTER 3: EPR METHOD FOR *EX VIVO* DETECTION OF REACTIVE OXYGEN

SPECIES IN CRYOPRESERVED TISSUE

In biology and medicine, the detection of free radicals that are involved in various important processes such as intercellular signaling, immune response, and the progression of disease is of immense interest. Oxygen free radicals as well as other reactive species are continually generated *in vivo* as a consequence of energy metabolism [1]. Although these free radicals have an extremely short lifetime, they are capable of extensive biological damage if the physiological oxidative balance is disturbed. In particular, increase in reactive oxygen species (ROS) can cause a variety of harmful effects such as lipid peroxidation, DNA modification, protein oxidation, and cell proliferation [2, 3]. Excessive production of ROS leads to oxidative stress, which can attenuate endothelium-dependent vasodilation by inactivating nitric oxide [4, 5]. These types of biological dysfunction are intimately associated with disease and aging.

Early electron paramagnetic resonance (EPR) techniques for measurement of free radicals in cells and tissues involved either freezing and drying of biological samples (lyophilization) to remove water or using aqueous samples in flat or tissue cells [6]. Lyophilization of biological material increases the amount of sample that can be placed in the microwave cavity. Since the EPR signal intensity is proportional to the number of unpaired electron spins in the sample, an increase in sample size will lead generally to a

larger signal. Removal of water and nutrients, however, leads to cell distress and then subsequent immune response causes additional free radical generation. Both methods eliminate the problem of non-resonant absorption of microwaves and allow sample size to be increased, but both methods are not ideal because they invariably lead to inaccurate free radical measurements. The objective of this study is to demonstrate the advantages of our EPR method of assaying ROS over other frequently employed ROS assays used in biology and medicine.

Spin trapping in conjunction with EPR spectroscopy is a widely used technique for measurement of short-lived free radical species of biological interest because of its high sensitivity and specificity [7, 8]. Spin traps chemically react with and stabilize free radicals, thus allowing *ex vivo* concentration measurements that are unambiguous. This method provides precise measurement of ROS concentrations, even at levels as low as micromolar at room temperature and one order of magnitude lower at liquid nitrogen temperature (77K) [9].

Materials and Methods

Experimental Procedures

The experiments were conducted on five healthy, 3 to 4 month-old Duroc swine weighing 32 kg ± 2 kg (range 30–35 kg). In each experiment, the heart was removed, and the coronary arteries were excised. All experiments were performed in accordance with national and local ethical guidelines, including the Institute of Laboratory Animal

Research Guide, Public Health Service policy, Animal Welfare Act and an approved Indiana University School of Medicine IACUC protocol.

Immediately after dissection of the coronary arteries, two similar-sized coronary vessels were videotaped from the side (approximately 5 mm in length) and cross views under a stereo microscope. The volume of each segment was calculated based on the product of cross-sectional area and axial length. One segment was then divided into 10 sections but kept as one sample while the other segment remained intact. This is done to investigate whether slicing tissue produces more ROS. EPR spectra were normalized with respect to tissue volume.

To elucidate ROS detection by PBN, the arterial segments were treated as follows: Porcine arteries were harvested then incubated in the dark with HEPES physiological saline solution, 10% dimethyl sulphoxide (DMSO), and 190-mM PBN (Sigma, USA) for 120 min at 37°C while being stirred gently. Subsequently, the tissue was inserted into a 1-ml tuberculin syringe along with the supernatant and stored at -80°C until EPR analysis was performed.

EPR Spectroscopy, Settings and Data Analysis

All EPR measurements were conducted with a Bruker (Billerica, MA, USA) ESP 300 X-band EPR spectrometer equipped with a TE_{102} cavity and a 500-ml finger dewar (Wilmad, NJ, USA). The tip of the plastic tuberculin syringe that contained the sample was cut off, and the icicle was quickly pushed out with the plunger and placed in a dewar

containing liquid nitrogen. To overcome EPR noise due to bubbling of nitrogen gas, the sample was weighed down with a glass rod. The rod remained outside the EPR cavity to eliminate any extraneous signal at g ≈ 2 and rested on the top of the cylindrical icicle which in turn protruded slightly outside the cavity. The volume of icicle inserted in the EPR cavity was carefully adjusted by moving the dewar vertically to the same position for each sample (Figure 3.1). The cryopreserved tissue as well as the supernatant remained frozen at 77K throughout the analysis. The microwave cavity was re-tuned after each scan since maintaining the cavity on resonance is difficult at liquid nitrogen temperature. ROS concentrations were determined with 2,2,6,6-tetramethylpiperidine 1-oxyl, TEMPO, solution (0.1-μM, Sigma, USA) used as a concentration standard. Parameters for experiments were as follows: 9.4-GHz microwave frequency, 2.52-mW incident microwave power, 100-kHz field modulation, 4.0-G modulation amplitude, 1×10^5 receiver gain, 5.24-s time constant, ~3350-G center magnetic field, and 100-G magnetic field sweep width. Four scans were taken and analyzed with Bruker WINEPR software (Version 2.11). The concentration of ROS was calculated based on the signal intensity and peak-to-peak derivative line-width (Figure 3.2). All EPR parameters and conditions were applied to both standard and experimental samples.

<u>Results and Discussion</u>

Comparison of two typical first-derivative spectra from the two data sets in Figure 3.3 shows that the dashed trace, Sliced Tissue (ST), reflects a larger ROS concentration. Both the signal intensity and the linewidth are greater than with the solid trace, Whole

Tissue (WT). The whole coronary arterial tissue segment (solid trace) and the sliced coronary arterial tissue (dashed trace) spectra were normalized with respect to tissue volume.

The additional ROS production in the ST group as compared to the WT group (Figure 3.4) is believed to be primarily due to the extra cellular trauma caused by further slicing of tissue. The ST group had a ROS concentration value of 173.64±16.10 nanomolar (black column) and the WT group had a ROS concentration value of 98.53±15.12 nanomolar (gray diagonal line column), with a sample size of N = 5 pigs.

EPR spin trapping has often been cited as the gold standard for measurement of ROS concentrations in biological samples [8, 10-13]. With this assertion in mind, we have compared two sets of coronary arterial tissue samples. The first data set contains artery segments with each individual segment divided into ten pieces to mimic typical ROS assay requirements [7, 14, 15]. The second data set consists of whole coronary segments (no further slicing). This second data set likely represents ROS measurement that is more reflective of the *in vivo* environment of arterial tissue. Figure 3.4 demonstrates that minimally perturbing arterial tissue (whole segment) reduces extraneous ROS generation by nearly 50%. Since the coronary arteries were harvested from young, healthy animals without any coronary artery disease; it is plausible that ROS generation in both cases is primarily due to tissue dissection. The WT group effectively represents basal levels of ROS in un-stimulated coronary arteries.

Although absorption of microwaves by an aqueous sample at room temperature limits the size of the sample; this method can accommodate as large as 20-mm^3 tissue volume into our standard, rectangular, X-band EPR cavity at liquid nitrogen temperature.

In our experiments the tissue volumes were in a range of values between 2 mm^3 and 5 mm^3, and the EPR spectra were normalized with respect to tissue volume.

In biological studies, either the tissue or the supernatant is often evaluated alone for free radical content, or an organic extraction of EPR spin adducts is applied to whole blood serum, cells or tissue [3, 16, 17]. In evaluating ROS concentrations in the supernatant, an inevitable pitfall is that some of the spin adducts are contained inside the tissue and cells and therefore go unmeasured. In evaluating tissue only, typically the tissue is homogenized [18, 19] or thinly sliced [20], which will cause additional free radical generation that compromises the integrity of the experiment as noted above. Employing an organic extraction of spin adducts from whole blood, cells and tissue is an improvement over evaluating either supernatant or tissue alone. This is not ideal, however, since it is likely that some spin adduct will remain trapped inside the tissue or solubilized in aqueous media; i.e., only the organic layer is analyzed for free radical content. Furthermore, centrifugation and the addition of an organic solvent may cause extraneous free radical generation as the biological sample becomes necrotic. Although frozen blood serum has been widely used in EPR liquid nitrogen experiments to determine the concentration of nitric oxide that is bound to the intrinsic spin trap, hemoglobin [10, 14, 18, 19, 21, 22], frozen tissue experiments [23, 24] have not been as successful, in part, due to the problem of EPR noise as a result of bubbling of nitrogen gas in the dewar that contains the sample. Our method employed in this study and in previous ones [15, 25] places the cryopreserved tissue in a *quasi*-live state into the EPR cavity along with the supernatant, allowing more precise EPR concentration measurements [18].

Fluorescent staining methods of ROS detection in tissue are ubiquitously employed in medicine and require freezing the sample and finely slicing of tissue to image ROS [15]. This staining method is popular both in terms of cost and ease of use. Fluorometric assays are also commonly used as ROS assays in homogenized tissue [26]. The chemiluminescence method of ROS detection utilizes small pieces of sliced tissue that are immersed in physiological saline; the experiment is run at physiological temperature, which is improvement in experimental protocol since the tissue is in a *quasi-live* state during data acquisition [27].

Although spin traps are more stable than the radical that they capture, these chemical species still remain reactive since they possess unpaired electrons. Many biologically relevant free radicals have short half-lives, which makes accurate measurement of ROS concentrations challenging. N-*tert*-butyl-α-phenylnitrone (PBN) forms relatively stable alkoxyl-radical spin-adducts that result from the oxidation of lipids. The spin-adducts' stability is enhanced at liquid nitrogen temperature. PBN is also lipid soluble and cell membrane permeable, which makes PBN an appropriate choice as a spin trapping agent in tissue. PBN spin adducts detected by EPR are believed to be lipid hydroperoxides that are secondary species resulting from free radical attack on cell membranes, and thus the presence of the spin-adducts is reflective of ROS levels [1, 3, 17, 28].

Ex vivo tissue experiments conducted at liquid nitrogen temperature have distinct advantages over experiments conducted at room or physiological temperature. Adduct, and by inference ROS concentrations on the order of tens of nanomolars can be gleaned from frozen samples. At liquid nitrogen temperature, the dielectric constant of the frozen

aqueous sample is reduced from its value at room temperature and in the liquid counterpart. This phenomenon allows a larger volume of sample to be placed in the EPR cavity without degrading the cavity Q so much as to render a signal undetectable. As a result, roughly one order of magnitude smaller concentrations of spin adducts can be detected from arterial samples at liquid nitrogen temperature versus room temperature. This technique places frozen tissue and supernatant directly into the EPR cavity for ROS detection.

In addition to the ability to place unfragmented or unfractioned tissue samples into the EPR cavity for ROS detection, conduction of the experiment with the samples at liquid nitrogen temperature has further advantages such as larger sample size (vide infra), extension of free radical stability, and cryopreservation of tissue sample. An upper limit on the size of aqueous sample that can be placed into an EPR cavity at room temperature leads to two possibilities for sample content. Either the supernatant alone is sampled or the tissue is minced or homogenized [21, 25]. Homogenization of tissue triggers the release of free radicals and causes cell necrosis. Since tissue contains approximately 70% water, increasing the tissue sample size can be achieved by freezing it. The dielectric constant of ice is greatly reduced relative to its liquid counterpart, which decreases the loading of the microwave cavity for an icy sample as compared with an aqueous one of the same volume. Therefore more frozen sample volume can be placed in the EPR cavity without overload, which can lead to disappearance of the cavity resonance to disappear. Although we used tissue volumes of approximately 4mm^3 in our experiments, tissue volumes could be increased by an order of magnitude. This would result in an improvement in the signal to noise ratio for a given concentration of spins. Utilizing

larger tissue samples is desirable because at liquid nitrogen temperature there exists a small underlining $g \approx 2$ signal due to the glass finger dewar that holds the sample in the EPR cavity [10]. As Figure 3.4 implies, larger tissue size and fewer tissue excises reduces contributions to the measured ROS from sources that are not relevant to the physiological processes being studied. In addition, smaller concentrations of spin adducts can be detected at liquid nitrogen temperature relative to room temperature. Since the signal intensity is proportional to the number of unpaired electron spins in the microwave cavity, a larger sample volume leads to increased signal intensity. With typical spectrometer setups, concentrations in the micromolar range can be measured at room temperature, whereas at liquid nitrogen temperature, one order of magnitude smaller sample concentrations can be detected. Furthermore, at room temperature PBN spin adducts are relatively stable for twenty-four hours but gradually become EPR silent after a few days. Although spin traps are more stable than the free radical that they trap, they still possess an unpaired electron and are reactive as noted above. The freezing of the spin adducts renders them stable over a longer period, which allows ample time to analyze tissue samples for ROS. Due to Maxwell-Boltzmann statistics, the population difference goes up as the temperature goes down, so this phenomenon enhances the signal intensity as well. In EPR, a frozen sample does lead to inhomogeneous broadening of the spectrum because the effective motional narrowing that occurs in a liquid sample, no longer occurs, and one detects a powder pattern. The inhomogeneous broadening factor is manageable because the principal values of the g-tensor of typical spin adducts are nearly equal and hyperfine interactions are not so large as to negate the advantages of using lower temperatures.

It is common practice to include final sample concentrations of chemical ingredients in the experimental protocol section of reports of spin trapping experiments rather than stock solution concentrations, which can lead to difficulty in reproducibility. Since PBN is a lipid soluble chemical compound, it needs to be dissolved in an organic solvent prior to adding it to the final tissue/supernatant sample. Although omission of the use of a small amount of organic solvent may be considered unimportant given that the overall sample volume is large compared with that of the solvent, this information is critical for experimental reproducibility. DMSO was the organic solvent employed in this work for two reasons. Firstly, DMSO is a polar aprotic solvent that readily dissolves into aqueous solutions as well as lipid solutions. The spin trap can traverse both the lipid portion as well as the aqueous portion of the tissue sample. Secondly, 10% DMSO cryopreserves the tissue by eliminating ice formation inside tissue cells during freezing which can cause extraneous ROS generation [29, 30]. It has been reported that DMSO can trap hydroxyl radical [13]. In these experiments, the ability of DMSO to trap hydroxyl radical is not a significant problem because overall ROS concentration is being measured.

In conclusion, it is important to limit extraneous ROS generation that is not due to the ROS stimulus of interest. Use of more than one method to detect ROS in an investigative study is important. Although no ROS assay method is ideal, using EPR in conjunction with a non-invasive probe such as PBN to assay ROS in whole tissue before freezing may create an approximation to *in vivo* conditions and should be included as one of the multiple methods to quantify ROS in biological studies.

References

[1]   Ashton, T.; Rowlands, C. C.; Jones, E.; Young, I. S.; Jackson, S. K.; Davies, B.; Peters, J. R. Electron spin resonance spectroscopic detection of oxygen-centred radicals in human serum following exhaustive exercise. *Eur J Appl Physiol Occup Physiol* **77:**498-502; 1998.

[2]   Anderson, R. A.; Evans, M. L.; Ellis, G. R.; Graham, J.; Morris, K.; Jackson, S. K.; Lewis, M. K.; Rees, A.; Frenneaux, M. P. The relationships between post-prandial lipaemia, endothelial function and oxidative stress in healthy individuals and patients with type 2 diabetes. *Atherosclerosis* **154:**475-484; 2001.

[3]   Davison, G. W.; George, L.; Jackson, S. K.; Young, I. S.; Davies, B.; Bailey, D. M.; Peters, J. R.; Ashton, T. Exercise, free radicals, and lipid peroxidation in type 1 diabetes mellitus. *Free Radic Biol Med* **33:**1543-1551; 2002.

[4]   Kojda, G.; Harrison, D. Interactions between NO and reactive oxygen species: pathophysiological importance in atherosclerosis. *Cardiovascular Research* **43:**562-571; 1999.

[5]   Racasan, S.; Braam, B.; Koomans, H. A.; Joles, J. A. Programming blood pressure in adult SHR by shifting perinatal balance of NO and reactive oxygen species toward NO: the inverted Barker phenomenon. *American journal of physiology* **288:**F626-636; 2005.

[6]   Berliner, L. J. *In Vivo EPR (ESR): Theory and Applications.* Denver: Kluwer Academic/ Plenum Publishers; 2003.

[7]   Villamena, F. A.; Rockenbauer, A.; Galllucci, J.; Velayutham, M.; Hadad, C. M.; Zweier, J. L. Spin Trapping by 5-Carbamoyl-5-methyl-1-pyrroline N-Oxide (AMPO): Theoretical and Experimental Studies. *J. Org. Chem.* **69:**7994-8004; 2004.

[8]   Timmins, S. G.; Liu, K. J. Spin Trapping *in Vivo*: Facts and Artifacts. In: Berliner, L. J., ed. *College of Pharmacy*. New York: Kluwer Academic/Plenum Publishers; 2003: 285-308.

[9]   Janzen, E. D. Formation and removal of oxygen radicals: spin trapping. *Methods in Enzymology* **105:**188-198; 1984.

[10]   Jiang, J.; Corbett, J.; Hogg, N.; Mason, R. P. An electron paramagnetic resonance investigation of the oxygen dependence of the arterial-venous gradient of nitrosyl hemoglobin in blood circulation. *Free Radic Biol Med* **43:**1208-1215; 2007.

[11]   Hogg, N.; Kalyanaraman, B. Nitric oxide and lipid peroxidation. *Biochimica et Biophysica Acta (BBA) - Bioenergetics* **1411:**378-384; 1999.

[12]   Berliner, L. J.; Swartz, H. M. History of *in Vivo* EPR. In: .Berliner, L. J., ed. *In Vivo EPR (ESR): Theory and Applications*. New York: Kluwer Academic/Plenum Publishers; 2003: ix-ixxviii.

[13]   Berliner, L. J.; Khramtsov, V.; Fujii, H.; Clanton, T. L. Unique *in vivo* applications of spin traps. *Free radical biology & medicine* **30:**489-499; 2001.

[14]   Piknova, B.; Gladwin, M. T.; Schechter, A. N.; Hogg, N. Electron paramagnetic resonance analysis of nitrosylhemoglobin in humans during NO inhalation. *J Biol Chem* **280:**40583-40588; 2005.

[15]   Lu, X.; Dang, C. Q.; Guo, X.; Molloi, S.; Wassall, C. D.; Kemple, M. D.; Kassab, G. S. Elevated oxidative stress and endothelial dysfunction in right coronary artery of right ventricular hypertrophy. *J Appl Physiol* **110:**1674-1681; 2011.

[16]   Grech, E. D.; Dodd, N. J.; Jackson, M. J.; Morrison, W. L.; Faragher, E. B.; Ramsdale, D. R. Evidence for free radical generation after primary percutaneous transluminal coronary angioplasty recanalization in acute myocardial infarction. *Am J Cardiol* **77:**122-127; 1996.

[17]   Bailey, D. M.; Davies, B.; Young, I. S.; Jackson, M. J.; Davison, G. W.; Isaacson, R.; Richardson, R. S. EPR spectroscopic detection of free radical outflow from an isolated muscle bed in exercising humans. *J Appl Physiol* **94:**1714-1718; 2003.

[18]   Aldini, G.; Orioli, M.; Maffei Facino, R.; Giovanna Clement, M.; Albertini, M.; Mazzola, S.; Pirrone, F.; Carini, M. Nitrosylhemoglobin formation after infusion of NO solutions: ESR studies in pigs. *Biochem Biophys Res Commun* **318:**405-414; 2004.

[19]   Svistunenko, D. A.; Patel, R. P.; Voloshchenko, S. V.; Wilson, M. T. The globin-based free radical of ferryl hemoglobin is detected in normal human blood. *J Biol Chem* **272:**7114-7121; 1997.

[20]   Mariappan, N.; Elks, C. M.; Fink, B.; Francis, J. TNF-induced mitochondrial damage: a link between mitochondrial complex I activity and left ventricular dysfunction. *Free radical biology & medicine* **46:**462-470; 2009.

[21]   Kozlov, A. V.; Szalay, L.; Umar, F.; Fink, B.; Kropik, K.; Nohl, H.; Redl, H.; Bahrami, S. Epr analysis reveals three tissues responding to endotoxin by increased formation of reactive oxygen and nitrogen species. *Free Radic Biol Med* **34:**1555-1562; 2003.

[22]   Kirima, K.; Tsuchiya, K.; Sei, H.; Hasegawa, T.; Shikishima, M.; Motobayashi, Y.; Morita, K.; Yoshizumi, M.; Tamaki, T. Evaluation of systemic blood NO dynamics by EPR spectroscopy: HbNO as an endogenous index of NO. *Am J Physiol Heart Circ Physiol* **285:**H589-596; 2003.

[23]   Zweier, J. L.; Flaherty, J. T.; Weisfeldt, M. L. Direct measurement of free radical generation following reperfusion of ischemic myocardium. *Proc Natl Acad Sci U S A* **84:**1404-1407; 1987.

[24]   Kozlov, A. V.; Szalay, L.; Umar, F.; Kropik, K.; Staniek, K.; Niedermuller, H.; Bahrami, S.; Nohl, H. Skeletal muscles, heart, and lung are the main sources of oxygen radicals in old rats. *Biochim Biophys Acta* **1740:**382-389; 2005.

[25]   Lu, X.; Guo, X.; Wassall, C. D.; Kemple, M. D.; Unthank, J. L.; Kassab, G. S. Reactive oxygen species cause endothelial dysfunction in chronic flow overload. *J Appl Physiol* **110:**520-527; 2011.

[26]   Socci, D. J.; Bjugstad, K. B.; Jones, H. C.; Pattisapu, J. V.; Arendash, G. W. Evidence that oxidative stress is associated with the pathophysiology of inherited hydrocephalus in H-Tx rat model. *Experimental Neurology* **155:**109-117; 1999.

[27]   Judkins, C. P.; Diep, H.; Broughton, B. R. S.; Mast, A. E.; Hooker, E. U.; Miller, A. A.; Selemidis, S.; Dusting, G. J.; Sobey, C. G.; Drummond, G. R. Direct evidence of a role for Nox2 in superoxiode production, reduced nitric oxide bioavailability and early atherosclerotic plaque formation. *Am J Physiol Heart Circ Physiol* **298:**H24-H32; 2010.

[28]   Garlick, P. B.; Davies, M. J.; Hearse, D. J.; Slater, T. F. Direct detection of free radicals in the reperfused rat heart using electron spin resonance spectroscopy. *Circ Res* **61:**757-760; 1987.

[29]	Geiszt, M.; Kopp, J. B.; Varnai, P.; Leto, T. L. Identification of renox, an NAD(P)H oxidase in kidney. *Proc Natl Acad Sci U S A* **97:**8010-8014; 2000.

[30]	Garland, C. J.; Plane, F.; Kemp, B. K.; Cocks, T. M. Endothelium-dependent hyperpolarization: a role in the control of vascular tone. *Trends Pharmacol Sci* **16:**23-30; 1995.

Figures
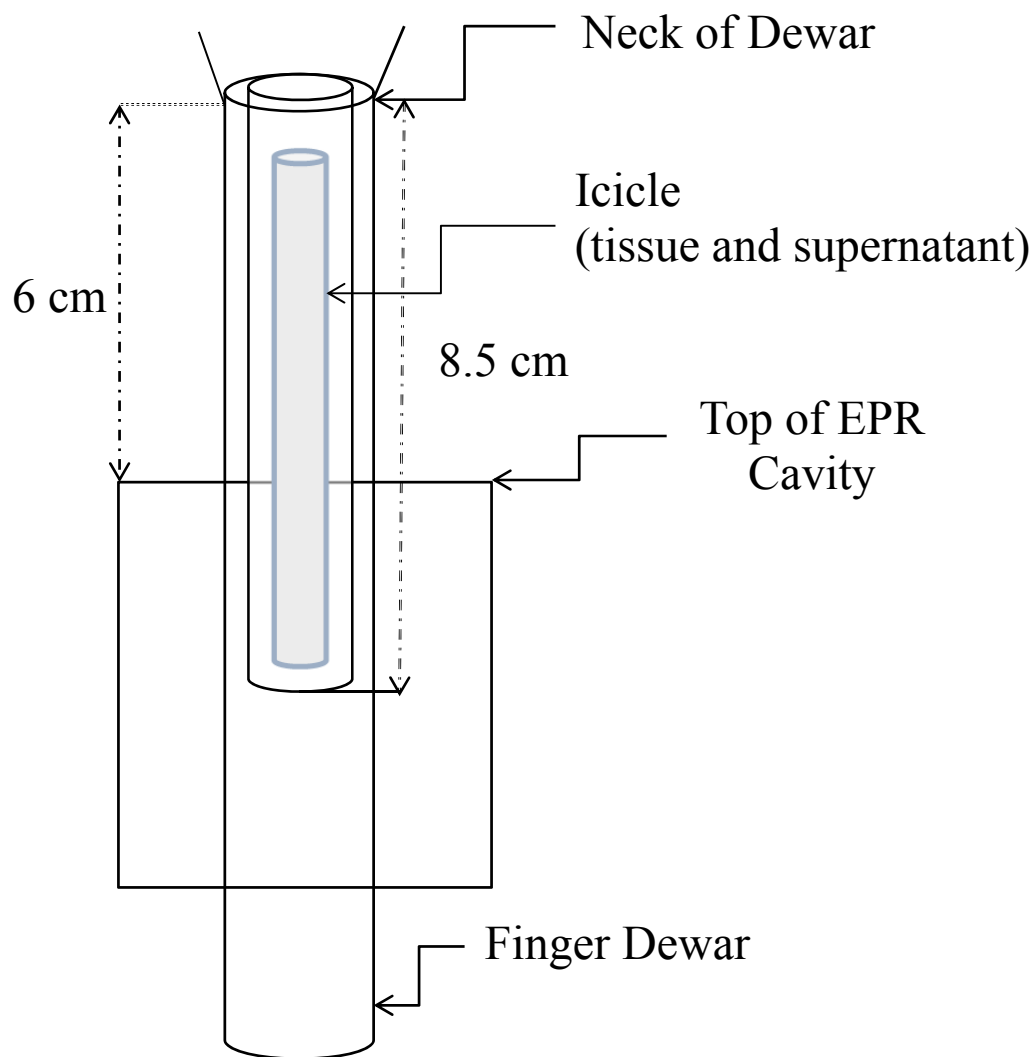
Figure 3.1: A diagram of the vertical dimensions of the icicle (tissue and supernatant) that is submerged in liquid nitrogen with respect to the neck of the dewar and the top of the EPR microwave cavity.
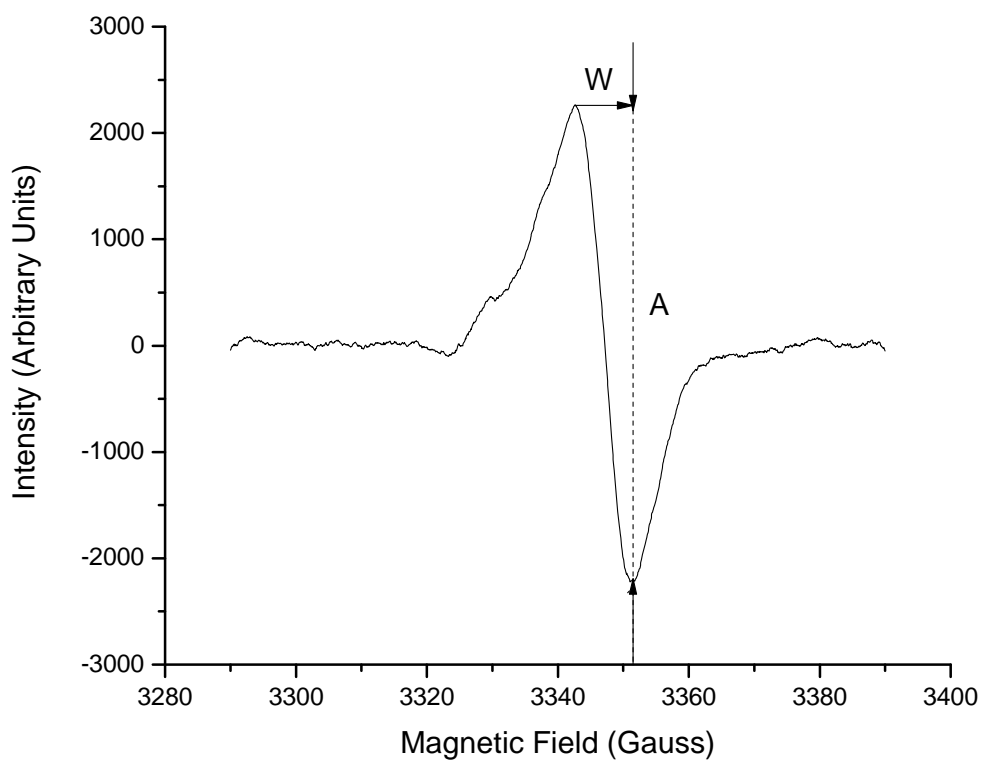
Figure 3.2:   A representative first-derivative spectrum of the PBN spin adduct at liquid
nitrogen temperature in pig arterial tissue. The concentration of ROS is determined from
the signal intensity (distance between the vertical arrows, A) and the line width (distance
along the horizontal arrow, W). Concentration $= 3W^2A$; this equation was derived from a
Lorenzian line function.
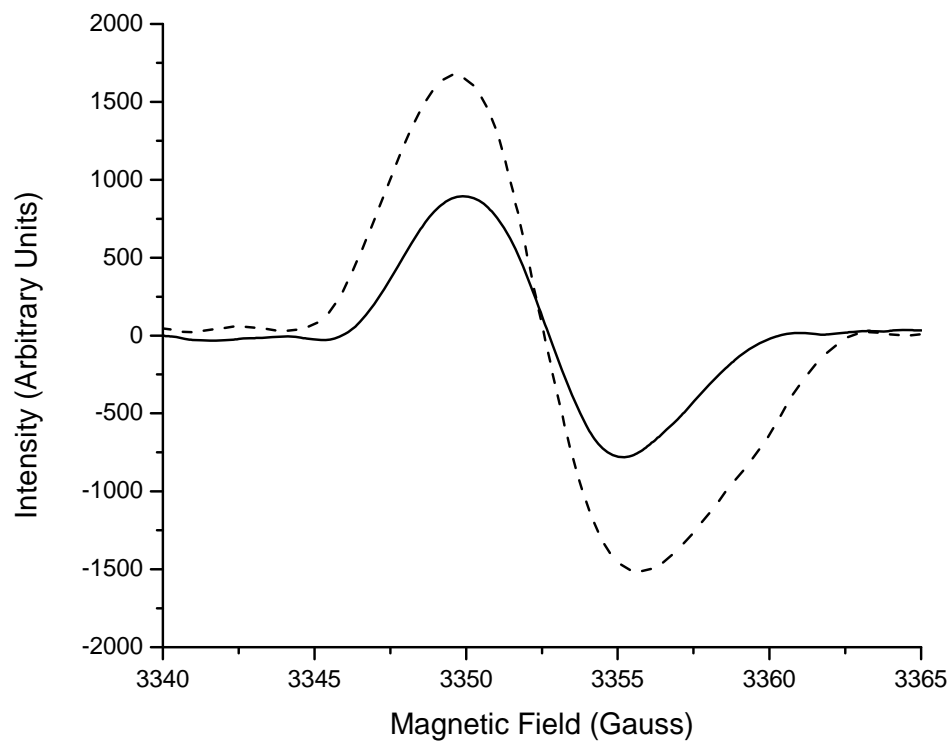
Figure 3.3: The graph compares two typical first-derivative spectra between Sliced Tissue (ST), dashed trace, and Whole Tissue (WT), solid trace.
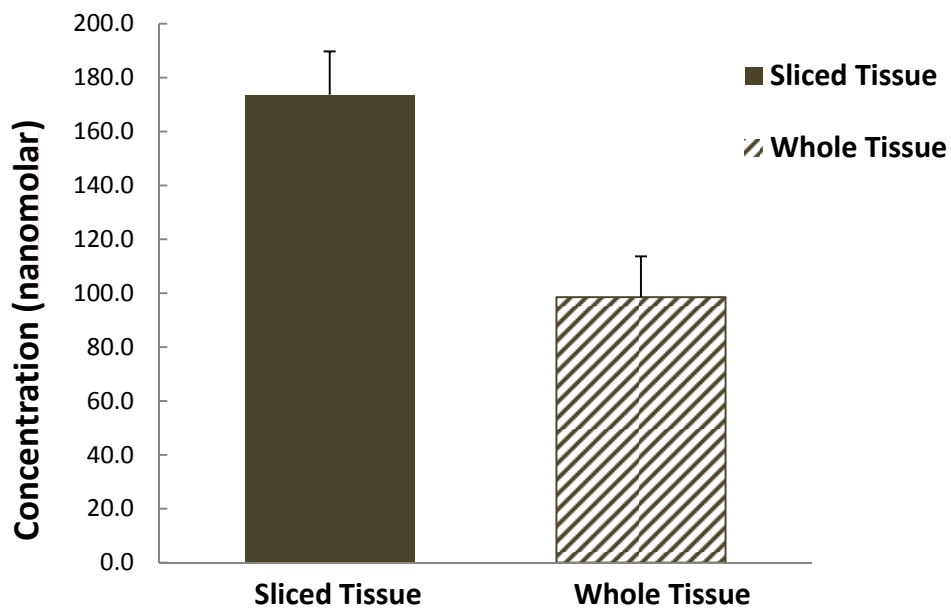
Figure 3.4:   Comparison between the Sliced Tissue (ST) group and the Whole Tissue (WT) group. ROS generation was significantly higher in the ST group with respect to the WT group (two-way ANOVA, $P < 0.05$). Values are means ± standard error.

CHAPTER 4: REACTIVE OXYGEN SPECIES CAUSE ENDOTHELIAL

DYSFUNCTION IN CHRONIC FLOW OVERLOAD

Flow overload (FO) is defined as an increase in blood flow rate in blood vessels over its normal physiological level. FO manifests during exercise, pregnancy or due to diseases of the circulatory system such as cardiac hypertrophy [1], arteriovenous fistula [2], or contralateral stenosis. Blood flow rate must be carefully regulated by the body since flow-induced shear stress on the endothelium induces structural homeostasis in the blood vessel wall. In response to FO in the endothelium, rigorous vasodilation of the blood vessel by nitric oxide (NO), prostacyclin (PGI_2), and endothelium-derived hyperpolarizing factor (EDHF) occurs [3-5]. An increase in reactive oxygen species (ROS) has been documented in FO in the three following cases: normal conduit arteries of rabbits [6], carotid arteries of mice [7] and coronary resistant arteries of humans [8].

There is an enlarging body of scientific evidence that ROS are involved in many physiological processes some of which are pathological in nature [9]. In particular, superoxide, a volatile ROS, has been recognized as a signaling molecule that elicits specific cellular responses in the vasculature. Reactions to superoxide signaling include activating matrix metalloproteinases (MMPs) [10], vascular remodeling, vascular smooth muscle cell (VSMC) hypertrophy, and cellular apoptosis. Superoxide production sometimes leads to the formation of hydrogen peroxide, which is believed to regulate

potassium ion channels [8]. In a study, superoxide was shown to dilate cerebral arterioles by opening calcium-activated potassium channels; hydrogen peroxide and peroxynitrite, a byproduct of endothelial NO synthase (eNOS) uncoupling, were also shown to reversibly dilate cerebral arterioles by activation of ATP-sensitive potassium channels [11]. Xanthine oxidase, NADPH oxidase, mitochondria and uncoupled eNOS are sources of superoxide in the endothelium [12-15].

In response to chemical and physical stimuli, NADPH oxidase has been recognized as a major source of ROS in blood vessels [14, 16-19]. It is well established in the literature that increases in ROS production in diseases such as hypertension, diabetes, hypercholesterolemia, and atherosclerosis lead to endothelial dysfunction [16, 20-23].

Little is known about the effect of chronic flow overload (CFO) on endothelial function of elastic (carotid) arteries of large animals, although CFO induced increase in ROS production has been established in various mammalian small arteries [7, 10, 24]. Therefore, we hypothesize that the ROS increase is deleterious to endothelial function in CFO, and that the source of ROS is primarily NADPH oxidase. To investigate our hypotheses, we take an intact porcine carotid artery that was exposed to CFO for 1 wk by contralateral ligation. ROS were detected with the spin trap N-*tert*-butyl-α-phenylnitrone (PBN) by electron paramagnetic resonance (EPR). The expressions of eNOS and NADPH oxidase were measured. Endothelial function was examined through endothelium-dependent relaxation in response to acetylcholine (ACh). Uncoupled eNOS in CFO was found with acute administration of eNOS cofactor tetrahydrobiopterin (BH$_4$). One additional group of swine was orally fed apocynin (4-hydroxy-3-methoxy-acetophenone) to ascertain the effect of NADPH oxidase in the vessel wall. The

experimental results support our hypotheses and show that CFO causes endothelial dysfunction in conduit vessels.

Materials and Methods

Twelve male Duroc swine weighing 34±4 kg (range 30–39 kg) were randomly divided into two groups. In group I, the right carotid artery was exposed to CFO for 1 wk by ligation of the contralateral carotid artery. In group II (CFO+A), the right carotid artery was exposed to CFO for 1 wk while animals were orally fed apocynin at the dose of 60 mg·kg^{-1}·day^{-1} from the postoperative first day to the termination. The left carotid artery served as a control for each group and was harvested at the time of ligation.

Animal Preparation

Surgical anesthesia was induced with ketamine (20 mg/kg im) and atropine (0.04 mg/kg im) and maintained with isofluorane (1–2%). Blood gas values were measured, and ventilation was adjusted to maintain normal values of PO_2 and PCO_2. In preliminary experiments, we measured the flow rates and external diameters to confirm that the left and right common carotid arteries are equivalent to ensure that one can serve as control for the other. Furthermore, the flow rates and external diameter of the right carotid artery were immediately measured after the left carotid artery was excised to quantify the immediate FO.

Subsequent to a left cervicotomy, the left common carotid artery was exposed gently to avoid vasomotion by dissection, and the *in vivo* external diameter was measured with the aid of a stereo microscope. The vessel was further dissected to place a flow probe (TS420 Transonic System). After data collection, the artery was ligated by suture and excised (length of 3 cm); the right carotid artery was not exposed to any surgical trauma. This measurement was taken on day 0 to avoid interference to the experimental vessel. The incision was closed, and the animal was recovered. The animals in group II were fed apocynin (60 mg·day^{-1}) orally. After 1 wk and following a right cervicotomy, the vessel segment was excised. The excised vessels from control and experimental groups were immediately stored at 4°C in HEPES physiological saline solution (HEPES-PSS, pH 7.4, with 142-mM NaCl, 4.7-mM KCl, 2.7-mM sodium HEPES, 3-mM HEPES acid, 1.17-mM MgSO4, 2.79-mM CaCl, 5.5-mM glucose) and divided into segments after dissection of adjacent tissue. HEPES and HEPES salt were purchased from Sigma, whereas other chemicals were purchased from Fisher Scientific.

The endothelium-dependent vasorelaxation was performed with an isovolumic myograph. The vessels were pre-contracted to an approximate transluminal pressure (170±20 mmHg) with acetylcholine at submaximal dose (10^{-8} mol/L to 10^{-6} mol/L), and thereafter the endothelium-dependent relaxation was induced with a series of doses of bradykinin (10^{-10} mol/L to 10^{-5} mol/L). The endothelium-independent vasorelaxation in response to sodium nitroprusside (10^{-10} mol/L to 10^{-5} mol/L) was measured to verify the responsiveness of vascular smooth muscle to nitric oxide.

All experiments were performed in accordance with national and local ethical guidelines, including the Institute of Laboratory Animal Research (ILAR) Guide, Public

Health Service policies, Animal Welfare Act, and an approved Indiana University School of Medicine IACUC protocol.

<div style="text-align:center">Vasoactivity</div>

An isovolumic myograph was employed to ascertain the vasoactivity of the artery [25]. Cannulating the carotid vessel on connectors that was fixed in a bath containing HEPES-PSS and adjusting the in situ length with a digital caliper (resolution of 0.1mm) while preloading it at physiological pressure of 80 mmHg, the vessel was submerged and incubated in a bath at 37˚C for forty minutes. Contraction or relaxation of the vessel was chemically induced with both ends closed. The diameter of the carotid artery remained approximately constant during the vasoactivity process. The pressure and external diameter were measured with a pressure transducer (Mikro-Tip SPR-524, Millar Instruments) and a dimensional tracer (DiamTrak 3 +, Australia; 10-μm resolution), respectively.

All arterial segments were precontracted (increase in pressure) to an approximate transluminal pressure (170 ± 20 mmHg) with phenylephrine (10^{-8} M to 10^{-6} M), and thereafter endothelium-dependent relaxation (decrease in pressure) was assessed with a series of doses of acetylcholine (Ach, 10^{-9} M to 10^{-6} M). The effect of eNOS uncoupling on endothelium-dependent relaxation was detected by incubation of the vessel segments in CFO with L-arginine (10^{-5} M) and eNOS cofactor BH_4 (10^{-5} M) for 40 min. The circumferential tension of the vessel at every dose was calculated by Laplace's law, tension = pressure × radius. The % decrease in tension was calculated by the equation:

%Tension = $(T_d - T_i)/(T_{max} - T_i) \times 100$. where, T_d, T_i, and T_{max} are the tension at every dose (T_d), physiological level (T_i), and maximum tension (T_{max}) at submaximal concentration of phenylephrine, respectively. Non-receptor-dependent contraction to potassium (KCl, 60 mM) was used to verify identical contractility of VSMC in CFO. Endothelium-independent vasorelaxation to sodium nitroprusside (SNP, 10^{-5} M) was measured to verify the sensitivity of VSMC in response to NO.

Electron Paramagnetic Resonance

Immediately after the vessel was divided, the vessel ring for electron paramagnetic resonance (EPR) was videotaped from the side (5 mm in length) and cross-views under stereo microscope. The volume of the segment was calculated based on the product of cross-sectional area and axial length. After measurement by EPR as described below, ROS generation was expressed as mole per unit of volume. ROS concentration in tissue samples was determined from the EPR spectra obtained by incubating the tissue samples with the spin-trapping agent N-tert-butyl-phenylnitrone (PBN; Sigma) at 190 mM in HEPES-PSS for 30 min at 37°C in the dark. A ring incubated with 4-Hydroxy-TEMPO (a superoxide dismutase mimic) served as the control for ROS measurement. The tissue was subsequently inserted into a syringe along with the supernatant, immediately frozen in liquid nitrogen, and stored at -80°C until EPR analysis was performed. To avoid ROS produced during freezing and thawing of samples, the sample was quickly removed while in its frozen state from the syringe and placed in a Dewar containing liquid nitrogen. The Dewar was then inserted into the microwave cavity of

the EPR spectrometer. The sample remained at liquid nitrogen temperature throughout the EPR analysis (1, 21). The EPR equipment and settings were as follows. A Bruker ESP X-band spectrometer equipped with a TE_{102} cavity was utilized to detect signals. Parameters for the spectra were 9.4-GHz microwave frequency, 25.2-mW microwave power, 4.0-G modulation amplitude, 1×10^5 receiver gain, 5.24-s time constant, 3,330-G center magnetic field, and 100-G magnetic field sweep width. All experiments were completed at liquid nitrogen temperature. Four EPR scans were taken per tissue sample and analyzed with Bruker WINEPR software (version 2.11) based on the spectral intensity and line width. ROS concentrations were determined with 2,2,6,6-tetramethylpiperidine 1-oxyl, TEMPO, solution (0.1 M, Sigma) used as a concentration standard. All EPR parameters and conditions were applied to both standard and experimental samples.

Protein Expression

The segment for Western blotting was homogenized in a lysis buffer and then incubated on ice for 1 h. The sample was centrifuged at 1,000 g for 15 min at 1°C, and the supernatant was drawn off. The total value of protein was measured by a BCA kit (Bio-Rad). Equal amounts of protein (25 μg) were loaded, electrophoresed in 10% SDS-PAGE gel, and transferred onto a ployvinylidene difluoride membrane. After blocking the sample for 2 h in 8% dried milk in TBS-Tween buffer, the membrane was incubated overnight at 4°C with specific primary antibody with either anti-eNOS (1:1,000 dilution in blocking buffer, BD transduction laboratory), anti-p22phox (1:1,000, Santa Cruz

Biotech), anti-p47phox (1:500, Santa Cruz Biotech), anti-NOX2 (1:250, Santa Cruz Biotech), or anti-NOX4 (1:250, Santa Cruz Biotech). The membrane was then rinsed and incubated with horseradish peroxidase-conjugated secondary antibody (Santa Cruz Biotech) for 2 h (eNOS: goat anti-mouse 1:3,000 dilution in blocking buffer; p22phox and p47phox: goat anti-rabbit 1:5,000, NOX2 and NOX4: bovine anti-goat 1:5,000). The specific protein was detected by enhanced chemiluminescence (ECL; Amersham) and evaluated by densitometry (Sigma Scan). All samples from each group were simultaneously probed with anti--actin, a mouse monoclonal antibody (primary antibody 1:1,000 dilution in blocking buffer, Santa Cruz Biotech), to correct for sample loading.

Statistical Analysis

All data given in the text and figures are expressed as means SD. Student's t-test (two-tailed distribution, two-sample unequal variance) and Duncan's test following ANOVA were used to detect differences between groups. For all analyses, $P < 0.05$ was used to indicate statistical significance.

Results

There was a significant increase in blood flow in carotid arteries in CFO and CFO+A after contralateral ligation (189.2 ± 25.3, 369.6 ± 61.9, and 382.3 ± 62.5 ml/min in the control, CFO, and CFO+A groups, respectively; $P < 0.001$). The flow rate in the apocynin treatment group was not significantly different than the untreated group. Figure

1 represents a typical tracing of a control and a carotid artery exposed to CFO. The mean and peak of the blood flow doubled in CFO (Figure 4.1A). After normalization of pulsatile blood flow with mean flow rate, the two curves with respect to their mean values largely overlapped (Figure 4.1B), which suggests that the oscillatory components of pulsatile blood flow were not significantly changed in the CFO model.

The outer diameter of the vessel significantly increased by 8.6% (4.60 ± 0.41 to 4.98 ± 0.46 mm) after 1 wk of exposure to CFO (P < 0.05) and did not change significantly after treatment with apocynin (4.98 ± 0.46 to 5.06 ± 0.48 mm). We did not observe a significant change of arterial wall thickness in the CFO or the CFO+A group compared with the control group (data not shown). The systemic blood pressure measured at the femoral artery did not change after either surgical ligation of the carotid artery or after treatment with apocynin compared with the pressure before ligation (88 ± 12 vs. 86 ± 11 mmHg). The wall shear stress (WSS; WSS ~ QD^{-3}, where Q and D represent flow rate and inner diameter, respectively) was found to remain elevated by ~ 50% after 1 wk of the CFO and CFO+A groups.

Endothelial Function

Endothelial function was assessed by monitoring the decrease in tension brought on by the addition of acetylcholine (ACh) (Figure 4.2); i.e. by measuring the effectiveness of the endothelial relaxation. The dose curves suggested that endothelial function was compromised in the CFO group (P < 0.05) but was retained with the treatment of apocynin. This result implied that endothelial dysfunction in CFO was

related to ROS upregulation. Furthermore, we found that the endothelial dysfunction of the vessels in CFO was completely reserved after acute incubation with BH4 and L-arginine, which suggests that eNOS uncoupling may play a role in CFO. The endothelium-independent vasorelaxation in response to SNP did not show differences in groups, which implied that the VSMC did not develop resistance to nitric oxide (103.5 ± 15.5, 102.6 ± 17.2, and 103.6 ± 21.1% for control, CFO, and CFO + A, respectively). The potassium-induced contraction, which is not receptor-dependent, did not reveal differences of VSMC contractility (tension) in the three groups (49.6 ± 6.98, 51.3 ± 7.66, and 51.1 ± 7.96 mN/mm for control, CFO, and CFO + A, respectively).

ROS Generation

The EPR measurements are presented in Figures 4.3 and 4.4. ROS generation significantly increased in the CFO group. Apocynin treatment restored ROS generation to the control value. Since PBN is lipophilic and forms stable lipid-derived, spin adducts (radical bound to spin trap), it provides reliable overall indication of ROS concentration measurements in biological tissue under physiological conditions without lipid radical adduct extraction that may involve artifacts such as failure to retrieve all of the adducts from the biological sample and additional ROS generation during centrifugation. Since PBN is indeed able to trap NO in vascular tissue, we verified that NO was not significantly produced in our experimental preparation with DAF-2DA (NO probe) and L-NAME (an eNOS inhibitor).

Expression of eNOS and NADPH Oxidase

The expression of eNOS was significantly upregulated in the CFO group and unaffected by apocynin treatment (Figure 4.5). The subunits p22phox and p47phox are well known to be expressed ubiquitously in endothelial and VSMC. The protein expression of cytosolic assembling subunits of NADPH oxidase (p22phox and p47phox) were significantly elevated in carotid segments exposed to CFO but not in CFO+A (Figure 4.5). NOX2 and NOX4 (NADPH oxidase 2 and 4) were found to be upregulated in CFO and CFO+A.

Discussion

The major findings are that chronic shear stress elevation of ~50% increases ROS production mediated by NADPH oxidase and induces endothelial dysfunction in swine carotid artery. Recent observations suggest that NADPH oxidase is directly involved in superoxide production in mouse carotid arteries where the flow was increased by a factor of three to five by construction of an arteriovenous fistula. The present study demonstrates a similar finding in conduit artery of the porcine model in response to a more modest increase in WSS. Moreover, we show for the first time endothelial dysfunction as a consequence of increased oxidative stress in conduit artery where eNOS uncoupling may play a role during CFO.

The porcine carotid artery was exposed to approximately twice the physiological flow rate for 1 wk in this study. Although the change of flow rate was relatively small

compared with a typical arteriovenous fistula (over fivefold increase in flow rate), the objective was to study a model with minimal disturbance since surgery elicits inflammatory response and consequent oxidative stress. The diameter enlargement of the artery was accordingly small (8.6%). Such a change in flow and diameter in a conduit artery may occur under physiological conditions, such as in exercise. Interestingly, ROS generation increased by onefold in response to the relatively small changes in flow or WSS (56% increase). Although mechanical stimulations, including oscillatory WSS and cyclic stretch, have been shown to increase ROS production in the vasculature; this is the first report of increased ROS generation in response to CFO in a conduit vessel of a large animal.

The diameter increase during CFO is attributed to a physiological response to restore the homeostatic shear stress on the endothelium. It is well known that acute vasodilatation is stimulated by WSS elevation. Following acute vasodilatation, chronic remodeling occurs and further increases the diameter. Interestingly, the complete restoration of WSS requires a relatively long period in an arteriovenous fistula; e.g., over 4 wk in carotid arteries of rabbits [10], over 3 wk in the carotid arteries of mice [7], and 6 mo in the carotid arteries of dogs [26]. In the present study, the WSS was not restored and remained elevated after 1 wk. In fact, a conduit artery possesses the capacity to acutely increase its diameter up to 15% in response to a 10- to 20-fold increase in flow [1]. Even in the 1-wk study, the diameter may enlarge by 15–20% in response to a three- to fivefold increase in flow rate. Hence, acute diameter enlargement in response to CFO depends on the magnitude of WSS and the subsequent remodeling duration since the restoration of WSS may be very long. Since vasodilatation increases vascular stretch,

which can activate NADPH oxidase in blood vessel wall [27], the stretch may play a role in CFO. The elevated stretch results from diameter increase (flow-induced vasodilatation) and vascular wall softening due to NO-induced vascular tone reduction. Both effects increase the magnitude of stretch at pulsatile blood pressure.

The expansive remodeling of the blood vessel wall in response to an increase in flow rate has been previously viewed as a physiological adaptation to restore the WSS [1, 23]. Here, we show that the remodeling response leads to compromised endothelial function (over a 1-wk period). The endothelium-dependent vasodilation in the present study (Figure 4.2) is significantly decreased in response to a modest flow increase in a relatively short period. In resistance arteries, Pourageaud et al. observed that CFO increased the endothelium-dependent vasodilation to ACh, and flow-induced vasodilation was slightly but not statistically attenuated. In diabetic rats, CFO results in significant endothelial dysfunction in mesenteric arteries. The mechanism involved in the different endothelial responses in large conduit arteries and small resistance arteries to CFO is unclear. It may be that resistance arteries are exposed to more significant variations of blood flow under physiological conditions due to lateral-contralateral adjustment of microcirculation and adapt to larger variation of blood flow compared with large conduit arteries.

NADPH oxidase (NOX) has been recognized as a major source of superoxide in the vasculature in response to mechanical stimulation [14, 18]. It is known that p22phox is an important trans-membrane protein that combines with NOX to assemble NADPH oxidase complex and is known to be upregulated by WSS [28]. The p47phox, as cytosolic subunit of NADPH oxidase, may also affect the activity of NOX. NOX4 is a

p22phox-dependent enzyme [29] and does not require cytosolic proteins (p47phox, p67phox) for its activity [30, 31].

Apocynin is an inhibitor of NADPH oxidase under *in vivo* condition where H_2O_2 and myeloperoxidase are present and is suggested to inhibit the translocation of cytoplasmic subunits. It is also possible that treatment by apocynin in this study shifted the balance of oxidative stress in vascular tissue through nonspecific antioxidant effects. Since the expression of NOX isoforms may be located in endothelial and VSMC, we cannot separate the effect of WSS on endothelium and circumferential stretch acting throughout the vessel wall on NOX isoforms. The elucidation of the role of NOX in endothelial and VSMC during CFO requires further study.

A fundamental question involves the mechanism by which elevated WSS sensed by the endothelium transmits its effect on more remote regions of the wall. A possible mechanism may be similar to hypertension via the NADPH oxidase pathway. The common factor in CFO and hypertension is the increase in circumferential stretch and stress. Hypertension increases circumferential stress and strain by an increase in blood pressure, whereas flow-induced vasodilation increases vessel stretch similarly through an increase in diameter. The circumferential stress or strain, mediated by mechanotransduction in CFO, may activate NADPH oxidase and elicit ROS generation.

In summary, ROS production increases in porcine carotid arteries in response to a onefold increase in the blood flow rate, which leads to endothelial dysfunction. NOX2 and NOX4 oxidase and p22phox and p47phox are upregulated in CFO, and NADPH oxidase is likely involved in the increase in oxidative stress. The chronic use of apocynin prevents the elevation of ROS levels, even though NOX2 and NOX4 are upregulated, and

preserves endothelial function. The mechanisms by which apocynin prevents the upregulation of p22phox and p47phox but not NOX2 and 4 remain unclear. Although the process of CFO-induced remodeling to restore WSS has previously been thought of as a physiological response, the present data suggest that CFO mediated by ROS causes endothelial dysfunction, which may result from eNOS uncoupling in the first week of outward vascular remodeling.

Acknowledgements

References

[1]   Di Stefano, I.; Koopmans, D. R.; Langille, B. L. Modulation of arterial growth of the rabbit carotid artery associated with experimental elevation of blood flow. *J Vasc Res* **35:**1-7; 1998.

[2]   Miyagishima, T.; Hara, T.; Inoue, M.; Terano, N.; Ohno, H.; Okamoto, K.; Hasuo, K. Pontine venous congestion due to dural arteriovenous fistula of the cavernous sinus: Case report and review of the literature. *Surg Neurol Int* **3**; 2012.

[3]   Brandes, R. P.; Schmitz-Winnenthal, F. H.; Feletou, M.; Godecke, A.; Huang Vanhoutte, P. M. P. L.; Fleming, I.; Busse, R. An endothelium-derived hyperpolarizing factor distinct from NO and prostacyclin is a major endothelium-dependent vasodilator in resistance vessels of wildtype and endothelial NO synthase knockout mice. *Proc Natl Acad Sci USA* **97:**9747-9752; 2000.

[4]   Garland, C. J.; Plane, F.; Kemp, B. K.; Cocks, T. M. Endothelium-dependent hyperpolarization: a role in the control of vascular tone. *Trends Pharmacol Sci* **16:**23-30; 1995.

[5]   Scotland, R. S.; Madhani, M.; Chauhan, S.; Moncada, S.; Andresen, J.; Nilsson, H.; Hobbs, A. J.; Ahluwalia, A. Investigation of vascular responses in endothelial nitric oxide synthase/cyclooxygenase-1 double-knockout mice: key role for endothelium-derived hyperpolarizing factor in the regulation of blood pressure *in vivo*. *Circulation* **111:**796-803; 2005.

[6]   Pagano, P. J.; Ito, Y.; Tornheim, K.; Gallop, P. M.; Tauber, A. I.; Cohen, R. A. An NADPH oxidase superoxide-generating system in the rabbit aorta. *Am J Physiol* **268:**H2274-2280; 1995.

[7]   Castier, Y.; Brandes, R. P.; Leseche, G.; Tedgui, A.; Lehoux, S. p47phox-dependent NADPH oxidase regulates flow-induced vascular remodeling. *Circ Res* **97:**533-540; 2005.

[8]   Liu, Y.; Zhao, H.; Li, H.; Kalyanaraman, B.; Nicolosi, A. C.; Gutterman, D. D. Mitochondrial sources of H_2O_2 generation play a key role in flow-mediated dilation in human coronary resistance arteries. *Circ Res* **93:**573-580; 2003.

[9]   Taniyama, Y.; Griendling, K. K. Reactive oxygen species in the vasculature: molecular and cellular mechanisms. *Hypertension* **42:**1075-1081; 2003.

[10]   Tronc, F.; Mallat, Z.; Lehoux, S.; Wassef, M.; Esposito, B.; Tedgui, A. Role of matrix metalloproteinases in blood flow-induced arterial enlargement: interaction with NO. *Arterioscler Thromb Vasc Biol* **20:**E120-126; 2000.

[11]   Wei, E. P.; Kontos, H. A.; Beckman, J. S. Mechanisms of cerebral vasodilation by superoxide, hydrogen peroxide, and peroxynitrite. *American Journal of Physiology - Heart and Circulatory Physiology* **271:**H1262-H1266; 1996.

[12]   Guzik, T. J.; Mussa, S.; Gastaldi, D.; Sadowski, J.; Ratnatunga, C.; Pillai, R.; Channon, K. M. Mechanisms of increased vascular superoxide production in human diabetes mellitus: role of NAD(P)H oxidase and endothelial nitric oxide synthase. *Circulation* **105:**1656-1662; 2002.

[13]   Griendling, K. K.; Sorescu, D.; Ushio-Fukai, M. NAD(P)H oxidase: role in cardiovascular biology and disease. *Circ Res* **86:**494-501; 2000.

[14]   McNally, J. S.; Davis, M. E.; Giddens, D. P.; Saha, A.; Hwang, J.; Dikalov, S.; Jo, H.; Harrison, D. G. Role of xanthine oxidoreductase and NAD(P)H oxidase in endothelial superoxide production in response to oscillatory shear stress. *Am J Physiol Heart Circ Physiol* **285:**H2290-2297; 2003.

[15]   Sonta, T.; Inoguchi, T.; Tsubouchi, H.; Sekiguchi, N.; Kobayashi, K.; Matsumoto, S.; Utsumi, H.; Nawata, H. Evidence for contribution of vascular NAD(P)H oxidase to increased oxidative stress in animal models of diabetes and obesity. *Free radical biology & medicine* **37:**115-123; 2004.

[16]   Cai, H.; Harrison, D. G. Endothelial dysfunction in cardiovascular diseases: the role of oxidant stress. *Circ Res* **87:**840-844; 2000.

[17]   De Keulenaer, G. W.; Chappell, D. C.; Ishizaka, N.; Nerem, R. M.; Alexander, R. W.; Griendling, K. K. Oscillatory and steady laminar shear stress differentially affect human endothelial redox state: role of a superoxide-producing NADH oxidase. *Circ Res* **82:**1094-1101; 1998.

[18]   Hwang, J.; Saha, A.; Boo, Y. C.; Sorescu, G. P.; McNally, J. S.; Holland, S. M.; Dikalov, S.; Giddens, D. P.; Griendling, K. K.; Harrison, D. G.; Jo, H. Oscillatory shear stress stimulates endothelial production of O2- from p47phox-dependent NAD(P)H oxidases, leading to monocyte adhesion. *J Biol Chem* **278:**47291-47298; 2003.

[19]   Fukui, T.; Ishizaka, N.; Rajagopalan, S.; Laursen, J. B.; Capers, Q. t.; Taylor, W. R.; Harrison, D. G.; de Leon, H.; Wilcox, J. N.; Griendling, K. K. p22phox mRNA expression and NADPH oxidase activity are increased in aortas from hypertensive rats. *Circ Res* **80:**45-51; 1997.

[20]   Drexler, H. Endothelial dysfunction: clinical implications. *Prog Cardiovasc Dis* **39:**287-324; 1997.

[21]   Ohara, Y.; Peterson, T. E.; Harrison, D. G. Hypercholesterolemia increases endothelial superoxide anion production. *J Clin Invest* **91:**2546-2551; 1993.

[22]   Touyz, R. M.; Schiffrin, E. L. Reactive oxygen species in vascular biology: implications in hypertension. *Histochem Cell Biol* **122:**339-352; 2004.

[23]   Zarins, C. K.; Zatina, M. A.; Giddens, D. P.; Ku, D. N.; Glagov, S. Shear stress regulation of artery lumen diameter in experimental atherogenesis. *J Vasc Surg* **5:**413-420; 1987.

[24]   Laurindo, F. R.; Pedro Mde, A.; Barbeiro, H. V.; Pileggi, F.; Carvalho, M. H.; Augusto, O.; da Luz, P. L. Vascular free radical release. *Ex vivo* and *in vivo* evidence for a flow-dependent endothelial mechanism. *Circ Res* **74:**700-709; 1994.

[25]   Lu, X.; Kassab, G. S. Vasoactivity of blood vessels using a novel isovolumic myograph. *Ann Biomed Eng* **35:**356-366; 2007.

[26]   Kamiya, A.; Togawa, T. Adaptive regulation of wall shear stress to flow change in the canine carotid artery. *Am J Physiol* **239:**H14-21; 1980.

[27]   Oeckler, R. A.; Kaminski, P. M.; Wolin, M. S. Stretch enhances contraction of bovine coronary arteries via an NAD(P)H oxidase-mediated activation of the extracellular signal-regulated kinase mitogen-activated protein kinase cascade. *Circ Res* **92:**23-31; 2003.

[28]   Silacci, P.; Desgeorges, A.; Mazzolai, L.; Chambaz, C.; Hayoz, D. Flow pulsatility is a critical determinant of oxidative stress in endothelial cells. *Hypertension* **38:**1162-1166; 2001.

[29]   Bedard, K.; Krause, K. H. The NOX family of ROS-generating NADPH oxidases: physiology and pathophysiology. *Physiol Rev* **87:**245-313; 2007.

[30]   Geiszt, M.; Kopp, J. B.; Varnai, P.; Leto, T. L. Identification of renox, an NAD(P)H oxidase in kidney. *Proc Natl Acad Sci U S A* **97:**8010-8014; 2000.

[31]   Martyn, K. D.; Frederick, L. M.; von Loehneysen, K.; Dinauer, M. C.; Knaus, U. G. Functional analysis of Nox4 reveals unique characteristics compared to other NADPH oxidases. *Cell Signal* **18:**69-82; 2006.

Figures
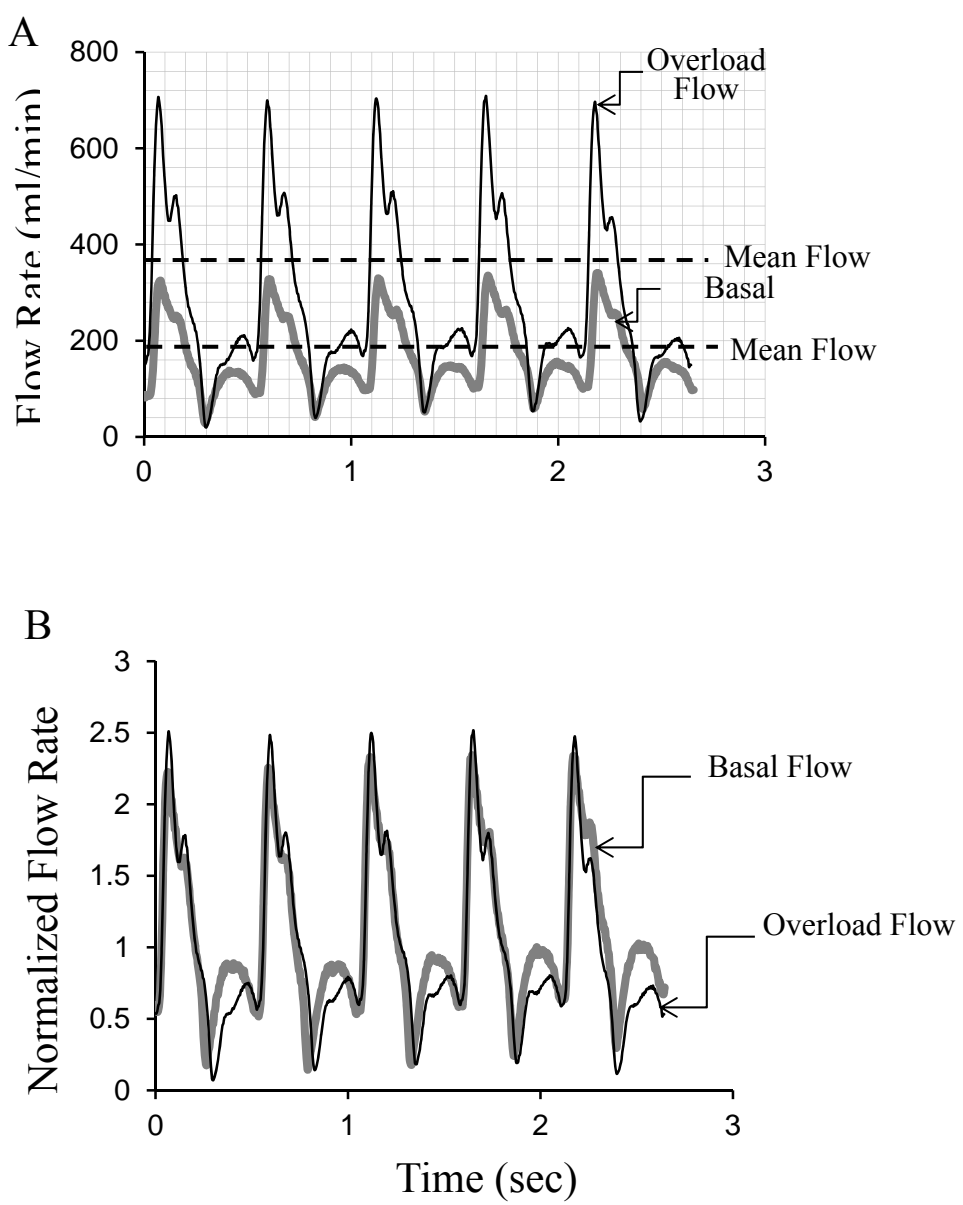
Figure 4.1: Representative waveform of blood flow in the carotid artery at rest (basal) and flow overload (CFO). (A) real time recordings. (B) tracing normalized by the mean flow rate. The normalized chronic flow overload trace approximately overlays the normalized baseline trace.
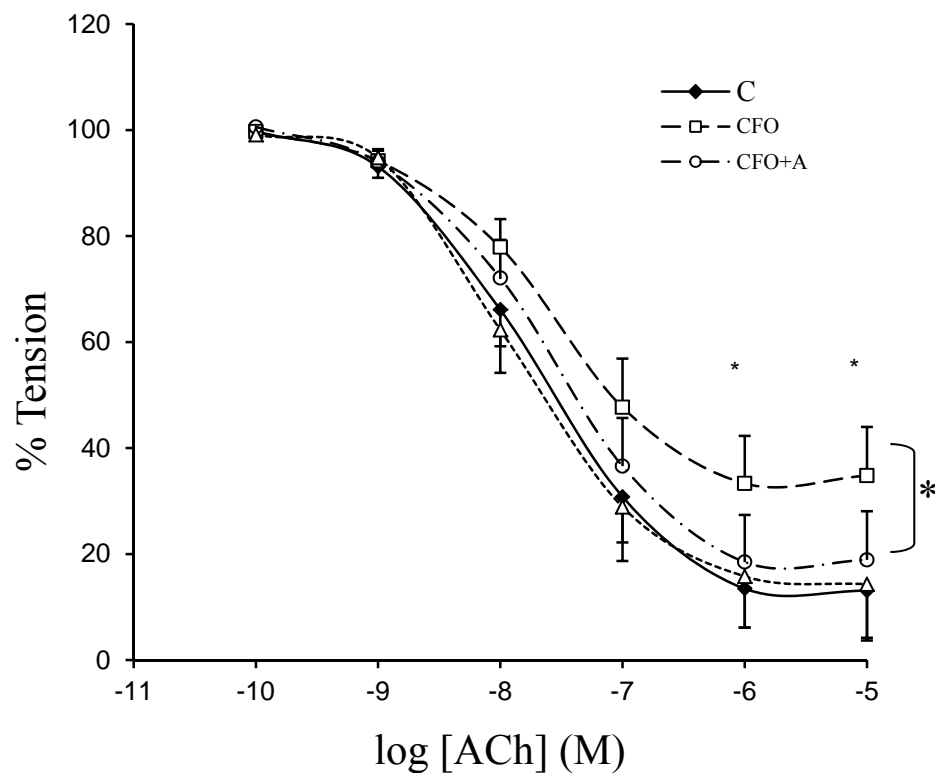
Figure 4.2: Endothelium-dependent vasorelaxation of carotid arteries. Initially the arteries were contracted to the same approximate tension with phenylephrine (PE) and dose-responsive vasorelaxation was induced by acetylcholine (ACh). C, control group; CFO, chronic flow overload group; CFO + A, chronic flow overload with administration of apocynin; CFO + BH_4, acute incubation with tetrahydrobiopterin (BH_4) in carotid arterial segment in CFO. *Significant difference between groups ($P < 0.05$; ANOVA followed by Duncan's test for multiple groups).
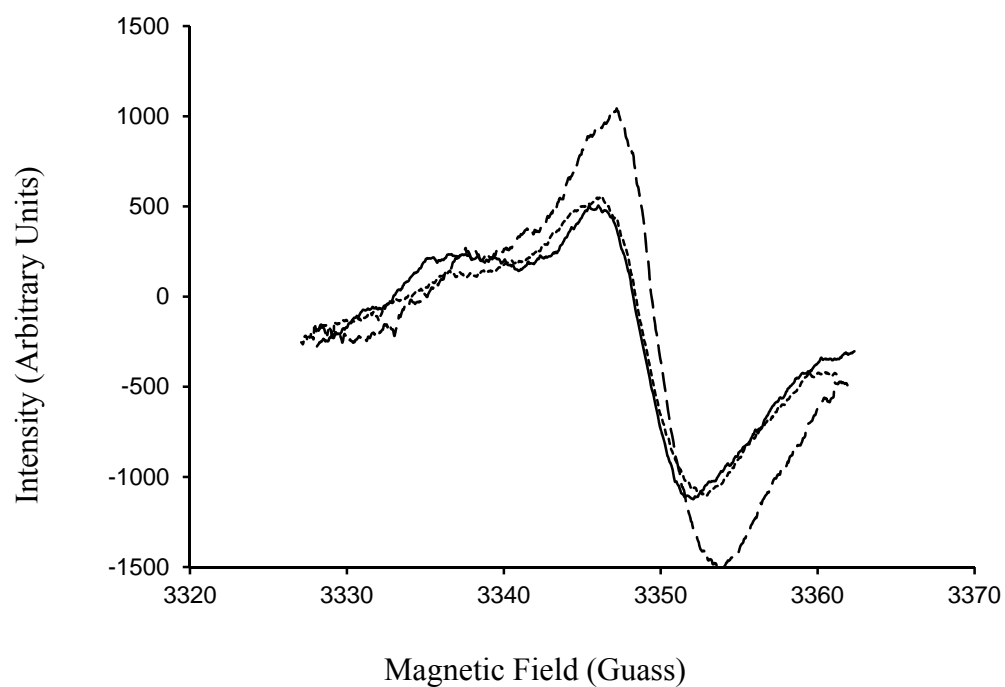
Figure 4.3: The three, first derivative spectra of the PBN spin adduct are as follows: the dashed trace is the CFO case, the solid trace is C (control) case and the dotted trace is CFO + A (chronic flow overload with administration of apocynin).
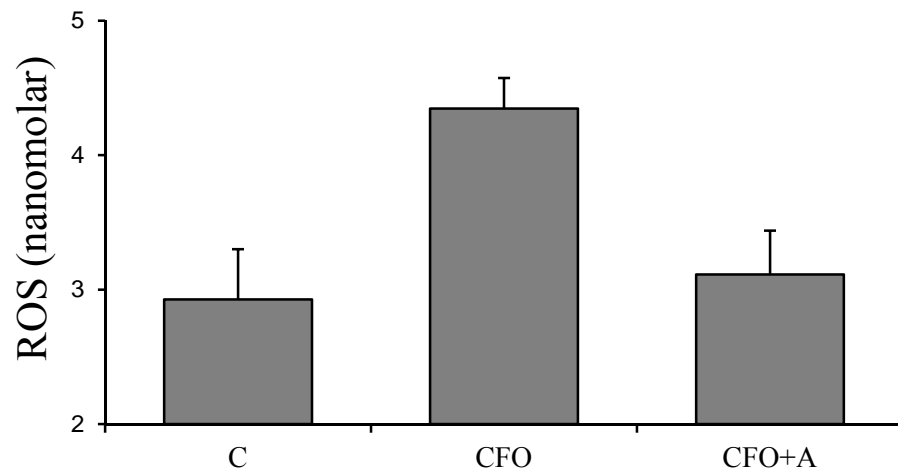
Figure 4.4: Concentration of ROS in n = 12 pigs due by EPR. The CFO case has the largest concentration of ROS, (4.35 nmolar). C and CFO + A groups are both low with the control group having the lowest concentration of ROS (2.9 nmolar).
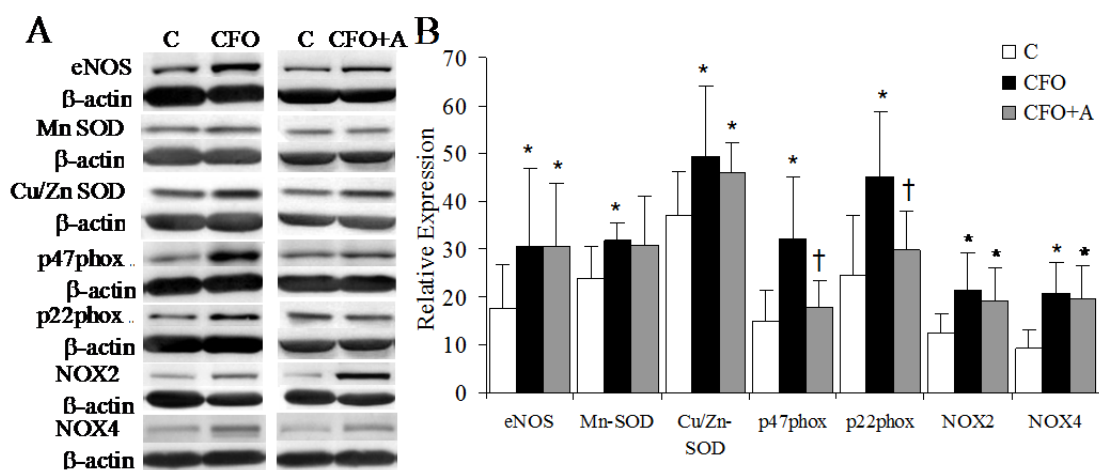
Figure 4.5: The proteins expression evaluated with Western blot. (A) Western Blotting bands. The molecular weight was confirmed as eNOS: 120 kD, p22phox: 22 kD, p47phox: 47 kD, NOX2: 91 kD, and NOX4: 55 kD. (B) Ratios of total pixels of the bands were measured by use of imaging software. C: Control group. CFO: Chronic flow-overload group. CFO+A: Chronic flow-overload group treated with apocynin. * P<0.05 in comparison between control and CFO or CFO+A. † P<0.05 in comparison between CFO and CFO+A.

CHAPTER 5: ELEVATED OXIDATIVE STRESS AND ENDOTHELIAL

DYSFUNCTION IN RIGHT CORONARY ARTERY OF RIGHT VENTRICULAR

HYPERTROPHY

Right ventricular hypertrophy (RVH) results in significant remodeling of right coronary artery (RCA) [1-7]. The morphometric data of RCA main trunk, arterioles, and capillaries in RVH suggest outward remodeling in main trunk and increase in numbers of resistance and capillary vessels [1]. A hemodynamic analysis showed RCA compensatory adaption during RVH to restore the perfusion at the arteriolar and capillary levels and increase blood flow in the main trunk [2], in proportion to increase in right ventricle (RV) mass [1]. The effect of RVH on RCA endothelial function, however, remains unclear.

Endothelial function plays an important role in vascular pathophysiology and is a biomarker/mediator of cardiovascular risk factors [1, 3-6]. Endothelial dysfunction has also been shown to be a predictor of adverse outcomes in patients with coronary artery disease [1, 7]. NO is well known as endothelium-dependent vasodilator and is believed to play an atheroprotective role. ROS are free radicals found in all vascular cells that are involved in remodeling in both physiological and pathological conditions [3, 4, 8-11]. ROS can inactivate NO and decrease NO bioavailability in blood vessels that may compromise endothelium-dependent vasorelaxation [3, 12-14]. Recent studies suggest

that an imbalance between superoxide and NO levels, rather than the individual levels, may have harmful consequences on the endothelium [3, 6, 12].   Numerous observations suggest that ROS are involved in vascular remodeling in response to mechanical stimulations, including stretch [6, 12, 15].   The RCA in RVH experiences outward remodeling (increase in diameter) and axial elongation [1]. It is unknown whether ROS, endothelial function, and vascular tone change during RCA remodeling in RVH. Our hypothesis is that elevated ROS, endothelial dysfunction, and increased tone accompany RCA remodeling in RVH.   Uncoupled endothelial NO synthase (eNOS) due to insufficient tetrahydrobiopterin (BH_4) may also contribute to endothelial dysfunction. We used digital subtraction angiography (DSA) to quantify RCA remodeling longitudinally based on quantitative angiographic images in swine.   The *ex vivo* endothelium-dependent vasorelaxation in response to vasodilator was measured to evaluate endothelial function. ROS production was confirmed by electron paramagnetic resonance (EPR) spectroscopy. The expression of NADPH oxidase was also measured to underscore the role of ROS production in a circumferentially stretched RCA at constant wall shear stress (WSS).

Materials and Methods

The experiments were conducted on seven 3-to 4-mo-old Yorkshire pigs, and five age and weight matched animals served as a sham group. A thoracotomy was performed along the fourth intercostal space. The chest cavity was exposed to provide access to the pulmonary artery (PA), as well as the RCA. A glycerin-filled silicone occlude was fitted

around the PA, and the filling tube was exteriorized to allow for cuff occlusion at a later time. A transonic flow probe (TD420, Transonic) was acutely placed on the proximal RCA, and flow rate was recorded. Once the probe was removed at the conclusion of coronary flow measurements, the chest was closed, and the animal was allowed to recover for 1 wk.

The degree of RVH, and the related increase in coronary blood flow, was imposed by the pressure gradient across the PA. A 7-Fr Swan-Ganz catheter was inserted through the jugular sheath and guided into the RV. The PA was banded upon inflation of the silicone occluder. The banding was set, and the occluder was locked when the desired systolic RV pressure was reached. The pressure increase ranged from 35% to 50% of baseline. The pressure gradient across the PA was monitored throughout the duration of the study. The sham group was treated identically, except the occluder was not inflated.

The RCA was imaged before and immediately after banding and again on scheduled days for the duration of the study. A period of 4 wk after onset of occlusion was deemed sufficient to observe most of the remodeling in RVH [1, 16-19]. At the end of 4 wk, the animal was anesthetized, and the heart was exposed similar to prior surgery. The transonic flow probe was placed in the same previous RCA region to record coronary flow rate, and the animal was euthanized. The heart was excised and immediately stored in 4°C HEPES physiological saline solution (HEPES-PSS, noted above). The RCA was carefully excised.

All experiments were performed in accordance with national and local ethical guidelines, including the Institute of Laboratory Animal Research (ILAR) Guide, Public

Health Service policies, Animal Welfare Act, and an approved Indiana University School of Medicine IACUC protocol.

A thoracotomy was performed along the fourth intercostal space. The chest cavity was exposed to provide access to the pulmonary artery (PA), as well as the RCA. A glycerin-filled silicone occlude was fitted around the PA, and the filling tube was exteriorized to allow for cuff occlusion at a later time. A transonic flow probe (TD420, Transonic) was placed on the proximal RCA, and flow rate was recorded. Once the probe was removed at the conclusion of coronary flow measurements, the chest was closed, and the animal was allowed to recover for 1 wk. The degree of RVH, and the related increase in coronary blood flow, was imposed by the pressure gradient across the PA. A 7-Fr Swan-Ganz catheter was inserted through the jugular sheath and guided into the RV. The PA was banded upon inflation of the silicone occluder. The banding was set, and the occluder was locked when the desired systolic RV pressure was reached. The pressure increase ranged from 35% to 50% of baseline. The pressure gradient across the PA was monitored throughout the duration of the study. The sham group was treated identically, except the occluder was not inflated.

The RCA was imaged before and immediately after banding and again on scheduled days for the duration of the study. A period of 4 wk after onset of occlusion was deemed sufficient to observe most of the remodeling in RVH. At the end of 4 wk, the animal was anesthetized, and the heart was exposed similar to prior surgery. The transonic flow probe was placed in the same previous RCA region to record coronary flow rate, and the animal was euthanized. The heart was excised and immediately stored in 4°C HEPES physiological saline solution (HEPES-PSS) (in mmol/l: 142 NaCl, 4.7

KCl, 2.7 sodium HEPES, 3 HEPES acid, 1.17 $MgSO_4$, 2.79 CaCl, 5.5 glucose). The RCA was excised carefully and used for various measurements. The degree of hypertrophy was assessed by measuring RV-to-left ventricle (LV) mass ratio (RV/LV).

EPR Spectroscopy

The vascular segment for EPR was videotaped from the side (~4 mm in length) and cross-sectional views were obtained under a stereo microscope. The volume of the segment was calculated based on the product of cross-sectional area and axial length. The ROS generation was expressed as moles per unit of volume. A measure of the ROS concentration in the tissue samples was determined from EPR spectra obtained by incubating the tissue samples with the spin trapping agent *N-tert*-butyl-α-phenylnitrone 190 mM in HEPES-PSS for 30 min at 37°C in the dark. A Bruker ESP X-band spectrometer equipped with a TE102 cavity was utilized to detect signals (frequency: 9.4 GHz, power: 25.2 mW). All experiments were done at liquid nitrogen temperature. ROS concentrations were determined with 2,2,6,6-tetramethylpiperidine 1-oxyl solution (0.1 μmol/l) used as a concentration standard. All EPR parameters and conditions applied to both standard and experimental samples.

NOXs and eNOS

Briefly, the protein extracts (~25 μg) from arterial tissues were fractionated on 10% SDS-PAGE gel, transferred onto polyvinylidene difluoride membrane, and probed

with the following primary antibodies: anti-NOX1 (1:250, Santa Cruz Biotechnology), anti-NOX2 (1:250, Santa Cruz Biotechnology), anti-NOX4 (1:250, Santa Cruz Biotechnology), anti-p47phox (1:500, Santa Cruz Biotechnology), or anti-eNOS (1:1,000 dilution in blocking buffer, BD Transduction Laboratory). Blots were incubated with horseradish peroxidase-conjugated secondary antibody. The signal was detected by enhanced chemiluminescence (Amersham) and evaluated by densitometry (Sigma Scan). β-Actin was used for normalization.

Ex Vivo Endothelium-dependent Relaxation

An isovolumic myograph recently developed by Kassab's group was employed to evaluate the endothelial function of RCA [20], which maintains physiological loading similar to a pressure myograph, but measures tension with the high sensitivity of a wire myograph. Briefly, the RCA was cannulated on both ends in a physiological bath with HEPES-PSS and stretched to in situ length. The pressure and external diameter were measured with pressure transducer (Mikro-Tip SPR-524, Millar Instruments) and digital diameter tracking (DiamTrak v3+, Australia), respectively. The internal diameter was computed using the incompressibility assumption of vessel wall. The circumferential tension (product of pressure and internal radius) of the vessel was calculated.

The vessel segment was precontracted to an approximate pressure by acetylcholine at submaximal concentration (10^{-7} mol/l - 10^{-5} mol/l), which resulted in a somewhat different concentration of acetylcholine for each segment. In general, the concentration was ~80% higher in sham than in RVH vessels. The precontracted RCA

was relaxed by bradykinin at a series of doses from 10^{-12} mol/l to 10^{-7} mol/l. The endothelium-dependent vasodilatation was expressed as percent decrease in tension, which is calculated by the equation: %Tension = $(T_d - T_i)/(T_{max} - T_i) \times 100$. The tension at every dose (T_d), physiological level (T_i), and sub-maximum tension (T_{max}) by vasoconstrictor (acetylcholine) are shown. In additional experiments, the vessel segments were incubated with either BH$_4$ (10^{-7} mol/l) and L-arginine (10^{-7} mol/l) or apocynin (10^{-6} mol/l) for 40 min, and the endothelium-dependent relaxation of RCA was measured. The endothelium-independent vasorelaxation to sodium nitroprusside (dose-response relaxation: 10^{-10} mol/l -10^{-5} mol/l) served as reference.

Statistical Analysis

The data are expressed as means ± SD, unless otherwise stated. The correlation of ROS production, NOX, and endothelium-dependent relaxation were analyzed using a linear least squares fit. Variance analysis (ANOVA) was used with time- and dose-dependent comparisons (Bonferroni). Student's *t*-test was used to detect differences between pairwise groups. For all analyses, a P <0.05 level was used to indicate statistical significance.

Results

The body weight and systemic blood pressure of PA banded animals were not significantly changed compared with the sham group. RV systolic pressure in the PA

banding group was significantly higher than that in the sham group (Table 5.1). The RV/LV was defined as the ratio of the RV free wall mass to LV plus septal wall mass. In the PA banding group, RV/LV was over three times that of the sham group, which indicated significant RV hypertrophy during PA banding (Table 5.1).

The blood flow in RCA based on measurement of Transonic probe significantly increased in the PA banding group compared with the sham group (Table 5.1). The flow rate measured by Transonic Doppler (Figure 5.1) shows a similar waveform pattern with a mean value of 23.8 ± 4.3 ml/min in sham control and 44.3 ± 7.3 ml/min after 4 wk of PA banding (Figure 5.1A). When the phasic flow curves were normalized relative to the respective mean values of flow rate, the waveforms appears similar, which suggests that only the mean value changed and not the oscillatory component (Figure 5.1B). Angiographic DSA was used weekly to longitudinally quantify RCA blood flow and luminal diameter, and the typical images are shown in Figure 5.2A. The RCA experienced a small step increase in blood flow with the onset of PA banding and a gradual increase in blood flow over time (Figure 5.2B). The gradual chronic increase in blood flow was accompanied by an increase in RCA diameter. The RCA diameter cubed in Figure 5.2B shows a close proportion to blood flow. Since WSS is proportional to the ratio of blood flow to diameter cubed, the WSS was essentially unchanged throughout the experimental duration. The total increase in blood flow after 4 wk was 1.82 times the sham control using DSA measurement, which was not statistically different from the Transonic measurement (1.87 times). Furthermore, we determined the WSS at onset of banding and after 4-wk banding with Transonic measurement to be 11.0 ± 0.9 and 10.4 ± 0.8 dyn/cm^2, respectively ($P = 0.37$).

The oxidative stress in arterial tissue was measured by EPR spin trapping. The typical tracing curves of spin trapped ROS are presented in Figure 5.3. ROS species concentration measured using the spin trap indicates an increase in ROS after 4 wk of PA banding (Figure 5.4). We further evaluated the expression of subunits of NOX: NOX1, NOX2, NOX4, and p47phox (Figure 5.5) to identify the sources of ROS. NOX oxidase is the major source of superoxide, and p47phox is essential to NOX oxidase function. The upregulation of enzyme expression increased the generation of superoxide and elevated oxidative stress in the tissue. Although the expression of eNOS was attenuated after 4 wk of PA banding, the difference was not statistically significant (Figure 5.5). Endothelial function was evaluated in this study by *ex vivo* acetylcholine precontractile endothelium-dependent vasorelaxation in response to bradykinin. The endothelium-dependent relaxation was compromised after 4 wk of PA banding (Figure 5.6A) compared with the sham group (two-way ANOVA, $P < 0.05$).

The supplement of BH_4 and L-arginine restored the endothelial function in the PA banding group (Figure 5.6A), which suggests insufficient eNOS cofactors in the PA banding model. Administration of apocynin did not restore the endothelial function (Figure 5.6), which implies that ROS may affect endothelial function through oxidization of eNOS cofactor (BH_4). NO donor (sodium nitroprusside) induced endothelium-independent vasorelaxation showed that vascular smooth muscle relaxation in response to NO was unchanged (Figure 5.6B).

Discussion

This is the first study to show a compromised endothelial function in RCA during RVH as verified in an *ex vivo* isovolumic myograph [20]. Our findings suggest that the RCA endothelial dysfunction stems from eNOS uncoupling. The angiographic analysis of *in vivo* volume ratio suggests an increase in the basal tone of RCA during RVH. The increase in ROS production was also observed in the RCA of RVH. Although increased ROS production in hypertension and coronary artery disease has been well documented [3-5], [14, 21] as has the predilection for vasospasm in hypertension and LV hypertrophy [9, 22, 23]; this is the first study to suggest increased ROS production and compromised endothelial function in response to a gradual increase in blood flow under constant WSS conditions.

We observed a chronic increase of blood flow in the RCA in PA banding-induced RVH. Despite the increase in RV pressure, the systemic blood pressure in RCA was unchanged, indicating that coronary hypertension was not a factor in this study. The progression of RVH was monitored in the same pig longitudinally using angiography, which allowed each animal to serve as its own control. To our knowledge, this is the first porcine longitudinal model that reflects remodeling of a coronary artery at different time points in the same animal. In this model, the increase in diameter cubed of RCA is proportional to the increase in blood flow, which is proportional to the increase in myocardial mass of RV, since RVH progresses slowly under the pressure overload. Therefore, WSS remained constant during increases in both diameter and blood flow in

RCA during RVH. The constant WSS is also underscored by the unchanged expression of eNOS in contrast to increase of eNOS with elevated WSS [24].

In addition to WSS, other hemodynamic factors, especially the circumferential and axial distension on blood vessel, may be the stimuli for the biochemical, molecular, and functional responses of blood vessel [15]. DSA measurement in this study clearly showed the progression of RCA expansion (Figure 5.2), which is consistent with our previous observation; i.e., diameter increase and axial elongation simultaneously take place in the RCA during RVH [1]. The axial elongation of RCA may result from dimensional remodeling (e.g., enlargement) of RV during RVH [1]. It is well established that stretch activated integrin, ion channels, and G protein-coupled receptors mediate cellular signaling and function in blood vessels. Endothelial dysfunction and increase in ROS production in this study are indeed similar to the pathological responses of blood vessels in hypertension that also entails stretch. An increase in ROS production is involved in changes of vaso-reactivity [25], endothelial dysfunction [6, 8], and vascular remodeling [3, 13]. ROS may reduce NO bioavailability by reaction with NO and, therefore, compromise endothelium-dependent vasorelaxation [3, 11].

An increased volume ratio indicates significant geometric remodeling of RCA during RVH (Figure 2C). With administration of vasodilators (nitroglycerin in the present study), the basal vascular tone can be estimated as the differences of volume ratio with and without the vasodilator. The analysis of *in vivo* volume ratio suggests a progression of elevated basal tone in the RCA during RVH (Figure 2C), which may predispose the vessel to vasospasm. The data from *ex vivo* vaso-reactivity (SNP-induced vasorelaxation) using isovolumic myograph suggest that vascular smooth muscle of RCA

is the same in sham and RVH groups (Figure 5.6). Therefore, we conclude that the increased basal tone is likely from endothelial dysfunction, i.e., eNOS uncoupling.

The upregulation of oxidative stress (Figures 5.3, 5.4 and 5.5) also may compromise endothelial function by oxidizing BH_4 (an eNOS cofactor) to form uncoupled eNOS, which produces ROS instead of NO. As an important cofactor of eNOS, BH_4 plays a critical role in endothelial function [26]. In the present study, the result shows that BH_4 can reverse the endothelial dysfunction of RCA by *ex vivo* administration of BH_4 (Figure 5.6A), which suggests eNOS uncoupling. But *ex vivo* administration of apocynin (an antioxidant and inhibitor of NOX) did not restore the endothelial function (Figure 5.6A). This implies that the deficiency of BH_4 in the RCA is not acute oxidization of ROS and needs further study.

In blood vessel, NOX, xanthine oxidase, mitochondria, and eNOS uncoupling are recognized as the sources of ROS. Among them, NOX has been identified as a major source of superoxide in blood vessels in response to pathological stimulation (hypertension, hypercholesterolemia, and diabetes) and mechanical stimulation [4, 10, 11]. In this study, we examined the expression of NOX in RCA using Western blot and chemiluminescence analysis. The upregulation of expression of NOX underscores its role in RCA remodeling during RVH. The result of the addition of BH_4 in *ex vivo* studies implies that eNOS uncoupling is one of the sources of ROS in the RCA during RVH. The administration of inhibitors of various oxidases and *in vivo* manipulation of BH_4 requires additional study.

The interaction of ROS between RCA and RV during RVH is likely to be small, since our measurement of ROS in RV tissue showed a relatively small increase (8%)

during RVH compared with the changes in the vessel tissue. In this model, we established stretch rather than WSS as the major stimulus. Accordingly, we chose DSA rather than conventional implantable probe-based or Doppler wire methods based on several reasons. The video densitometry-based DSA is independent of geometry or velocity profile and is less invasive to the vessel. Ultrasonic flow wire provides flow velocity as opposed to volumetric flow rate. The flow rate can be calculated if the velocity is measured from the centerline, which is often not the case. The flow rate calculation also requires the assumption of laminar flow (a condition that is not necessarily true in RCA) and an accurate area measurement. DSA was selected over a transonic flow probe in this study, since implantation of a flow probe around the RCA presented a technical challenge; i.e., access to the RCA is difficult from a left lateral thoracotomy. Even when surgical implantation of the flow probe was successful, as was the case in several test animals, the implant may induce an inflammatory response in the RCA, which contributes strong oxidative stress. Additionally, the flow probe itself may cause a focal stenosis when vessel growth is retarded by the flow probe. Microsphere techniques were not used to measure flow or its profile, because they require withdrawal of blood per measurement. Furthermore, any degradation of microspheres lodged in the capillary bed within the 1-mo measurement period would underestimate flow. Finally, the change in heart weight makes the normalization of flow (perfusion) inaccurate. The DSA technique has been validated *in vivo* against an ultrasonic flow probe with a discrepancy of 4% [27].

Conclusion

We confirmed that WSS remains constant in this model of RVH and implicated stretch as the major stimulus. ROS production and NOX content increased significantly in this RCA model of RVH. Endothelial function of RCA was compromised after 4 wk of RVH, and eNOS uncoupling was implicated in the endothelial dysfunction. *In vivo* analysis suggests an increased basal tone in the RCA during RVH and, therefore, increases the potential risk of vasospasm.

Acknowledgements

References

[1]   Kassab, G. S.; Imoto, K.; White, F. C.; Rider, C. A.; Fung, Y. C.; Bloor, C. M. Coronary arterial tree remodeling in right ventricular hypertrophy. *Am J Physiol* **265:**H366-375; 1993.

[2]   Huo, Y.; Linares, C. O.; Kassab, G. S. Capillary perfusion and wall shear stress are restored in the coronary circulation of hypertrophic right ventricle. *Circ Res* **100:**273-283; 2007.

[3]   Cai, H.; Harrison, D. G. Endothelial dysfunction in cardiovascular diseases: the role of oxidant stress. *Circ Res* **87:**840-844; 2000.

[4]   Castier, Y.; Brandes, R. P.; Leseche, G.; Tedgui, A.; Lehoux, S. p47phox-dependent NADPH oxidase regulates flow-induced vascular remodeling. *Circ Res* **97:**533-540; 2005.

[5]   Laurindo, F. R.; Pedro Mde, A.; Barbeiro, H. V.; Pileggi, F.; Carvalho, M. H.; Augusto, O.; da Luz, P. L. Vascular free radical release. *Ex vivo* and *in vivo* evidence for a flow-dependent endothelial mechanism. *Circ Res* **74:**700-709; 1994.

[6]   McIntyre, M.; Bohr, D. F.; Dominiczak, A. F. Endothelial function in hypertension: the role of superoxide anion. *Hypertension* **34:**539-545; 1999.

[7]   Kai, H.; Mori, T.; Tokuda, K.; Takayama, N.; Tahara, N.; Takemiya, K.; Kudo, H.; Sugi, Y.; Fukui, D.; Yasukawa, H.; Kuwahara, F.; Imaizumi, T. Pressure overload-induced transient oxidative stress mediates perivascular inflammation and cardiac fibrosis through angiotensin II. *Hypertens Res* **29:**711-718; 2006.

[8]   Bedard, K.; Krause, K. H. The NOX family of ROS-generating NADPH oxidases: physiology and pathophysiology. *Physiol Rev* **87:**245-313; 2007.

[9]   Chutkow, W. A.; Pu, J.; Wheeler, M. T.; Wada, T.; Makielski, J. C.; Burant, C. F.; McNally, E. M. Episodic coronary artery vasospasm and hypertension develop in the absence of Sur2 K(ATP) channels. *J Clin Invest* **110:**203-208; 2002.

[10]   Fukui, T.; Ishizaka, N.; Rajagopalan, S.; Laursen, J. B.; Capers, Q. t.; Taylor, W. R.; Harrison, D. G.; de Leon, H.; Wilcox, J. N.; Griendling, K. K. p22phox mRNA expression and NADPH oxidase activity are increased in aortas from hypertensive rats. *Circ Res* **80:**45-51; 1997.

[11]   Guzik, T. J.; Mussa, S.; Gastaldi, D.; Sadowski, J.; Ratnatunga, C.; Pillai, R.; Channon, K. M. Mechanisms of increased vascular superoxide production in human diabetes mellitus: role of NAD(P)H oxidase and endothelial nitric oxide synthase. *Circulation* **105:**1656-1662; 2002.

[12]   Landmesser, U.; Spiekermann, S.; Dikalov, S.; Tatge, H.; Wilke, R.; Kohler, C.; Harrison, D. G.; Hornig, B.; Drexler, H. Vascular oxidative stress and endothelial dysfunction in patients with chronic heart failure: role of xanthine-oxidase and extracellular superoxide dismutase. *Circulation* **106:**3073-3078; 2002.

[13]   Valko, M.; Leibfritz, D.; Moncol, J.; Cronin, M. T.; Mazur, M.; Telser, J. Free radicals and antioxidants in normal physiological functions and human disease. *Int J Biochem Cell Biol* **39:**44-84; 2007.

[14]   Zhu, X. Y.; Daghini, E.; Chade, A. R.; Rodriguez-Porcel, M.; Napoli, C.; Lerman, A.; Lerman, L. O. Role of oxidative stress in remodeling of the myocardial microcirculation in hypertension. *Arterioscler Thromb Vasc Biol* **26:**1746-1752; 2006.

[15]   Oeckler, R. A.; Kaminski, P. M.; Wolin, M. S. Stretch enhances contraction of bovine coronary arteries via an NAD(P)H oxidase-mediated activation of the extracellular signal-regulated kinase mitogen-activated protein kinase cascade. *Circ Res* **92:**23-31; 2003.

[16]   Botham, M. J.; Lemmer, J. H.; Gerren, R. A.; Long, R. W.; Behrendt, D. M.; Gallagher, K. P. Coronary vasodilator reserve in young dogs with moderate right ventricular hypertrophy. *Ann Thorac Surg* **38:**101-107; 1984.

[17]   Manohar, M. Transmural coronary vasodilator reserve, and flow distribution during tachycardia in conscious young swine with right ventricular hypertrophy. *Cardiovasc Res* **19:**104-112; 1985.

[18]   Murray, P. A.; Vatner, S. F. Reduction of maximal coronary vasodilator capacity in conscious dogs with severe right ventricular hypertrophy. *Circ Res* **48:**25-33; 1981.

[19]   White, F. C.; Nakatani, Y.; Nimmo, L.; Bloor, C. M. Compensatory angiogenesis during progressive right ventricular hypertrophy. *Am J Cardiovasc Pathol* **4:**51-68; 1992.

[20]   Lu, X.; Kassab, G. S. Assessment of endothelial function of large, medium, and small vessels: a unified myograph. *Am J Physiol Heart Circ Physiol* **300:**H94-H100; 2011.

[21]   McNally, J. S.; Davis, M. E.; Giddens, D. P.; Saha, A.; Hwang, J.; Dikalov, S.; Jo, H.; Harrison, D. G. Role of xanthine oxidoreductase and NAD(P)H oxidase in endothelial superoxide production in response to oscillatory shear stress. *Am J Physiol Heart Circ Physiol* **285:**H2290-2297; 2003.

[22]   Koshiba, K.; Hoka, S. Clinical characteristics of perioperative coronary spasm: reviews of 115 case reports in Japan. *J Anesth* **15:**93-99; 2001.

[23]   Mohri, M.; Takeshita, A. Coronary microvascular disease in humans. *Jpn Heart J* **40:**97-108; 1999.

[24]   Tuttle, J. L.; Nachreiner, R. D.; Bhuller, A. S.; Condict, K. W.; Connors, B. A.; Herring, B. P.; Dalsing, M. C.; Unthank, J. L. Shear level influences resistance artery remodeling: wall dimensions, cell density, and eNOS expression. *Am J Physiol Heart Circ Physiol* **281:**H1380-1389; 2001.

[25]   Matsubara, T.; Nakazawa, M.; Yoshida, Y.; Imai, S.; Suzuki, K.; Hori, T.; Konno, T.; Higuchi, K.; Tamura, Y.; Yamazoe, M.; Izumi, T.; Aizawa, Y. Increasing vasoconstrictor response to ergonovine with oxidative injury in canine coronary artery. *Coron Artery Dis* **8:**1-7; 1997.

[26]   Vasquez-Vivar, J.; Kalyanaraman, B.; Martasek, P. The role of tetrahydrobiopterin in superoxide generation from eNOS: enzymology and physiological implications. *Free Radic Res* **37:**121-127; 2003.

[27]   Molloi, S.; Kassab, G. S.; Zhou, Y. Quantification of coronary artery lumen volume by digital angiography: *in vivo* validation. *Circulation* **104:**2351-2357; 2001.

Table

Table 5.1: Hemodynamic and physiological parameters

	PA banding		Sham	
	Day 0	Day 28	Day 0	Day 28
Body weight (kg)	41.2 ± 3.3	49.8 ± 4.7	40.7 ± 3.8	53.6 ± 6.2
RV/LV ratio (g/g)	N/A	0.73 ± 0.11	N/A	0.21 ± 0.06
Systemic pressure (mmHg)	68 ± 8	64 ± 6	69 ± 8	70 ± 11
RV pressure (mmHg)	37 ± 7	52 ± 11	36 ± 7	38 ± 9
RCA blood flow (ml/min)	23.8 ± 4.3	44.3 ± 7.2	22.7 ± 4.6	25.9 ± 5.1

Values are means ±SD. PA, pulmonary artery; RV/LV, weight ratio of right to left ventricles; RV, right ventricle; RCA, right coronary artery; N/A, not applicable. *P < 0.05, significant difference vs. sham group.

Notes: RV: right ventricle; LV: left ventricle; RV/LV: weight ratio of right to left ventricles; RCA: right coronary artery.

Figures

A
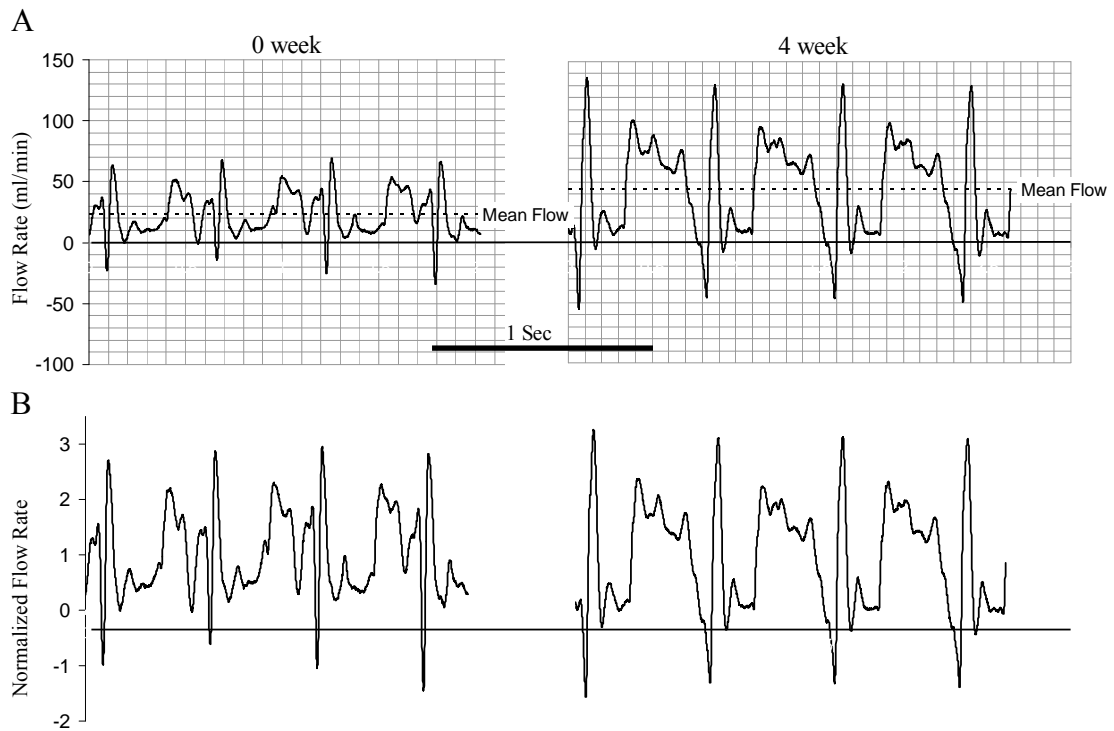
Figure 5.1: The Transonic flow tracing curves of blood flow in right coronary artery (RCA) at day 0 and day 28 (4 wk) of right ventricular (RV) hypertrophy (RVH). (A) real-time recordings at *day 0* and 4 wk of RVH. (B) flow curves were normalized by the mean flow rate.

A

| Day 0 | Day 14 | Day 28 |

B
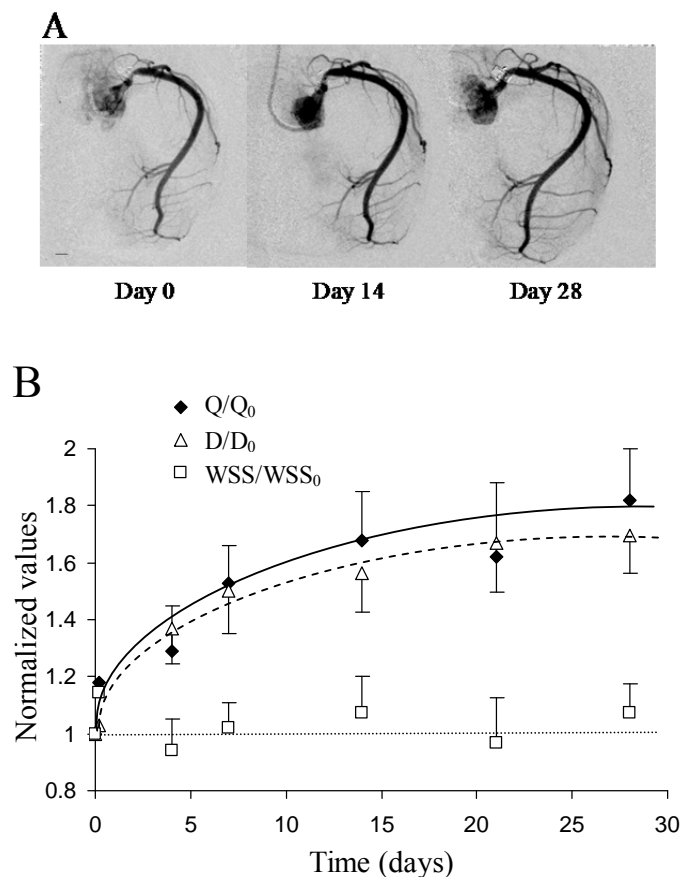
Figure 5.2: (A) The video densitometric images of RCA were from the same pig to show the progress (day 0, day 7, and day 28) of RCA remodeling after PA banding. All images are taken at the same magnification. Scale length is 5 mm. (B) The flow and inner diameter were measurements based on DSA and WSS was calculated based on the ratio of flow to diameter cubed. Normalized flow (Q/Q_0), diameter cubed ($[D/D_0]^3$), and WSS (WSS/WSS_0) were defined as the ratio at a given day relative to day 0. Both Q/Q_0 and $[D/D_0]^3$ increased gradually with time (one way ANOVA, $P < 0.05$). The increase is exponential thereafter as shown through the best-fit line. WSS/WSS_0 showed no significant change with time (one way ANOVA, $P > 0.05$). Data are expressed as mean $\pm$ SEM.
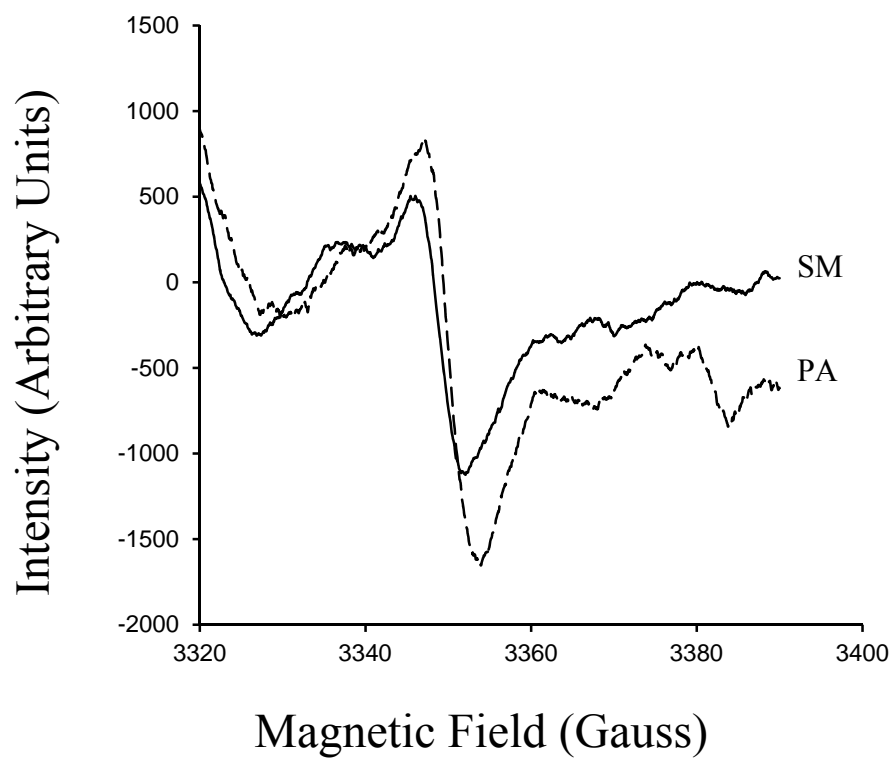
Figure 5.3: Typical EPR spectra of the PBN spin adduct for a RCA segment. ROS production measured with EPR normalized by volume of vessel tissue.
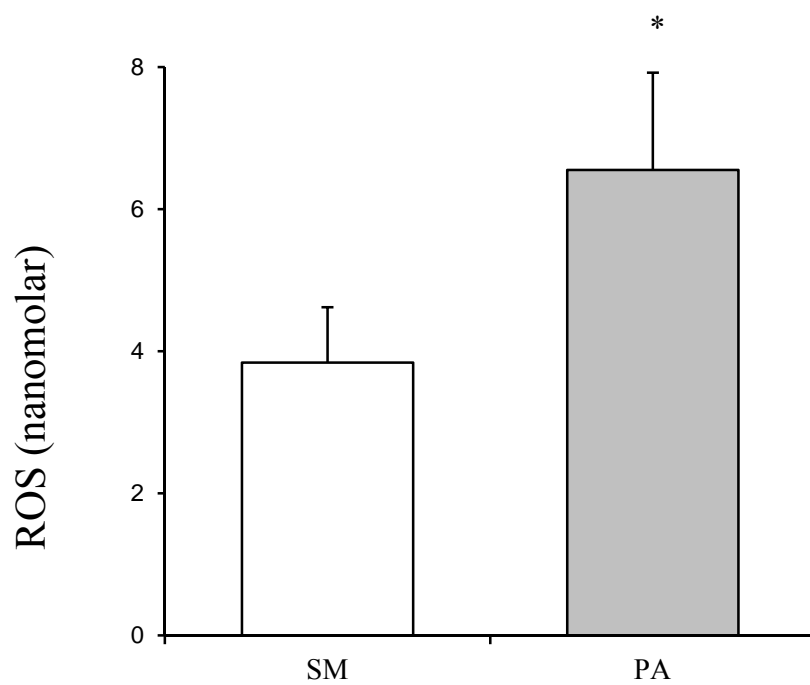
Figure 5.4: Reactive oxygen species (ROS) production measured with EPR normalized by volume of vessel tissue.
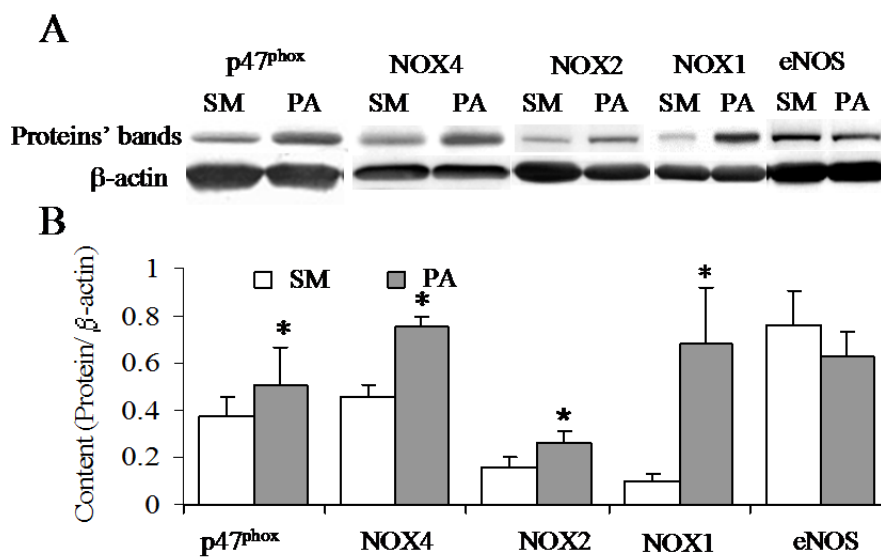
Figure 5.5: Expression of the proteins of p47phox, NADPH oxidase (NOX4, NOX2, NOX1), and endothelial nitric oxide synthase (eNOS). (A) Western blotting bands of the proteins. (B) the semi-quantification of the proteins content normalized by β-actin content. Values are means ±SD, *statistical difference ($P < 0.05$).
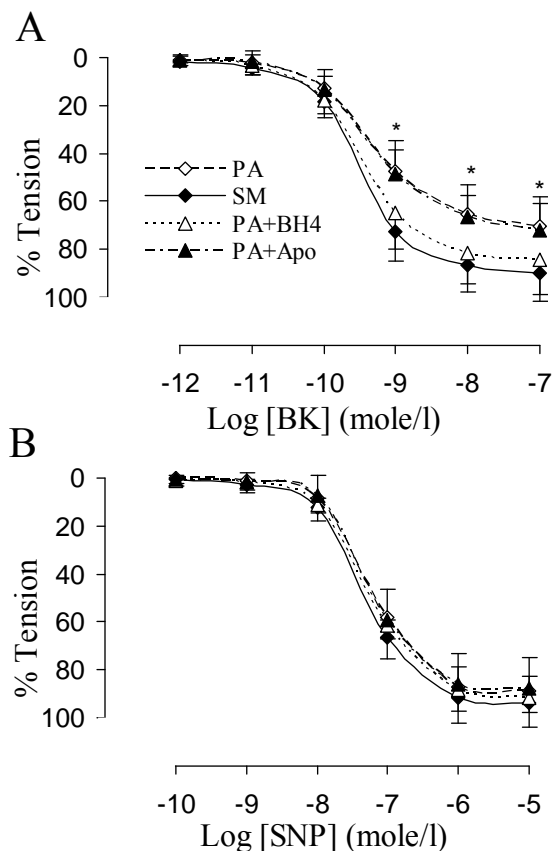
Figure 5.6: (A) endothelial function represented by endothelium-dependent vasorelaxation in response to bradykinin (BK; precontracted with acetylcholine 10^{-7} mol/l -10^{-6} mol/l). The endothelial function of RCA in PA banding (PA) was significantly dysfunctional compared with SM (two-way ANOVA, *P < 0.05). Vessel segments in PA banding incubated with tetrahydrobiopterin (PA+BH$_4$) for 40 min showed restoration of endothelium-dependent vasorelaxation. Apocynin (PA+Apo) did not improve endothelium-dependent vasorelaxation of vessel segment in PA banding. (B) endothelium-independent vasorelaxation in response to sodium nitroprusside (SNP; precontracted with acetylcholine 10^{-7} mol/l -10^{-6} mol/l) (two-way ANOVA, P < 0.05). Values are means ±SD.

CHAPTER 6: ROLE OF STRETCH ON ENDOTHELIAL DYSFUNCTION AND
ACTIVATION OF ANGIOTENSIN II TYPE 1 RECEPTOR IN CORONARY ARTERY

The mechanical stretch induced by hypertension or blood flow overload is recognized as a signal that elicits mechanotransduction and vascular remodeling in blood vessels. Stretch deforms endothelial and vascular smooth muscle cells and activates the signaling pathway in the cells which trigger functional and structural remodeling [1-5]. The detailed mechanisms of the activation remain unclear in various cellular signaling systems, e.g., the rennin-angiotensin system which is well-known to play an important role in hypertension [5-7].

The AT1 receptor has been shown to mediate most of the physiological and pathological actions of Angiotensin II (Ang II) in vascular cells [6]. Ang II which binds to the AT1 receptor has been thought to play a critical role in hypertension [8]. The inhibition of AT1 receptors has been shown to have pharmaceutical benefit for cardiovascular diseases such as hypertension [9]. Pretreatment with AT1 receptor blockers significantly attenuates the mechanical stretch-induced hypertrophy and the activation of myocytes [5, 10].

Ang II binds to AT1 receptor and activates the cytosolic subunits of NADPH oxidase (p47phox, p67phox) and thereafter NADPH oxidase recruits NAD(P)H as an electron donor to catalyze the trans-membrane transfer of electrons to oxygen to form

superoxide [11, 12]. It has been observed in cultured cells that the AT1 receptor signaling cascade may be activated by mechanical stimulation through integrin which is a well-established mechano-sensor that bridges the extracellular matrix to the cytoskeleton [12-14]. The AT1 receptor cascade activated by integrin was suggested to be mediated by cytosolic Ang II [12]. It is also reported that mechanical stress can activate AT1 receptors without the involvement of Ang II but the mechanism remains unclear [10, 15].

Endothelial dysfunction is a salient feature of hypertension, atherosclerosis, and heart failure [16-18]. A decline in bioavailability of nitric oxide (NO) is an important cause of endothelial dysfunction. In hypertension, activation of NADPH oxidase increases production of ROS which suppresses NO bioavailability by rapid quenching of NO [1, 16, 17, 19-21]. Activation of the AT1 receptor causes endothelial dysfunction by reduction of NO bioavailability due to an increase in ROS production. Although the roles of AT1 receptor and the Angiotensin system in hypertension have been extensively studied, it remains unclear whether the AT1 receptor plays a role in non-hypertensive distension, e.g., outward remodeling of blood vessels.

The signaling pathway of distension-induced endothelial dysfunction is not completely understood. The distension of a blood vessel may trigger multiple cellular signaling pathways in the vessel wall (see Figure 6.1). Here, we hypothesize that the distension activates AT1 receptors in coronary arteries and in turn the NADPH oxidase system which causes ROS-mediated endothelial dysfunction. Chronic *in vivo* and acute *ex vivo* experiments were used to test these hypotheses. In the former, the RCA of swine was exposed to chronic distension through a flow-overload model that maintains constant wall shear stress. In the latter, *ex vivo* RCA segments were distended acutely to

determine the AT1 receptor activation response, ROS production, and endothelial function. An external cuff was used to validate the role of distension or circumferential stretch in the activation of AT1 receptor in acute *ex vivo* over-inflation.

Materials and Methods

Animals

Six male Duroc swine weighing 34 kg ± 4 kg (range 30–39 kg) were used to induce right ventricle (RV) hypertension and subsequent RV hypertrophy by pulmonary artery (PA) banding and an additional six animals (shams) served as controls. Eighteen normal male Duroc swine weighing 38 kg ± 6 kg (range 31–47 kg) were used in acute *ex vivo* stimulation. The animal experiments were performed in accordance with the guidelines of Institute of Laboratory Animal Research Guide, Public Health Service Policy, Animal Welfare Act, and an approved Indiana University School of Medicine IACUC protocol.

Right Ventricle Hypertrophy

A thoracotomy was performed along the fourth intercostal space. The chest cavity was exposed to provide access to the pulmonary artery (PA). A glycerin filled silicone occluder was fitted around the PA, and the filling tube was exteriorized to allow for cuff occlusion and PA stenosis at a later time. One week after recovery, the animal

was anesthetized again and the silicone occluder was inflated and locked when the desired systolic RV pressure was reached (35 – 50% above baseline). In the shams, the silicone occluder was not inflated. The RCA was X-ray imaged before and immediately after banding and again on the terminal day of the study. The angiographic blood flow rate and RCA lumen diameter were obtained to determine the wall shear stress as WSS = $\mu Q/\pi D^3$, where μ is the viscosity of blood, Q is blood flow rate, and D is the inner diameter of blood vessel.

Heart and Coronary Artery Harvest

On the termination day, surgical anesthesia was induced with ketamine (20 mg/kg im) and atropine (0.04 mg/kg im) and maintained with isofluorane (1–2%). A thoracotomy was performed and the heart was exposed. The heart was excised and immediately stored in 4°C HEPES physiological saline solution (HEPES-PSS) (in mmole/l: 142 NaCl, 4.7 KCl, 2.7 Sodium HEPES, 3 HEPES acid, 1.17 MgSO4, 2.79 CaCl, 5.5 Glucose). The main trunks of the right coronary artery (RCA) and the left anterior descending coronary artery (LAD) were excised carefully. The RCAs from PA banding or sham controls were directly evaluated with various measurements, whereas the RCA segments harvested from the acute pigs were first exposed to *ex vivo* stimulations and then evaluated for various endpoints. The LAD served as a control for the RCA in the same heart since the LAD artery essentially remained at normal hemodynamic state during PA banding.

Ex Vivo Stimulations

The RCA was cannulated with connectors and secured with 6-0 suture twice to avoid any leakage. The vessel was warmed up to 37°C slowly (20 – 25 min) and equilibrated for 40 minutes at a transmural pressure of 15 mmHg and *in situ* length before stimulation. After establishment of the base line, the RCA segments in the PA banding group were incubated with either AT1 receptor inhibitor (Losartan, 10 μM) for 30 minutes, or the inhibitor of NADPH oxidase (gp91-ds-TAT, 1 M) for 40 minutes, respectively. The RCA segments in the acute inflation group were stimulated for 1 hour by either 180 mmHg inflation pressure, 180 mmHg inflation pressure with cuff-restriction, 180 mmHg with pre-incubation of Losartan (10 μM) for 30 minutes, or 180 mmHg with pre-incubation of gp91-ds-TAT (1 μM) for 40 minutes. A 100 mmHg (physiological pressure of RCA) inflation pressure served as control. The external cuff is a plastic porous tube that was opened and externally applied to the vessel, where the inner diameter of the tube was precisely made to equal to the outer diameter of the vessel at 100 mmHg of inflation pressure. The activations of AT1 receptor and endothelium of the segments were verified and the data were discarded if the activations did not meet the following criteria: maximal incremental tension < 40% and maximal endothelium-dependent relaxation < 90%.

AT1 Receptor Activation

The activation of the AT1 receptor was verified with Ang II-induced vasoconstrictions in a series of doses from 10^{-11} mol/l to 10^{-6} mol/l. The contraction of the vessel wall against the luminal fluid increases the intraluminal pressure at isovolumic conditions. The pressure and the external diameter were measured with a pressure transducer (Mikro-Tip SPR-524, Millar Instruments, USA) and a dimensional tracer (DiamTrak 3+, Australia), respectively. Potassium chloride (KCl, 60 mM) was used to verify the receptor-independent vasoconstriction of vessel segments. The contractile tension (T) was calculated according to Laplace's equation ($T = p \cdot r/2$) from the luminal pressure (p) and radius (r).

Vasoreactivity

Endothelium-dependent vasorelaxation was monitored with an isovolumic myograph. The vessels were pre-contracted to an approximate transluminal pressure (170 ± 20 mmHg) with acetylcholine at submaximal dose (10^{-8} mol/l to 10^{-6} mol/l), and thereafter the endothelium-dependent relaxation was induced with a series of doses of bradykinin (10^{-10} mol/l to 10^{-5} mol/l). The endothelium-independent vasorelaxation in response to sodium nitroprusside (10^{-10} mol/l to 10^{-5} mol/l) were measured to verify the responsiveness of vascular smooth muscle in response to nitric oxide.

ROS Detection by Electron Paramagnetic Resonance (EPR)

A measure of ROS concentration in tissue samples was determined from the EPR spectra obtained by incubating the tissue samples with the spin trapping agent N-*tert*-butyl-α-phenylnitrone (PBN, Sigma, USA) at 190 mM in HEPES-PSS for 30-min at 37°C in the dark. A ring incubated with 4-Hydroxy-TEMPO (a superoxide dismutase mimic) served as a control of ROS measurement. The tissue was subsequently inserted into a syringe along with the supernatant, immediately frozen in liquid nitrogen, and stored at -80°C until EPR analysis was performed. To avoid ROS produced during freezing and thawing samples, the sample was quickly removed while in its frozen state from the syringe and placed in a dewar containing liquid nitrogen. The dewar was then inserted into the microwave cavity of the EPR spectrometer. The sample remained at liquid nitrogen temperature throughout the EPR analysis [22, 23]. ROS generation was expressed as mole per unit volume of tissue.

The EPR equipment and settings were as follows: A Bruker ESP X-band spectrometer equipped with a TE_{102} cavity was utilized to detect signals. Parameters for the spectra were: 9.4-GHz microwave frequency, 25.2-mW microwave power, 4.0-G modulation amplitude, 1×105 receiver gain, 5.24-s time constant, 3330-G center magnetic field, and 100-G magnetic field sweep width. All experiments were run at liquid nitrogen temperature.

Four EPR scans were taken per tissue sample and analyzed with Bruker WINEPR software (Version 2.11) based on the spectral intensity and linewidth. ROS concentrations were determined with 2,2,6,6-tetramethylpiperidine 1-oxyl, TEMPO,

solution (0.1 µM, Sigma, USA) used as a concentration standard. All EPR parameters and conditions were applied to both standard and experimental samples.

Statistics

The data were presented as mean ± SD and significant differences between two data points were determined by Student's *t*-test. Significant differences between the dose-response relationships between groups were determined by use of Analysis Of Variance (ANOVA) between groups. A probability of $P < 0.05$ was considered to be indicative of a statistically significant difference.

Results

Chronic Right Ventricular Hypertrophy

The PA banding caused an increase in RV pressure from 377 to 529 mmHg. RV pressure did not change in sham animals (367 versus 356 mmHg). The systemic blood pressure remained nearly constant in the PA banding animals and the shams. In PA banding, the blood flow increased in the RCA after the four-week period and the diameter of the RCA increased accordingly such that the wall shear stress (WSS) was not significantly changed. It went from 11.009 dynes/cm^2 at baseline to 11.408 dynes/cm^2 at termination (Figure 6.2). The blood flow and diameter of the RCA in the shams did not

change (data not shown). The blood flow remained unchanged in the LAD during PA Banding since the left ventricle (LV) is normotensive.

In PA banding, the RCA significantly augmented the contractile responsiveness of the vessel to Ang II in comparison with the LAD in the same heart and the RCA in the sham (Figure 3A). Acute application of losartan, an inhibitor of AT1 receptor, blocked the contractile responsiveness of the RCA and LAD to Ang II, which verified the role of AT1 receptor in contraction. The Western Blotting analysis indicated that the expression of AT1 receptor in the RCA was upregulated during PA Banding but not in the LAD (Figure 6.3B).

Endothelium-dependent relaxation was attenuated in the RCA but not the LAD during PA Banding (Figure 6.3) in comparison with the shams. The acute inhibition of AT1 receptor with losartan restored the endothelial function of RCA in PA banding. Since the angiotensin system may activate NADPH oxidase which augments the production of ROS, we investigated the effects of an inhibitor of NAPDH oxidase; i.e., gp91-dis-TAT. The acute inhibition of NADPH oxidase did not completely restore endothelium-dependent relaxation in the RCA exposed to PA banding. The results are based on EPR (Figure 6.3B). The acute inhibition of AT1 receptor and NADPH oxidase reduced the production of ROS in the RCA wall exposed to PA banding (Figure 6.3B).

Ex Vivo Stimulation

After exposure to *ex vivo* distension at 180 mmHg for 1 hour, the RCA showed an elevation in contractile responsiveness to Ang II (Figure 6.5). This observation combined

with the inhibition of AT1 receptor, implies that the angiotensin system is activated by the 180 mmHg inflation. When an external cuff was applied to the vessel segment to restrain the distension, a pressure of 180 mmHg did not increase the contractile responsiveness to Ang II in comparison with physiologic pressure of 100 mmHg (Figure 6.5). The endothelium-dependent relaxations are shown in Figure 6.4. An inflation of 180 mmHg pressure attenuated the endothelium-dependent relaxation. The inhibition of AT1 receptor and the use of external cuff maintained the endothelial function at hyper-distension. The inhibition of NADPH oxidase did not completely restore endothelium-dependent relaxation. The production of ROS significantly increased when the vessel segment was inflated to 180 mmHg (Figure 6.5). The inhibition of AT1 receptor, NADPH oxidase, and circumferential stretch (external cuff) reduced the production of ROS to lower level than physiologic pressure of 100 mmHg.

Discussion

In the present study, we found that the expression and activation of AT1 receptor was upregulated in the RCA exposed to chronic *in vivo* distension by PA banding and acute *ex vivo* distension (over inflation), which is a typical stimulus-response in cellular signal pathways (Figure 6.1). AT1 receptor is implicated in the production of ROS induced by distension. The inhibition of the distension by an external cuff, AT1 receptor, and ROS provide evidence that distension plays a major role in activation of AT1 receptor and endothelial dysfunction in the vascular wall.

The PA banding causes RV hypertension and secondarily hypertrophy. In this model, the RCA is not exposed to high blood pressure but a gradual increase in blood flow due to increase in RV mass. The diameter of RCA increased progressively, i.e., the RCA was gradually circumferentially stretched while maintaining a constant WSS. Although laminar WSS is considered as a stimulator of endothelial NO, the effect of WSS was not significant in this model since the WSS on the endothelial surface of RCA did not change significantly during the duration of PA banding. The major mechanical stimulus in this model is the gradual increase in circumferential stretch of the vessel wall. The circumferential stretch accompanies vascular relaxation but is different than the vascular stretch accompanied by higher vascular tone in hypertension. The similarity of this model and hypertension lies in the observation that both stretches can activate vascular mechanotransduction, cellular signaling pathway, and remodeling. Although the role of angiotensin system is intensively investigated in hypertension, the effect of the circumferential stretch on the local angiotensin system is not completely understood. The experimental observation from vascular smooth muscle cells exposed to cyclic stretch suggests that the AT1 receptor may be activated in the mechanotransduction of vascular smooth muscle cells. The present study provides evidence that distension of blood vessel wall by either pressure or dilatation can activate the AT1 receptor and elicits endothelial dysfunction (Figures 6.3, 6.4, and 6.5). We used an external cuff to inhibit the circumferential stretch during increase in inflation pressure. We found that the cuff prevents the increase in response of AT1 receptor to Ang II by an increase in inflation pressure (Figure 6.5). Although the mechanism of the AT1 receptor activated by distension remains unclear, the integrin (trans-membrane proteins) may play a role which

mediates the deformation of extracellular matrices due to distention and intracellular signaling pathway [24]. The signaling pathway needs to be further explored.

Activation of the rennin-angiotensin system is involved in endothelial synthesis (eNOS) in cardiovascular diseases [22-27]. Up-regulation of AT1 receptor or increase in activation of the AT1 receptor may inhibit the activation of eNOS or NO production [28, 29]. Most physiological and pathological actions of Ang II in vascular cells are mediated by the AT1 receptor [6]. Inhibition of the AT1 receptor blocks the Ang II-induced signaling pathway in cells. Losartan is an Ang II receptor antagonist drug used mainly to treat hypertension. The application of losartan in our *ex vivo* studies restores the endothelial function in acute over inflation (Figure 6.5), which implicates the AT1 receptor in the distension-induced endothelial dysfunction. The acute inhibition of AT1 receptor did not completely restore the endothelial function in the RCA exposed to PA banding for 4 weeks. There may be other signaling pathway involved in the distension-induced remodeling, such as ROS, protein kinase C (PKC), and others.

Mechanical forces are stimulators of ROS [30, 31]. Activation of NADPH oxidase is one of the signaling components downstream of the activated angiotensin system [4]. The production of ROS tightly couples with vascular remodeling, endothelial dysfunction, atherogenesis, etc. Here, we inhibited NADPH oxidase with a peptide inhibitor gp91-ds-TAT which is a specific inhibitor of NADPH oxidase. This inhibitor attenuated the distension-induced AT1 receptor-mediated product of ROS in over-inflation or distension. This inhibitor did not completely eliminate the effect of distension in PA banding on the production of ROS in the RCA (Figure 6.5). The chronic distension may activate not only AT1 receptor but also other signaling pathways

(Figure 6.1). Activation of the angiotensin system has several downstream signaling pathways [6, 8]. The production of ROS tightly couples with vascular remodeling, endothelial dysfunction, and atherogenesis. Here, we inhibited NADPH oxidase with a peptide inhibitor gp91-ds-TAT which is a specific inhibitor of NADPH oxidase. This inhibitor attenuated the distension-induced AT1 receptor-mediated product of ROS in over-inflation or distension (Figure 6.5). This inhibitor did not completely eliminate the effect of distension in PA banding on the production of ROS in the RCA (Figure 6.5). Activation of angiotensin system has several downstream signaling pathways.

This chapter contains unpublished data. The Kassab group was responsible for the Western Blot and endothelium-dependent vasorelaxation data.

References

[1] Ungvari, Z.; Csiszar, A.; Huang, A.; Kaminski, P. M.; Wolin, M. S.; Koller, A. High pressure induces superoxide production in isolated arteries via protein kinase C-dependent activation of NAD(P)H oxidase. *Circulation* **108:**1253-1258; 2003.

[2] Griendling, K. K.; Sorescu, D.; Ushio-Fukai, M. NAD(P)H oxidase: role in cardiovascular biology and disease. *Circ Res* **86:**494-501; 2000.

[3] White, F. C.; Nakatani, Y.; Nimmo, L.; Bloor, C. M. Compensatory angiogenesis during progressive right ventricular hypertrophy. *Am J Cardiovasc Pathol* **4:**51-68; 1992.

[4] Kai, H.; Mori, T.; Tokuda, K.; Takayama, N.; Tahara, N.; Takemiya, K.; Kudo, H.; Sugi, Y.; Fukui, D.; Yasukawa, H.; Kuwahara, F.; Imaizumi, T. Pressure overload-induced transient oxidative stress mediates perivascular inflammation and cardiac fibrosis through angiotensin II. *Hypertens Res* **29:**711-718; 2006.

[5] Yamazaki, T.; Komuro, I.; Kudoh, S.; Zou, Y.; Shiojima, I.; Mizuno, T.; Takano, H.; Hiroi, Y.; Ueki, K.; Tobe, K.; et al. Angiotensin II partly mediates mechanical stress-induced cardiac hypertrophy. *Circ Res* **77:**258-265; 1995.

[6] Higuchi, S.; Ohtsu, H.; Suzuki, H.; Shirai, H.; Frank, G. D.; Eguchi, S. Angiotensin II signal transduction through the AT1 receptor: novel insights into mechanisms and pathophysiology. *Clin Sci (Lond)* **112:**417-428; 2007.

[7] Griendling, K. K.; Harrison, D. G. Dual role of reactive oxygen species in vascular growth. *Circ Res* **85:**562-563; 1999.

[8] Berk, B. C.; Corson, M. A. Angiotensin II signal transduction in vascular smooth muscle: role of tyrosine kinases. *Circ Res* **80:**607-616; 1997.

[9]   Griendling, K. K.; Lassegue, B.; Alexander, R. W. Angiotensin receptors and their therapeutic implications. *Annu Rev Pharmacol Toxicol* **36:**281-306; 1996.

[10]   Zou, Y.; Akazawa, H.; Qin, Y.; Sano, M.; Takano, H.; Minamino, T.; Makita, N.; Iwanaga, K.; Zhu, W.; Kudoh, S.; Toko, H.; Tamura, K.; Kihara, M.; Nagai, T.; Fukamizu, A.; Umemura, S.; Iiri, T.; Fujita, T.; Komuro, I. Mechanical stress activates angiotensin II type 1 receptor without the involvement of angiotensin II. *Nat Cell Biol* **6:**499-506; 2004.

[11]   Nakashima, H.; Suzuki, H.; Ohtsu, H.; Chao, J. Y.; Utsunomiya, H.; Frank, G. D.; Eguchi, S. Angiotensin II regulates vascular and endothelial dysfunction: recent topics of Angiotensin II type-1 receptor signaling in the vasculature. *Curr Vasc Pharmacol* **4:**67-78; 2006.

[12]   Browe, D. M.; Baumgarten, C. M. Angiotensin II (AT1) receptors and NADPH oxidase regulate Cl- current elicited by beta1 integrin stretch in rabbit ventricular myocytes. *J Gen Physiol* **124:**273-287; 2004.

[13]   Ross, R. S.; Borg, T. K. Integrins and the myocardium. *Circ Res* **88:**1112-1119; 2001.

[14]   Wang, N.; Butler, J. P.; Ingber, D. E. Mechanotransduction across the cell surface and through the cytoskeleton. *Science* **260:**1124-1127; 1993.

[15]   Hunyady, L.; Turu, G. The role of the AT1 angiotensin receptor in cardiac hypertrophy: angiotensin II receptor or stretch sensor? *Trends Endocrinol Metab* **15:**405-408; 2004.

[16]   Touyz, R. M.; Schiffrin, E. L. Reactive oxygen species in vascular biology: implications in hypertension. *Histochem Cell Biol* **122:**339-352; 2004.

[17]   Taniyama, Y.; Griendling, K. K. Reactive oxygen species in the vasculature: molecular and cellular mechanisms. *Hypertension* **42:**1075-1081; 2003.

[18]   Cai, H.; Harrison, D. G. Endothelial dysfunction in cardiovascular diseases: the role of oxidant stress. *Circ Res* **87:**840-844; 2000.

[19]   Oeckler, R. A.; Kaminski, P. M.; Wolin, M. S. Stretch enhances contraction of bovine coronary arteries via an NAD(P)H oxidase-mediated activation of the extracellular signal-regulated kinase mitogen-activated protein kinase cascade. *Circ Res* **92:**23-31; 2003.

[20]   Fukui, T.; Ishizaka, N.; Rajagopalan, S.; Laursen, J. B.; Capers, Q. t.; Taylor, W. R.; Harrison, D. G.; de Leon, H.; Wilcox, J. N.; Griendling, K. K. p22phox mRNA expression and NADPH oxidase activity are increased in aortas from hypertensive rats. *Circ Res* **80:**45-51; 1997.

[21]   Kataoka, H.; Otsuka, F.; Ogura, T.; Yamauchi, T.; Kishida, M.; Takahashi, M.; Mimura, Y.; Makino, H. The role of nitric oxide and the renin-angiotensin system in salt-restricted Dahl rats. *Am J Hypertens* **14:**276-285; 2001.

[22]   Bailey, D. M.; Davies, B.; Young, I. S.; Jackson, M. J.; Davison, G. W.; Isaacson, R.; Richardson, R. S. EPR spectroscopic detection of free radical outflow from an isolated muscle bed in exercising humans. *J Appl Physiol* **94:**1714-1718; 2003.

[23]   Kozlov, A. V.; Szalay, L.; Umar, F.; Fink, B.; Kropik, K.; Nohl, H.; Redl, H.; Bahrami, S. Epr analysis reveals three tissues responding to endotoxin by increased formation of reactive oxygen and nitrogen species. *Free Radic Biol Med* **34:**1555-1562; 2003.

[24]   Lee, J.; Kim, S.; Oh, Y.; Ryu, S. Y.; Kim, S. W. Upregulation of vascular renin-angiotensin and endothelin systems in rats inhibited of nitric oxide synthesis. *Pharmacol Res* **46:**383-387; 2002.

[25]   Molloi, S.; Kassab, G. S.; Zhou, Y. Quantification of coronary artery lumen volume by digital angiography: *in vivo* validation. *Circulation* **104:**2351-2357; 2001.

[26]   Molloi, S.; Zhou, Y.; Kassab, G. S. Regional volumetric coronary blood flow measurement by digital angiography: *in vivo* validation. *Acad Radiol* **11:**757-766; 2004.

[27]   Xu, H.; Fink, G. D.; Galligan, J. J. Tempol lowers blood pressure and sympathetic nerve activity but not vascular O2- in DOCA-salt rats. *Hypertension* **43:**329-334; 2004.

[28]   Itoh, T.; Kajikuri, J.; Tada, T.; Suzuki, Y.; Mabuchi, Y. Angiotensin II-induced modulation of endothelium-dependent relaxation in rabbit mesenteric resistance arteries. *J Physiol* **548:**893-906; 2003.

[29]   Harada, S.; Nakata, T.; Oguni, A.; Kido, H.; Hatta, T.; Fukuyama, R.; Fushiki, S.; Sasaki, S.; Takeda, K. Contrasting effects of angiotensin type 1 and 2 receptors on nitric oxide release under pressure. *Hypertens Res* **25:**779-786; 2002.

[30]   Oelze, M.; Warnholtz, A.; Faulhaber, J.; Wenzel, P.; Kleschyov, A. L.; Coldewey, M.; Hink, U.; Pongs, O.; Fleming, I.; Wassmann, S.; Meinertz, T.; Ehmke, H.; Daiber, A.; Munzel, T. NADPH oxidase accounts for enhanced superoxide production and impaired endothelium-dependent smooth muscle relaxation in BKbeta1-/- mice. *Arterioscler Thromb Vasc Biol* **26:**1753-1759; 2006.

[31]   Howard, A. B.; Alexander, R. W.; Nerem, R. M.; Griendling, K. K.; Taylor, W. R. Cyclic strain induces an oxidative stress in endothelial cells. *Am J Physiol* **272:**C421-427; 1997.

Figures
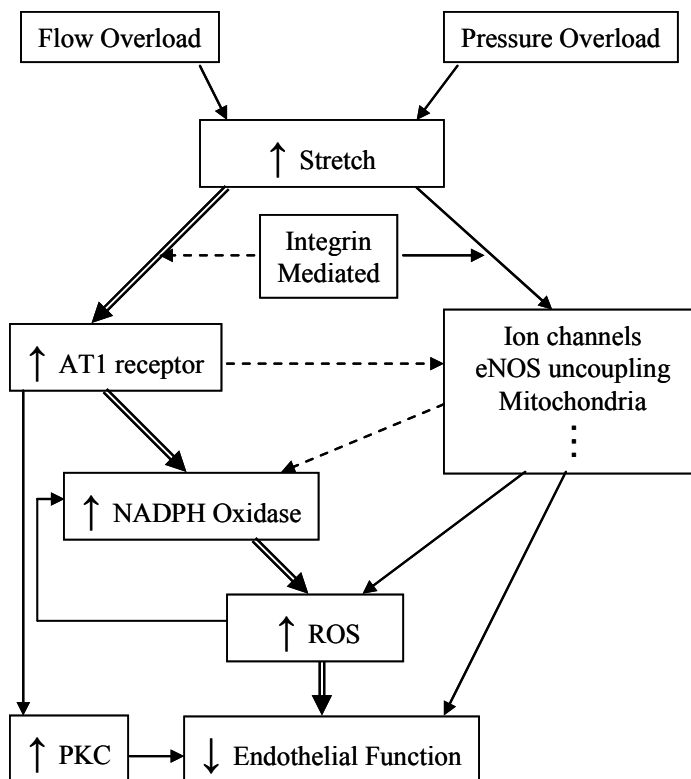
Figure 6.1: A schematic of stretch-induced cellular signaling pathway. Dual solid lines indicate pathways that were verified in the present study. Solid lines indicate established pathways. Dashed lines indicate uncertain pathways.
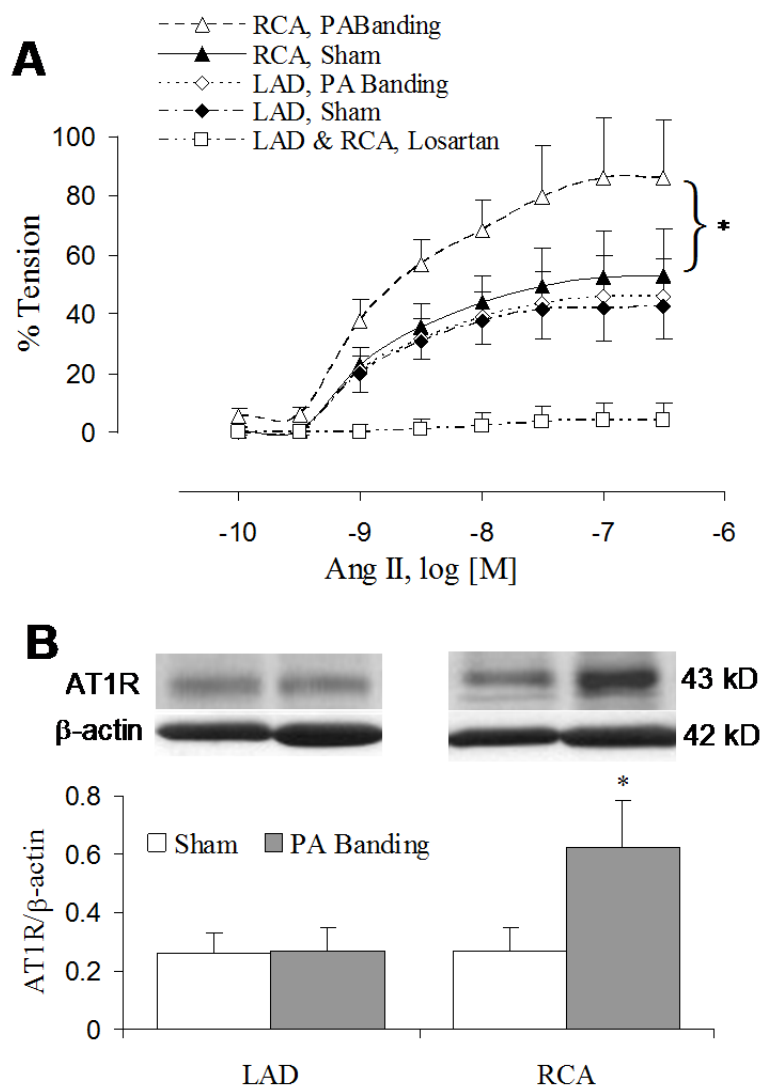
Figure 6.2: The evaluations of AT1 receptor activation in RCA exposed to PA banding and LAD as a control (unpublished data, X. Lu and G. Kassab). (A) The vascular contractile responsiveness to Ang II. The vascular contraction significantly increased in the RCA but not LAD. Losartan, an inhibitor of AT1 receptor, eliminated the vascular contractile responsiveness to Ang II. *: $P < 0.05$ two-way ANOVA analysis in comparison with control RCA. (B) The blots (top) and percent change (bottom) of protein expression of AT1 receptor in RCA and LAD tissue. *: $P<0.05$ Student t-test.
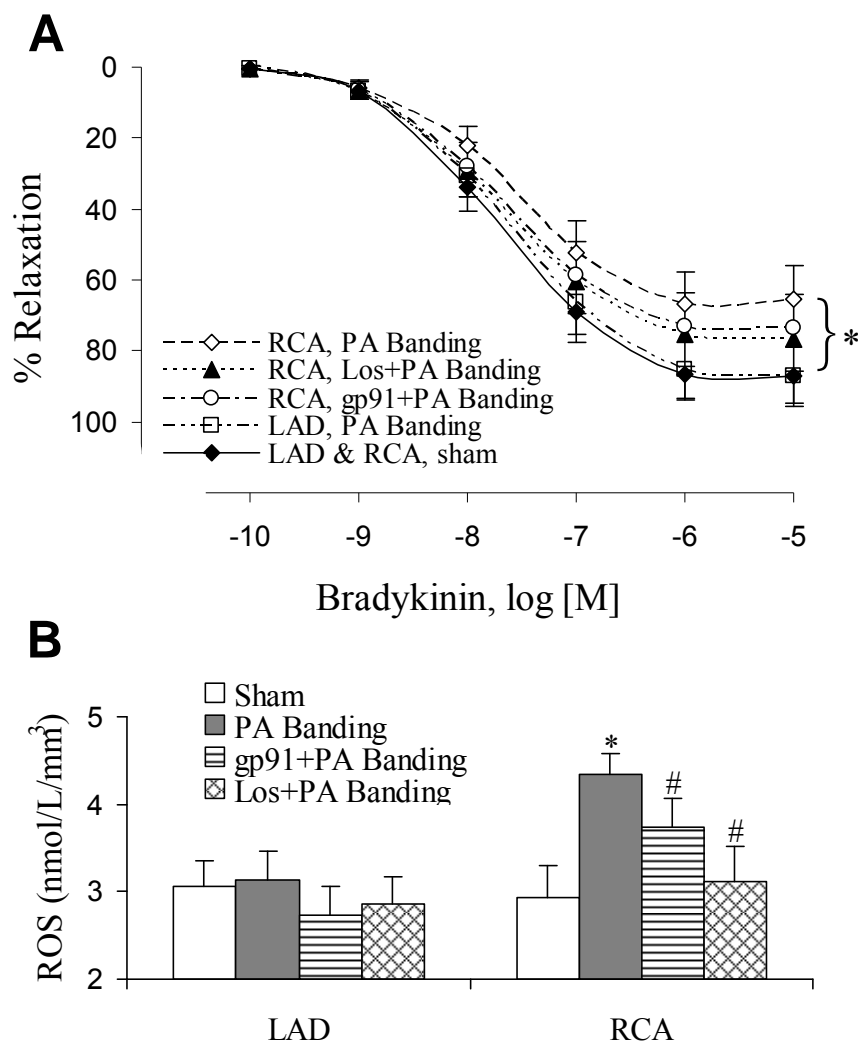
Figure 6.3: The endothelial function evaluated by endothelium-dependent vasorelaxation (unpublished data, X. Lu and G. Kassab), and the production of ROS measured by EPR (unpublished data). (A) The endothelial function. gp91: gp91-ds-TAT which is an inhibitor of NADPH oxidase. Los: losartan. Acute treatment of the inhibitors did not completely restore endothelium-dependent relaxation. *: $P < 0.05$ two way ANOVA analysis in comparison with control. (B) The production of ROS measured. with EPR. *: $P < 0.05$ Student's t-test in comparison with control. #: $P < 0.05$ Student's t-test in comparison with PAB.
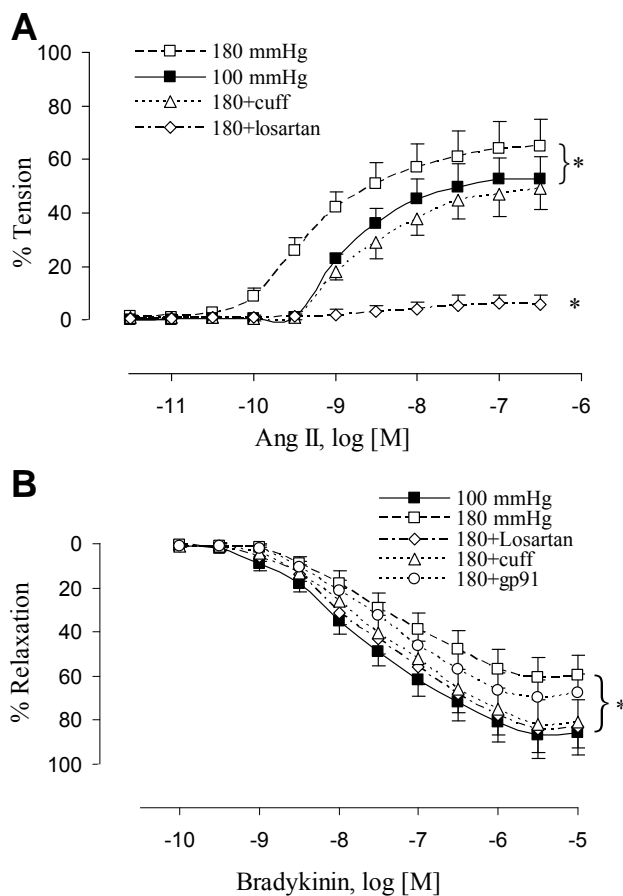
Figure 6.4: The effects of acute inflation (180 mmHg) on vascular reactivity to determine the role of stretch on Ang II induced contraction and endothelium-dependent relaxation (unpublished data, X. Lu and G. Kassab). (A) The vascular contractile responsiveness to Ang II. (B) The endothelium-dependent vasorelaxation. The endothelium-dependent relaxation was significantly weakened after 180 mmHg inflation. 100 mmHg: physiologic pressure. 180 mmHg: *ex vivo* inflation with 180 mmHg. 180+cuff: cuffed RCA was inflated at 180 mmHg. 180+Los: RCA incubated with losartan was inflated at 180 mmHg. 180+gp91: RCA incubated with gp91-ds-tat was inflated at 180 mmHg. *: $P < 0.05$ two-way ANOVA analysis in comparison with control.

Figure 6.5: The effects of *ex vivo* stimulation (180 mmHg) on the production of ROS of vessel segments, and EPR evaluation (unpublished data). 100 mmHg: physiologic pressure. 180 mmHg: *ex vivo* inflation at 180 mmHg. 180+cuff: cuffed RCA was inflated with 180 mmHg. 180+Los: RCA incubated with losartan was inflated at 180 mmHg. 180+gp91: RCA incubated with gp91-ds-TAT was inflated at 180 mmHg. *: $P < 0.05$ student t-test in comparison with control. #: $P < 0.05$ student t-test in comparison with PAB.

CHAPTER 7: SUMMARY AND FUTURE RESEARCH
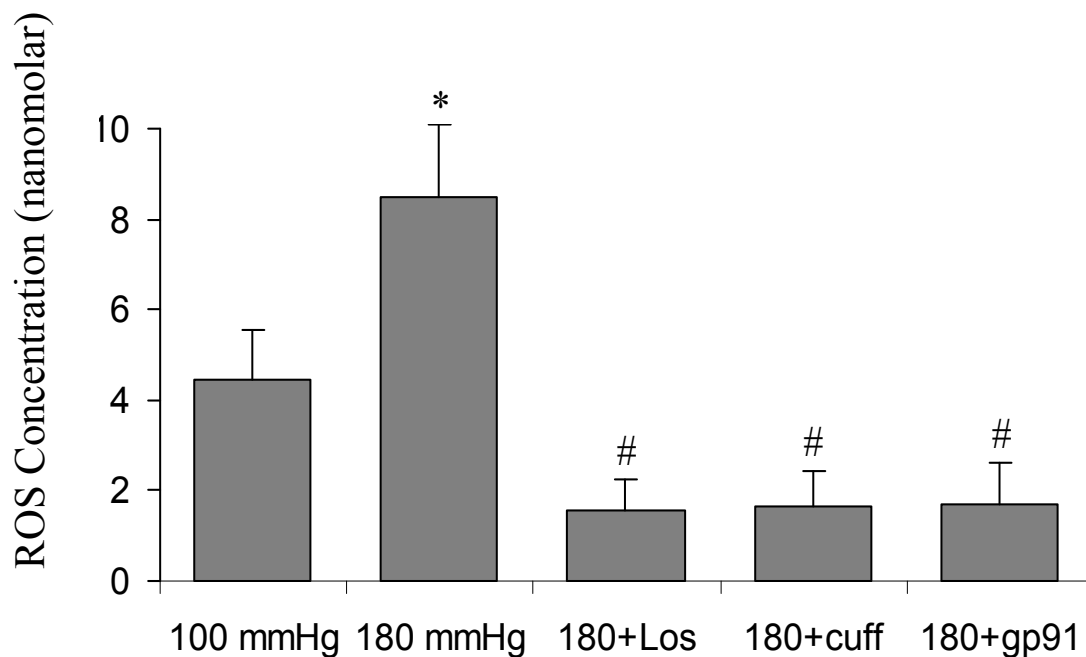
The endothelium, a thin layer of cells lining blood and lymphatic vessels, is particularly susceptible to free radical damage and is involved in many physiological reactions which are responsible for vascular tone. Free radical reactions involving superoxide and nitric oxide that are imbalanced in favor of superoxide lead to endothelial dysfunction through a process called eNOS uncoupling. Although these free radicals have extremely short lifetimes, they are capable of extensive cellular damage. In particular, ROS cause a variety of harmful effects such as lipid peroxidation, DNA modification, protein oxidation, and cell proliferation (cancer). In this thesis we have quantified free radicals, *ex vivo*, in biological tissue with continuous wave electron paramagnetic resonance (EPR) to determine the role that ROS play in endothelial dysfunction.

We have shown that conducting experiments at liquid nitrogen temperature leads to some experimental advantages. Freezing of the spin adducts renders them stable over a longer period, which allows ample time to analyze tissue samples for ROS. The dielectric constant of ice is greatly reduced over its liquid counterpart; this property of water enables larger sample volumes to be inserted into the EPR cavity without overloading it and leads to enhanced signal detection. Due to Maxwell-Boltzmann

statistics, the population difference goes up as the temperature goes down, so this phenomenon enhances the signal intensity as well.

We have found that it is important to limit extraneous ROS generation that is not due to the ROS stimulus of interest. Use of more than one method to detect ROS in an investigative study is important. Although no ROS assay method is ideal, using EPR in conjunction with a non-invasive probe such as PBN to assay ROS in whole tissue before freezing may create an approximation to *in vivo* conditions and should be included as one of the multiple methods to quantify ROS in biological studies.

In addition, we have demonstrated that ROS production increases in porcine carotid arteries in response to a onefold increase in the blood flow rate, which leads to endothelial dysfunction. NOX2 and NOX4 oxidase and p22phox and p47phox are upregulated in CFO, and NADPH oxidase is likely involved in the increase in oxidative stress. The chronic use of apocynin prevents the elevation of ROS levels, even though NOX2 and NOX4 are upregulated, and preserves endothelial function. The mechanisms by which apocynin prevents the upregulation of p22phox and p47phox but not NOX2 and NOX4 remain unclear. Although the process of CFO-induced remodeling to restore WSS has previously been thought of as a physiological response, the present data suggest that CFO mediated by ROS causes endothelial dysfunction, which may result from eNOS uncoupling in the first week of outward vascular remodeling.

We confirmed that WSS remains constant in this model of RVH and implicated stretch as the major stimulus. ROS production and NOX content increased significantly in this RCA model of RVH. Endothelial function of RCA was compromised after 4 wk of RVH, and eNOS uncoupling was implicated in the endothelial dysfunction. *In vivo*

analysis suggests an increased basal tone in the RCA during RVH and, therefore, increases the potential risk of vasospasm.

The study in Chapter 6 provides evidence that distension of the blood vessel wall by either pressure or dilatation can activate the AT1 receptor and elicits endothelial dysfunction. The signaling pathway needs to be further explored. The expression and activation of AT1 receptor and the production of ROS were upregulated and endothelial function deteriorated in the RCA. The acute inhibition of AT1 receptor and NADPH oxidase partially restored the endothelial function. The endothelial dysfunction and activation of AT1 receptor was also realized with acute hyper-inflation (180mmHg) of normal RCA. An external cuff inhibited the increase in activation of AT1 receptor and preserved endothelial function. In conclusion, we observed that stretch or distension activates the AT1 receptor which mediates ROS production which collectively leads to endothelial dysfunction in coronary arteries.

Our novel EPR spin trapping method can be applied to any tissue or cells. The spin trap, PBN, acts as a non-invasive probe of either tissue or cells, since it is non-toxic and cell permeable. In future, we plan to culture human aortic endothelial cells (HAECs) and incubate them with ω-3 fatty acids. We will elicit lipid peroxidation with an azo compound that delivers free radicals at a constant and temperature dependent rate; this free radical generator will mimic free radical attack of the cell membrane, since the free radicals are in the aqueous media outside of the cells. We want to investigate whether HAECs that are enhanced with ω-3 fatty acids are more or less susceptible to oxidation.

VITA

VITA

Cynthia D. Wassall

Education:

PhD.: Physics, 2012, Purdue University, Indianapolis, Indiana. (3.92, Cumulative)

MS: Physics, 2007, Purdue University, Indianapolis, Indiana. (3.82, Cumulative)

GRE General Test, January 2003: Verbal Score 600 and 85 percentile, Quantitative Score

710 and 75 percentile, Analytical Writing Score 5.0 on a 6.0 scale and 65 percentile.

BS: Physics, **with highest distinction,** 1994, Purdue University, Indianapolis, Indiana.

(3.87 Cumulative, 3.95 Major).

Awards:

Center for Membrane Biophysics Research Assistantship: IUPUI 2010-2011.

Minority in Science Fellowship: School of Science, IUPUI 2006-2009.

Indiana University Purdue University Fellowship: 2003-2004.

RMC Student Travel Award: 48[th]Annual Meeting of the Rocky Mountain Conference on

Analytical Chemistry 2006.

Outstanding Student Award in Physics: IUPUI 1993.

Upperclass Outstanding Scholars Award: IUPUI 1992-1994.

Challenger Scholarship: IUPUI 1991.

School of Science Scholar Award: 1989-1994.

Research:

My research work is focused on the application of EPR spin trapping techniques to the study of reactive oxygen species in porcine arteries. We employ a pig model because of its similarity to human cardiovascular physiology to investigate the role of reactive oxygen species in endothelial dysfunction. The objective of this research is to gain insight into the relationship between reactive oxygen species and cardiovascular disease.

I also have experience with culturing and performing oxidation experiments on human aortic endothelial cells using fluorescence spectroscopy as well as solid state nuclear magnetic resonance and differential scanning calorimetry of model membrane systems.

M.S.Thesis:

EPR detection of reactive oxygen and nitrogen species in biological systems.

Ph.D. Thesis:

The role of reactive oxygen species in endothelial dysfunction by electron paramagnetic resonance.

Published Manuscripts:

X. Lu, C. Q. Dang, X. Guo, S. Molloi, **C. D. Wassall**, M. D. Kemple, G. S. Kassab, Elevated Oxidative Stress and Endothelial Dysfunction in Right Coronary Artery of Right Ventricular Hypertrophy, J Appl Physiol, *110(6)*, 1674-1681 (2011).

Lu, X. Guo, **C. D. Wassall**, M. D. Kemple, J. L. Unthank, G. S. Kassab, Reactive Oxygen Species Cause Endothelial Dysfunction in Chronic Flow Overload, J Appl Physiol, *110(2)*, 520-527 (2011).

R. Wassall, M. A. McCabe, **C. D. Wassall**, R. O. Adlof and S. E. Feller, Solid State ^{2}H NMR and MD Simulations of Positional Isomers of a Monounsaturated Phospholipid Membrane: Structural Implications of Double Bond Location. J Phys Chem B, *114(35)*, 11474-83 (2010).

W. Stillwell, S. R. Wassall, A. C. Dumaual, W. Ehringer, **C. W. Browning (Wassall)** and L. J. Jenski, Use of Merocyanine (MC540) in Quantifying Lipid Domains and Packing in Phospholipid Vesicles and Tumor Cells, Biochim Biophys Acta, *1146*, 136-144 (1993).

Manuscripts in Progress:

X. Lu, **C. D. Wassall**, M. D. Kemple and G. S. Kassab. Role of Stretch on Angiotensin II type 1 Receptor and Endothelial Dysfunction.

C. D. Wassall, M. D. Kemple, X. Lu, and G. S. Kassab, Slicing tissue to assay for ROS produces inaccurate concentration values: an EPR investigation of cryopreserved tissue.

J. A. Williams, **C. D. Wassall**, M. W. Kagimbi, C. L. Eslinger, M. D. Kemple and S. R. Wassall, Cholesterol-lipid Affinity Determined by EPR.

Platform Presentations:

"Investigating reactive oxygen species' role in endothelial dysfunction by electron paramagnetic resonance." IUPUI, Department of Physics, Indianapolis, Indiana in January 2012.

"EPR detection of reactive oxygen and nitrogen species in biological systems".

Department of Physics, IUPUI, Indianapolis, Indiana in December 2007.

Poster Presentations:

C. D. Wassall, M. D. Kemple, X. Lu, and G. S. Kassab, EPR Method for ex vivo Detection of Reactive Oxygen Species in Tissue. Biophysical Society's 56th Annual Conference, San Diego, California, USA, February 2012.

J. A. Williams, **C. D. Wassall**, M. W. Kagimbi, C. L. Eslinger, M. D. Kemple and S. R. Wassall, Cholesterol-lipid Affinity Determined by EPR. Biophysical Society's 56th Annual Conference, San Diego, California, USA, February 2012.

C. D. Wassall, M. D. Kemple S. R. Wassall and W. Stillwell Spin Trapping the Oxidized Products of PUFA in Model Membranes: the Protection Conferred by Vitamin E. 3rd Annual IUPUI Research Day, Indiana University Purdue University Indianapolis, Indianapolis, Indiana, USA. April 2011.

C. D. Wassall, M. D. Kemple, S. R. Wassall and W. Stillwell, Vitamin E Forms Domains with PUFA during Lipid Peroxidation of Model Membranes: An EPR Spin Trapping Study. Biophysical Society's 55th Annual Conference, Baltimore, Maryland, USA, March 2011.

C. D. Wassall, M. D. Kemple, S. R. Wassall and W. Stillwell, Spin Trapping the Oxidized Products of PUFA in Model Membranes: the Protection Conferred by Vitamin E. Biophysical Society's 54th Annual Conference, San Francisco, California, USA, February 2010.

C. D. Wassall, M. D. Kemple, G. S. Kassab and Xiao Lu, Spin Trapping of Reactive Oxygen Species (ROS) in Porcine Tissue Exposed to Blood Flow-Overload. 1st Annual IUPUI Research Day, Indiana University Purdue University Indianapolis, Indianapolis, Indiana, USA. April 2009.

C. D. Wassall, P. M. Forester, M. D. Kemple, J. L. Unthank and S. Miller, EPR Detection EPR Detection of Reactive Oxygen and Nitrogen Species, Indiana Center for Vascular Biology & Medicine 2006 Retreat, Indianapolis, Indiana, USA, September 25, 2006.

C. D. Wassall, P. M. Forester, M. D. Kemple, J. L. Unthank, S. J. Miller and Michael Sturek, EPR Detection of Reactive Oxygen Species in Whole Blood of Diseased Animals, 48th Rocky Mountain Conference on Analytical Chemistry, Breckenridge, Colorado, USA, July 23-27, 2006.

S. P. Schuh, S. D. Harris, **C. D. Wassall**, M. A. McCabe and S. R. Wassall, Location of Unsaturation Determines the Thermal Behavior of Phospholipid Membranes: ^{2}H NMR Studies, 111th Annual Meeting Indiana Academy of Science, Indiana University Purdue University Indianapolis, Indianapolis, Indiana, November 2-3, 1995.

S. R. Wassall, M. A. McCabe, **C. D. Wassall**, S. P. Schuh and S. D. Harris, ^{2}H NMR Studies of Positional Isomers of a Monounsaturated Phospholipid Membrane, 19th Conference of the Australian Society for Biophysics in conjunction with the British Biophysical Society, University of Sydney, Sydney, Australia, July 21-23. 1995.

S. R. Wassall, M. A. McCabe, **C. W. Browning (Wassall)**, S. P. Schuh and S. D. Harris, 2H NMF Studies of Monounsaturated Lipid Bilayers, 39th Annual Meeting of the Biophysical Society, San Francisco, California, USA, February 12-16, 1995.

S. R. Wassall, M. A. McCabe, **C. W. Browning (Wassall)**, S. D. Harris and S. P. Schuh, ^{2}H NMR Studies of Unsaturated Lipid Bilayers, International Symposium on NMR as a Structural Tool for Macromolecules: Current Status and Future Directions, Indiana

University Purdue University Indianapolis, Indianapolis, Indiana, USA, October 30-November 1, 1994.

S. R. Wassall, M. A. McCabe, **C. W. Browning (Wassall)**, R. C. Yang McCabe, J. L. Thewalt and R. O. Adlof, ^{2}H NMR Studies of Positional Isomers of Monounsaturated Phospholipid Bilayers, 1994 March Meeting of the American Physical Society, Pittsburgh, Pennsylvania, USA, March 21-25, 1994.

S. R. Wassall, M. A. McCabe, **C. W. Browning (Wassall)**, R. C. Yang McCabe, W. D. Ehringer and W. Stillwell, ^{2}H NMR Studies of Unsaturated Phospholipid Membranes: Importance of Double Bond Location, 38th Annual Meeting of the Biophysical Society, New Orleans, Louisiana, USA, March 6-10, 1994.

S. R. Wassall, M. A. McCabe, **C. W. Browning (Wassall)**, J. L. Thewalt and R. O. Adlof, Broadline ^{2}H NMR Studies of Positional Isomers of Unsaturated Phospholipid Membranes, Eleventh International Meeting on NMR Spectroscopy of the Royal Society of Chemistry, University College of Swansea, Wales, July 4-9, 1993.

M. A. McCabe, **C. W. Browning (Wassall)**, J. L. Thewalt, R. O. Adlof and S. R. Wassall, Comparison of Isomeric Monounsaturated Phospholipid Membranes by ^{2}H NMR, 37th Annual Meeting of the Biophysical Society, Washington, D. C., USA, February 14-18, 1993.

S. R. Wassall, M. A. McCabe, G. L. Griffith, **C. W. Browning (Wassall)**, W. D. Ehringer and W. Stillwell, ^{2}H NMR Studies of Positional Isomers of Polyunsaturated Membranes, XV International Conference on Magnetic Resonance in Biological Systems, Jerusalem, Israel, August 16-21, 1992.

W. Stillwell, S. R. Wassall, **C. W. Browning (Wassall)**, W Ehringer, A. C. Dumual and L. J. Jenski, Use of Merocyanine (MC540) in Quantifying the Extent of Liquid Crystalline and Gel States in Lipid Vesicles, American Society for Biochemistry and Molecular Biology/Biophysical Society Joint Meeting, Houston, Texas, USA, Feb. 9-13, 1992.

Teaching:

Teaching assistantship at IUPUI. Heat Electricity Optics (152, 251) and General Physics I and II (201, 202), 2003-2006.

Teaching Mentor at IUPUI. Mechanics (152) and Heat, Electricity and Optics (251), 2011-2012.

Physics Tutor at IUPUI. All introductory physics courses. 2009-2011 and 1992-1994.

Computer Skills:

Proficient in MS-office, Chem Biodraw and Origin. Familiar with C, C++ and Fortran.

Services:

School of Science Women in Science Internal Advisory Board Member, 2005.

Student Council Member, School of Science, 1993.

Secretary of Physics Club, 1992.

Society of Physics Students Member

Affiliations:

Biophysical Society

American Physical Society

American Chemical Society

Society of Physics Students